University of Neuchâtel

Centre of Hydrogeology

Gas supersaturation, ^{222}Rn and CO_2 as tracers in karst water

PhD thesis presented to the Faculty of Sciences of the University of Neuchâtel
to satisfy the requirements of the degree of Doctor of Philosophy in Science

by

Domagoj Babić

Thesis defence date: *25.06.2013*
Public presentation date: *09.10.2014*

PhD thesis evaluation committee:

Prof. François Zwahlen	University of Neuchâtel, Switzerland	Thesis director
Dr. Heinz Surbeck	ETH-Zürich, Switzerland	Jury member
Prof. Antoine Kies	University of Luxembourg, Luxembourg	Jury member
Prof. D. Hunkeler	University of Neuchâtel, Switzerland	Jury member

UNIVERSITÉ DE NEUCHÂTEL

Faculté des sciences
Secrétariat-décanat de Faculté
Rue Emile-Argand 11
2000 Neuchâtel - Suisse
Tél: + 41 (0)32 718 2100
E-mail: secretariat.sciences@unine.ch

IMPRIMATUR POUR THESE DE DOCTORAT

La Faculté des sciences de l'Université de Neuchâtel autorise l'impression de la présente thèse soutenue par

Monsieur Domagoj BABIC

Titre:

Gas supersaturation, ^{222}Rn and CO_2 as tracers in karst water

sur le rapport des membres du jury composé comme suit :

- Prof. hon. François Zwahlen, Université de Neuchâtel, directeur de thèse
- Prof. Daniel Hunkeler, Université de Neuchâtel
- Prof. hon. Antoine Kies, Université du Luxembourg, Luxembourg
- Dr Heinz Surbeck Nucfilm GmbH, Cordast, Suisse

Neuchâtel, le 8 août 2013

Le Doyen, Prof. P. Kropf

Remerciements

Après ces quelque quatre années depuis le début du projet, c'est avec plaisir que j'arrive à la rédaction des remerciements. Je tiens à exprimer une réelle gratitude envers toutes ces personnes qui ont permis, de près ou de loin, de mener à bien cette étude.

En premier lieu, merci infiniment à François Zwahlen, mon directeur de thèse, pour m'avoir proposé cette aventure. Sa porte était toujours ouverte et sa bonne humeur salvatrice très motivante. Son expérience et ses idées ont grandement facilité la progression de ce projet. Merci également pour toutes ses petites anecdotes de vie qui vous font repartir avec le sourire. Je n'oublierai jamais l'élégance du marchandage de tapis à Damas.

Merci à Heinz Surbeck, grand spécialiste des radioisotopes dans les eaux souterraines, pour m'avoir fait entrevoir le potentiel des gaz dissous. Sa grande disponibilité, sa jovialité et ses précieux conseils ont rendu plus accessible la complexité de ce domaine. De plus, sa gestion efficace des données m'ont plus d'une fois sauvé la mise quand la situation semblait désespérée.

Je tiens également à remercier Pierre-André Schnegg, concepteur du fluorimètre de terrain, sans qui le travail des hydrgéologues du monde entier aurait été autrement plus difficile. Sa grande disponibilité et sa gentillesse ont toujours été au rendez-vous.

Un grand merci à Roberto Costa, pour son implication de tous les instants. Sa capacité à créer a grandement facilité le suivi de cette aventure.

Ma profonde gratitude va à Steve Gobert, grand connaisseur des Gorges de l'Areuse. Son incomparable soutien logistique et son équipe n'ont rendu que plus agréable ces journées passées sur le site d'étude.

J'exprime mes sincères remerciements à toute l'équipe du projet ALPEAU, en particulier Robert Jenni, Urs Moser et François Godi. Merci pour leur organisation sans failles, leur implication et leur bonne humeur.

Merci à également à Jean-Michel Gobat du Laboratoire Sol et Végétation pour sa disponibilité et sa capacité à rendre accessible ce monde extrêmement complexe qu'est le sol.

J'exprime une grande gratitude envers Thierry Schneider de chez Tetraedre SA, pour son appareillage de mesure et de contrôle à distance.

Une dédicace spéciale s'impose pour les secrétaires du CHYN, Carine Erard Brayek, Corinne Carraux-Drey, Sabine Erb-Robert et Gianfranca Cerrito. La bonne humeur des lieux leur doit beaucoup.

Toute ma gratitude va aussi à Bibiane Schlunegger, laborantine au CHYN.

Je tiens à remercier très chaleureusement tous mes collègues et amis, pour la très agréable ambiance de travail. Une mention toute spéciale au mythique troisième étage. Merci à Lorienne Thüler, mon compère du bureau E319 pour son dynamisme et pour avoir transformé les lieux. Merci à Andrea Borghi et Damian Glenz pour leur amitié, leur hébergement stratégique et tous ces fous rires. Merci à Gregory Deman et Lucien Blandenier pour m'avoir accompagné sur le terrain pendant des conditions dantesques et pour leur maîtrise parfaite du burger au BBQ. Merci à Geoffrey Undereiner, Cybèle Cholet, Julien Straubhaar, Pierik Falco, Giona Preisig éminences grises de l'étage et à Christian Moeck, Antoine Bailleux et Paul Bailleux. Merci également à Michiel Pronk, François Negro, Ellen Milnes et Jaouher Kerrou sans qui les pauses café et les soirées de Neuchâtel n’auraient pas eu la même saveur.

Merci à ma famille qui m'a toujours soutenu pendant ces aller-retours entre Genève et Neuchâtel.

Un grand merci final à Sofia, ma moitié pour ses encouragements constants et sa présence...

Abstract

Karst aquifers are among the most important water resources world-wide. Nevertheless, due to their intrinsic properties consisting in fast transport processes and reduced contaminant attenuation capacity, they are proved to be highly vulnerable.

Consequently, it is important to discriminate between water originating from the soil reservoir, the epikarst, the low permeability volume and the freshly infiltrated rainwater. To do so, the Prédernier artificial drainage gallery (Gorges de l'Areuse, Swiss Jura Mountains) was investigated by a combined continuous monitoring of radon, carbon dioxide and total dissolved gas pressure. Electrical conductivity, turbidity, total organic carbon and dissolved ions were also followed. The survey of various seepages spread throughout the drainage gallery, offered the unique feature of allowing to compare the dynamics of natural parameters characterized by different storage origins and watershed scales.

Radon and carbon dioxide are two gases produced in soil, hence their input function is well delimited. They both are characterized by good solubilities and can be dissolved in percolating water and transported to system outlets. Even tough originating from the same production area, these gases have different chemical and physical properties. On the one hand, radon is an inert radioactive noble gas produced through α-decay of radium present in soil and is characterized by a half-life of 3.8 days. It can be used to assess fast transport processes, as after 20 days its concentrations pass under detection limits. On the other hand, carbon dioxide reacts with carbonates on its way down to the saturated zone.

Total dissolved gas pressure (TDGP) represents water vapour pressure in addition to the individual dissolved gases partial pressures. When TDGP in water exceeds the atmospheric pressure, supersaturation occurs. Following a precipitation event, soil air entrapped in pore space, undergoes a newly applied hydrostatic pressure, allowing more gas to be dissolved. Hence, the percolating water acquires a supersaturation signature, which can easily be followed at system outlets.

These gases, characterized by good solubility, different chemical and physical properties and naturally and abundantly produced in soil or during rainfall events, were used as natural tracers. The temporal variations of their respective concentrations in underground water not only allow to gain valuable information about fast transport processes in karst systems, but also to identify the different water reservoirs contributing to the discharge.

Results demonstrated that the dissolved gases approach, revealed the importance of the soil sub-system with regards to its influence on the recharge of karst aquifers during high-flow conditions, and on the sustainability of its influence to the flow regime. The supersaturation base-level, a soil thickness specific feature, was used as a relevant surrogate to assess the temporal distribution of soil contribution to the selected karst system. Whereas, codependent radon, carbon dioxide and supersaturation peaks depict the influence of soil stored water, enriched in dissolved gases during rainfall events.

Keywords: karst hydrogeology; soil; ^{222}Rn; CO_2; total dissolved gas pressure; supersaturation, total organic carbon; turbidity.

Table of Contents

List of Figures

List of Tables

Appendices

1 Introduction

1.1 Aim of the thesis

The Alpeau project[1] aims at strengthening the protective role of forests with an eye to the sustainable management of groundwater resources and their quality. In order to do so, it promotes responsible forest management methods and evaluation of their costs. It is generally admitted that underground water filtered through forest soil is characterized by its excellent quality (e.g. Klapproth and Johnston, 2000). Nonetheless, forest harvesting may drastically impact the soil. Aggressive methods and industrial harvesting, that involves road construction and soil compaction, may noticeably affect the filtering features and storage capacity of forest soil. Indeed, soil compaction results in a decline in macropore flow, a reduced infiltration capacity, a high susceptibility to erosion and a decreased hydraulic conductivity (Zheng, 2008). Moreover, the Alpeau project tends to develop efficient cooperation methods, establishing contractual relationships, between actors of the water providing sector and those of forest management.

In karst aquifer systems, the soil layer is held accountable for an important part of contamination hazards. Therefore, several authors have proposed the monitoring of soil related parameters, such as turbidity and total organic carbon on their own (e.g. Nebbache *et al.*, 1997; Stadler *et al.*, 2008) and in combination with particle size distribution (Pronk, 2009), as surrogates for the occurrence of microbial contaminations.

This study, which is part of the Alpeau project, intends to assess the relevancy of a dissolved gases approach, to evaluate the soil contribution to the hydrodynamic of the selected karst aquifer. To do so, the selected test site was investigated by a combined continuous monitoring of radon, carbon dioxide and gas supersaturation. Indeed, both radon and CO_2 are characterized by a good solubility and are naturally and abundantly produced in soil, whereas the generation of supersaturation in soil occurs during precipitation events. These gases, along with supersaturation, can easily be monitored at system outlets and were used as natural tracers.

[1] http://www.alpeau.org/

1.2 Karst aquifers

1.2.1 Karst aquifers specificities and main features

A karst aquifer is made of soluble hard rock and is characterized by surface and underground phenomena of chemical dissolution. It is described by a karstified geological unit which contains groundwater. It may form in any types of rock that show some degree of chemical or physical water solubility. The most typical and important karst rocks are carbonate rocks, above all limestone but also dolomite. Gypsum, anhydrite, carbonatic conglomerate and sandstone can also show some karstifications.

Karst aquifers have a very specific structure and behaviour. They may be essentially described by their duality, also known as organised heterogeneity (Perrin, 2003). This heterogeneity can be schematized by a high permeability connected channel network formed by the dissolution of a low permeability fractured limestone unit (Drogue, 1971; Kiraly, 1975). This network drains a catchment basin and discharges to at least one perennial spring.

More specifically, the saturated and unsaturated zones are not necessarily superimposed (Mangin, 1975), hence part of the recharge can come from allogenic or adjacent non-karst areas. As such, the karst system term would be more appropriate than karst aquifer, as it is referred to the entire drainage unit of the system. Furthermore, this duality can also be found in the autogenic recharge conditions which may be diffuse (through the soil, the epikarst or the low permeability volumes), or concentrated (into the channel network or sinking streams). The groundwater flow field follows this duality, as low flow velocities occur in the fractured volume and high flow velocities characterized the channel network. The discharge conditions follow this dual behaviour as well. Indeed, diffuse seepage takes place from the low permeability volume, and concentrated discharge from the karst network at the spring (Kiraly, 1998). Finally, water storage within the system can occur in both the vadose and phreatic zone.
This heterogeneity found in the hydrogeological behaviour of karst systems can be related to the geological and geomorphological features of karst terrains (Ford and Williams, 1989).

Several conceptual models regarding karst aquifers are presented in the literature (Blavoux and Mudry, 1983; Doerfliger *et al.*, 1999; Drogue, 1992; Grenn *et al.*, 2006; Klimchouk, 2000; Lacroix *et al.*, 2000; Lee and Krothe, 2001; Mangin, 1975; Perrin, 2003; Sauter, 1992; Williams, 1983). Although some differences can be found among them, especially considering the origin of the base flow regime (the low permeability volume in the phreatic zone or the epikarst) and the origin of the water contributing to flood events (concentrated or diffuse infiltrations, phreatic or freshly infiltrated water, epikarst, soil or conduit storage, mixing of different tributaries) they all mostly agree on separating karst systems in different sub-systems:

- the infiltration sub-system
- the soil and epikarst sub-system
- the unsaturated zone
- the phreatic zone

1.2.2 The infiltration sub-system

The infiltration sub-system is defined according to its recharge constituting terrains. If they are characterized by karstic terrains only, it is referred to as a unary karst system and the recharge is said to be autogenic. If karstic and non-karstic terrains contribute to the recharge (allogenic recharge) it is known as a binary karst system.

1.2.3 Soil

Soil may be described as a three phases system: soil solid (minerals and organic matter), liquid and gaseous phase. It is the result of the alteration and the reorganisation of an underlying bedrock. Both these transformations are the direct consequences of biological activities and atmospheric influences (Aubert and Boulaine, 1980, in Lozet and Mathieu, 2002). It is generally referred to as soil pedogenesis. It can be described by three successive stages (Tissier, 2012).

The first stage consists of underlying rock physical and chemical alteration. The former is the result of temperature variations, wind erosion and plants growth (especially root impact). These phenomenons lead to the formation of soil skeleton referring principally to

altered rock, gravels, sand grains and silt particles. The latter implies rock dissolution and hydrolysis under the influence of acid and alkaline enriched water. This process leads to the generation of alteration features such as silt and iron-oxides.
The second stage is characterized by organic matter enrichment. Newly formed soil is colonized by pioneer plants and animals. Following their decomposition by microorganisms and fungi, humus formation occurs and CO_2 is released. Under the influence of CO_2 and water, rock alteration continues.
The third stage can be referred to as horizons formation. Depending on the total amount of precipitations, soil permeability and humus features, leaching takes place within soil. It results in soil horizons formation. These horizons are quite homogeneous, parallel to the surface and are characterized by their thickness, grain size distribution, alkalinity and rock alteration levels.
In this study, soil stands for the unconsolidated pedologic cover of a limestone bedrock.

1.2.3.1 Soil and hydrogeology

Perrin (2003) demonstrated the prominent role of the soil cover with regards to storage and transport processes through the unsaturated zone of karst aquifers. Indeed, soil influences the infiltration and the mixing of solutes. Following an isotopic survey of percolation water ($\delta^{18}O$) at the Milandre cave (Switzerland), an area covered wit thick soil, he suggested that significant mixing occurred in the soil zone, as the rain isotopic signature was highly buffered when reaching the unsaturated zone underneath.
Pedogenesis in the Jura mountains is strongly controlled by the underlying bedrock (Gaiffe and Bruckert, 1990). In some loacations loess plays a role as well (Havlicek and Gobat, 1996). As a result, two principal types of soil cover can be found in these areas: brown soils and humo-calcic (Calco soils) ones. Those soils present different features. Brown soils are found on solid limestone characterized by a low fracturing density (e.g. dolomitic and marly limestone, dip slope strata). Therefore, they are poorly drained and have a high humidity level. Humo-calcic soil develops on well fissured limestone. They are efficiently drained, thus have a low storage capacity. They contribute to significant calcium level in water as rock fragments are usually found. Aubert and Pochon (1977) compared these two soil types water chemistry. They obtained a mean concentration for bicarbonate and calcite ranging from 12.5 to 21.7 mg/l for the brown soils, and from 47.2 to 126.3 mg/l for calco-humic soils. Hence an observed diminishing mineralisation at a karst spring doesn't

necessarily mean a contribution of fresh infiltrated water, but could also show a brown soil zone influence.

1.2.3.2 Forest soil

It is generally admitted that underground water filtered through forest soil is characterized by its excellent quality (Davie, 2006). This can by explained by the fact that forest ecosystems are well preserved and rarely under influences of human activities and pollution, contrary to pastures and urban areas. Moreover, if any accidental spill was to happen forest soil is naturally rich in organic matter and hence efficiently minimises pollutions. Following precipitations, water will first percolate through the humus layer, described as the upper part of soil containing organic matter and highly influenced by biological activities (AFES, 2009). It is the soil horizon which is most likely to be subjected to human influences (Gobat *et al.*, 2010). The chemical and physical filtering role of this soil is achieved through the combination of high organic matter content and a diversified and dynamic biocenosis. Indeed, several natural processes, such as sorption, denitrification, oxydoreduction, ions exchanges and plant nutrient intake take place (Klapproth and Johson, 2000; Schürch *et al.*, 2003). Microorganisms turn out to be of significant importance (Gish *et al.*, 1998). They degrade organic matter and are involved in denitrification. All these statements can be considered to be true in “naturally” or “ethically” harvested forests. Moore (1999) links aggressive harvesting methods with significant high sediments loads and pesticides presence in surface and underground streams. Industrial harvesting, that involves road construction and soil compaction, seems to be a particularly ravaging result (Aust and Blinn, 2004), as pollution can occur and the filtering features of forest soil is drastically affected.

In contrast to Perrin's work, Lange *et al.* (2008) underlineded the role of preferential flow paths through the soil. These preferential flow paths can be directly related to vegetation and especially tree roots, as a densely developed tree roots network enhances the transport of water underground. Concentrated infiltration can also occur following tree trunk water accumulation (Gobat *et al.*, 1998). Bundt (2000) points out two mechanisms allowing rapid movement of water and solutes that bypass a portion of the soil matrix. The first one is known as macropore flow. It generally occurs through root channels, cracks and fissures and other biopores (Beven and Germann, 1982; Booltink and Bouma, 1991; Jacobsen *et al.*, 1997). The second one is referred to as finger flow. It takes place trough

macroscopically homogeneous soil in reaction to a wetting front contrast due to differences in water content, trapped air, water repellency of solid surfaces or inhomogeneous infiltration at the surface (Glass *et al.*, 1989; Selker *et al.*, 1992; Dekker and Ritsema, 1996).
It could easily be assumed that macropore flow could promote underground water pollution. However, the danger is only hypothetical, as macropores are characterized by high oxygen and organic matter content, resulting in flourishing microbial activity (Gish *et al.*, 1998).

1.2.4 The epikarst

Klimchouk (1997) defined the epikarstic zone (also referred to as subcutaneous zone) as the uppermost part of exposed karstified rocks. The permeability of this zone, which is the consequence of fissuring and diffuse karstification, is noticeably more important than the one characterizing the underlying vadose zone. Rock decompression and biochemical processes (dissolution and vegetation fissuring) result in an exponential increase in fissure density towards the rock ground surface.

The epikarstic zone structure and functioning has been described by several authors (Williams, 1985; Smart and Friedrich, 1986; Klimchouk, 2000). At the surface and within the uppermost part of the epikarst, vertical hydraulic conductivity is high and quite homogeneous. Consequently, diffuse infiltration is a dominant feature. Moreover, hydraulic conductivity drastically diminishes with depth in reaction to jointing density and diffuse karstification lessening. As a result, even though infiltration is efficient in the upper part of the epikarstic zone, drainage out is more problematical leading to water storage. These distinctive features can be summarized as a permeability contrast between the epikarstic zone and the underlying low permeability volume, leading to the formation of a perched aquifer. Water flow in this perched aquifer is characterized by a noticeable horizontal component which allows recharging of the vadose zone through the nearest vertical fissures. The epikarstic zone can thus support base flow and concentrates water fluxes into the uppermost part of the unsaturated zone (Jeannin, 1996).

Nevertheless, all the above described features are known to be true for mature epikarsts. According to Klimchouk (2004), interruption of epikarst maturation by glacial stripping is common, especially in mountain regions. Glaciers can strip away completely the epikarst

zone. The removal of the epikarst changes drastically the hydrological behaviour of the post-glacial karst system. The new epikarst zone tends to re-establish after glaciations, and its evolution follows a typical young epikarst stage. He states that a poorly developed epikarst is characterized by a low to negligible water storage capacity and mainly behaves as a flow concentrating media. Most of karst massifs that experienced glaciations during the last glacial maximum have the epikarst re-establishing on young stages.

1.2.5 The unsaturated zone

The unsaturated zone, also referred to as the vadose zone, connects the epikarstic sub-system and/or the soil to the phreatic zone. This transfer is mostly achieved by drainage through a vertical network of fissures and conduits, also known as concentrated or quick flow. Seepage flow through the low permeability volume (LPV), the rock matrix and the fractured limestone, also occurs. Indeed, Kiraly (2002) thanks to numerical simulations, estimated that 50% of water transiting through the vadose zone, does so in drainage conduits. These two types of flow lead to two hydraulic responses at karst systems outlet. Conduit flow leads to nervous hydraulic behaviour and seepage flow through the low permeability volume results in a more attenuated signature. The combination of these two hydraulic reactions lead to what is usually observed at karst systems sources. It is relevant to point out the unsaturated zone storage feature. During heavy flood events, fresh water may recharge the low permeability volume in reaction to a hydraulic gradient inversion. This matrix storage can then contribute to base flow recharge during low flow conditions (Emblanch *et al.*, 1998).

1.2.6 The phreatic zone

The phreatic zone, also named the saturated zone, can be described as a network of high permeability conduits within low permeability volumes characterized by a high storage capacity. It is the main storage unit of karst systems. The main part of flows occur in the drainage conduit and are known to be turbulent, whereas storage is mainly concentrated in the fractured limestone (White and White, 2005). A hydraulic gradient inversion between the conduits and the matrix during precipitation events recharges the low permeability volume as well. This inversion stops the contribution of the phreatic zone storage to spring discharge (Kiraly, 1998).

The saturated zone is sometimes overhanged by a so called epiphreatic zone, which can be partially saturated in reaction to floods or during high-flow conditions (Monroe, 1970).

1.2.7 Physical and chemical properties

1.2.7.1 Turbidity

The turbidity of water is a measure of the extent to which the intensity of light passing through is reduced, by absorption, diffusion or reflection, by suspended matter. The turbidity of underground water is the result of suspended particles, such as insoluble minerals, colloids originating from soil erosion, micro-organisms and organic particles resulting from the decomposition of plant and animal remains. Typical diameters range from less than 1µm for colloids to more than 1 mm for other particles. The index of refraction of water, the size and shape of suspended matter influence light diffusion. PH can also noticeably affect turbidity. Indeed, some substances can flocculate in reaction to the variation of these parameters.
In porous aquifers, turbidity content is generally low and quite stable in time. This behaviour is not observed in karst aquifers, prone to nervous system responses, where particles transport, implying turbidity presence, is a complex process involving sedimentation and suspension phenomenons (Fournier *et al.*, 2006). Indeed, limestones alteration and soil leaching result in the genesis of silt, which settles down after a discharge diminishing in the conduit network. Particles characterized by a larger diameter are more prone to settling down and sedimentation, as well to remobilisation following discharge variation within the intrakarstic conduit network. On the one hand, turbidity events occurring at karst springs, known as autochthonous turbidity, results from the resuspension of intrakarstic material; on the other hand, allochthonous turbidity is the consequence of direct transfer of particles from the soil or sinking surface streams (Amraoui *et al.*, 2003; Lacroix *et al.*, 2000; Mahler and Lynch, 1999; Massei *et al.* 2003; Pronk, 2009). Several authors have proposed turbidity as a surrogate indicator of microbial contamination (Nebbache *et al.*, 1997; Ryan and Meinman 1996). However, according to Kralik (2001), even though small turbidity events sometimes coincide with bacterial contamination, large turbidity variations may happen without any bacterial presence. Thus, the duality of turbidity origin, whether it is autochthonous or allochthonous, and the lack of clear microbial contamination correlation, doesn't allow turbidity alone to be used as a reliable water quality indicator (Dussart-Baptista *et al.*, 2003).

1.2.7.2 Total organic carbon

Natural organic compounds found in groundwater generally originate from the soil layer (Batiot *et al.*, 2003). On occasion, organic rich layers within aquifers also contribute to organic content. The natural organic compounds are mainly the result of decomposition of plants material by microorganisms. The fraction available for transport across the unsaturated zone is usually refractory (i.e. difficult to degrade), if not, it would be degraded by the time it reaches the phreatic zone and the system outlet. Natural organic particles are a complex combination of different molecules with variable composition. Each individual compound is very difficult to isolate and identify. Therefore, the content of organic matter is often characterized globally and referred to as dissolved organic carbon (DOC) or total organic carbon (TOC). Total organic carbon includes dissolved and particulate organic carbon (POC). Particulate organic carbon doesn't represent a significant part of total organic carbon (Thurman, 1985) in natural media. Dissolved organic carbon can thus be used as a surrogate for total organic carbon. According to its size distribution or its solubility at pH values, dissolved organic carbon is subdivided into different classes. Indeed, a common way to characterize DOC is to determine its fulvic and humic fraction, which belong to the group of humic substances. The fraction of humic substances insoluble in water at pH=2 but soluble at higher values is known as humic acid. On the contrary, fulvic acid is soluble under all pH conditions.

Total organic carbon (TOC) principally originates from the soil and surface water and is typically of allochthonous origin (Batiot *et al.*, 2003). Stadler *et al.* (2008) proposed it as an “early-event” warning surrogate for real-time monitoring of microbial contamination. Savoy (2007) underlined TOC propensity to behave as a solute in karst aquifers. Indeed, TOC signal at the system outlet, is not always synchronous with a bacterial peak and often trails behind (Auckenthaler *et al.*, 2002). In the simplest and most optimistic case, a combined increase of turbidity and TOC indicates the arrival microbial contamination. However, even a very low increase of both parameters, even below the water quality standards, may coincide with high allochthonous bacteria levels (Pronk, 2009). As a result the use of both these parameters as surrogate for water microbial contamination may appear problematical.

1.2.7.3 Electrical conductivity

The in situ measurement of the electrical conductivity (eC) is a common approach to characterize the total content of dissolved compounds in water. A strong correlation can usually be observed between the electrical conductivity and the total amount of dissolved compounds. Indeed, most dissolved particles are usually electrically charged. Water mineralisation directly depends on the different lithologies crossed along the flow path and on the transit time. Calcium and bicarbonate strongly influence measured electrical conductivity values (OFEV, 2009). In karst systems, their content variations, so water electrical conductivity, enhance different water contributions, whether it is during high flow or low flow conditions (Fournier *et al.*, 2006). Dilution by storm events water, low mineralized water from some type of brown soil and temperature can noticeably influence electrical conductivity values. Indeed, a negative shift in conductivity values can be used as a surrogate for freshly infiltrated water (Massei *et al.*, 2003).
The relationship linking mineral concentration and electrical conductivity varies depending on the type of ions present in the solution (Fig. 1). The electrical conductivity per amount of compound depends on how concentrated the solution is. For Ca-HCO3 waters, the conductivity of a solution containing 1meq/L Ca^{2+} and 1meq/L HCO_3^- is about 100 µS/cm. Thus 80 mg/L of dissolved compounds per 100 µS/cm of electrical conductivity can be expected at 25 °C. The electrical conductivity strongly depends on the temperature, as an increase of 2% is observed per °C. The precise relationship between temperature and conductivity depends on the considered temperature range and the water composition. Usually, the electrical conductivity is reported for a temperature of 25°C or 20 °C. If measured at a different temperature, it has to be transformed to a referenced one. It can be converted as follows:

$$EC_R = \frac{EC}{1+\frac{\alpha_R}{100}\cdot(T-T_R)}$$

EC_R → Electrical conductivity at reference temperature TR (e.g. 25°C)
EC → Electrical conductivity at temperature T
α_R → Correction factor: Percent variation of EC per °C depending on the reference temperature of the sample (Table 1)

Temperature °C	α_{20}	EC/EC_{20}	α_{25}	EC/EC_{25}
0	2.09	0.582	1.91	0.522
5	2.14	0.679	1.96	0.608
10	2.19	0.781	2.00	0.700
15	2.24	0.888	2.04	0.796
20	2.28	1.000	2.08	0.896
25	2.32	1.116	2.10	1.000
30	2.35	1.235	2.14	1.107
35	2.38	1.357	2.17	1.217

Table 1: Corrections factors depending on the reference temperature (modified after Rommel 1980).

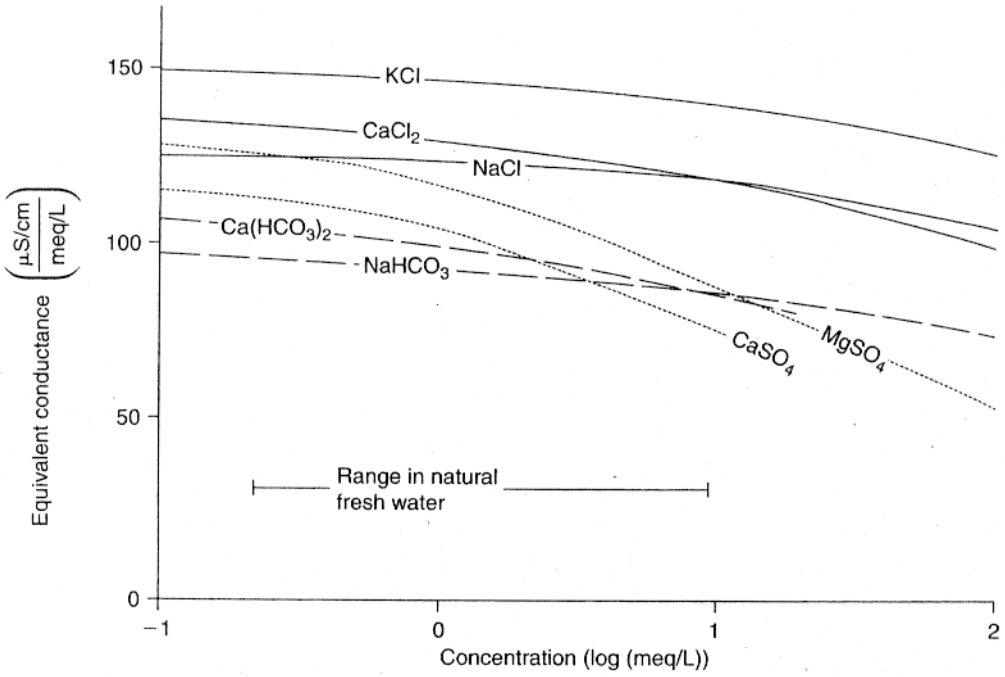

Fig. 1: Electrical conductivity as a function of the concentration of different ions in separate solution (modified after Rommel 1980).

1.3 Dissolved gases

When a gas phase is in contact with water, some of the gaseous molecules dissolve. The partial pressure of the gas in the gas phase and the equilibrium concentration of compound in the aqueous phase are related by the following equation known as the Henry's law:

$$K_h = \frac{C_{w,i}}{p_i}$$

where p_i is the partial pressure of compound i in the gas phase (e.g. atm), $C_{w,i}$ the concentration of the compound in the aqueous phase (mol/L) and K_h the Henry coefficient (mol/(L*atm)). In some studies, the Henry coefficient is defined as a dimensionless constant:

$$K_{gw} = \frac{C_{g,i}}{C_{w,i}}$$

where Cg,i and Cw,i are respectively the concentration of compounds in the gas and aqueous phase in any units as long as they are the same in both phases (e.g. mg/L, mol/L). Kh and Kgw are related by the following equation derived using the ideal gas law:

$$K_{gw} = \frac{C_{g,i}}{C_{w,i}} = \frac{p_i / R \cdot T}{C_{w,i}} = \frac{1}{R \cdot T \cdot K_h}$$

where R is the gas constant (0.08206 L atm mol^{-1} K^{-1}) and T is the absolute temperature.

Flow path and transit time of water in a hydrogeological system is of great importance in order to assess the vulnerability of an aquifer. Through time the use of tracers has been developed. Artificial tracers, characterized by a conservative behaviour, are widely used (Kaess, 1998). The clearly defined input function of the tracer and its very accurate detection are some of its biggest advantages. However, without mentioning how time consuming it is to set a tracing experiment, artificial tracers can only be applied over a very localized area and their persistence in the environment makes it quite difficult to repeat

the experiment during different hydrogeological conditions. To bypass these limitations natural tracers can be used. Indeed, they are naturally present and produced over the whole catchment. Environmental isotopes such as ^{18}O, ^{2}H and ^{3}H can give significant insight into the contribution of water from various origin, such as freshly infiltrated, low permeability volume or unsaturated zone stored water (Katz *et al.*, 1998; Lee and Krothe, 2001; Maloszewski *et al.*, 2002). The main drawback of these environmental tracers is the lack of continuous measurement methods and the complexity of defining an input function.

Turbidity, total organic carbon and electrical conductivity are also used as natural tracers, especially in karst systems, as they allow to define karst system dynamic (Amraoui *et al.*, 2003; Batiot *et al.*, 2003; Massei *et al.* 2003) and to assess the potential risk of microbial allochthonous contamination in combination with particle size distribution (Pronk, 2009).

An elegant way to combine the abundance of natural tracers and the artificial tracers ease of detection and continuous measurement possibility is the use of dissolved gases, such as radon, carbon dioxide and total dissolved gas pressure.

1.3.1 Radon

Radon (^{222}Rn) is a radioactive noble gas produced through decay of radium (^{226}Ra). It is part of the uranium (^{238}U) decay chain. Three different isotopes are found in nature: ^{219}Rn, ^{220}Rn and ^{222}Rn. ^{222}Rn, characterized by a half-life of 3.82 days is the most abundant. The two other isotopes are very short-lived, 55.6 s for ^{220}Rn and 3.96 s for ^{219}Rn, and are not expected to be transported far before decay. In this study ^{222}Rn will always be referred to as radon and ^{226}Ra as radium. Radon concentrations are measured in Bq/L. One Bq is defined as the activity of a quantity of radioactive material in which one nucleus decays per second.

1.3.1.1 Radon emanation

Radon is produced within the grains in rocks and soil. The propensity of radon to escape from the soil grain is known as radon emanation (Grolander, 2009). Emanation is a combination between diffusion, allowing radon to reach pore space within soil grains, making it available for transport through dissolution in percolating water; and alpha particle recoil, which produces simultaneously an alpha particle and a radon atom. This

recoil theory (Semkow, 1990), states that radon atoms produced during radium decay possess a recoil energy, which will allow them to be transported some 40 nm (considering ^{222}Rn) through the rock or the soil grain, permitting them to reach pore space or another grain. This implies that if radium atoms are situated near or on the surface of the grain, radon emanation is more efficient. The fraction of radon available for transportation is known as the radon emanation coefficient ε. It represents the percentage of produced radon atoms that reaches pore space (Fig. 2).

Several studies focused on radon emanation and transport in soil (Hubbard *et al.*, 1992; Hubbard and Hagberg, 1996, Washington and Rose, 1990; Holkko and Liukkonen, 1993; Washington and Rose, 1992). According to these authors, the concentration of radon within the soil evolves with time, under the influences of atmospheric pressure changes, pressure and temperature gradients, wind and moisture content. Grain composition (Morawska and Philips, 1993), grain size (Markkanen and Arvela, 1992), soil porosity, permeability and compaction (Holkko and Liukkonen, 1993), radium distribution (Greeman et Rose, 1996; Hogue *et al.*, 1997) also affect radon emanation and transport rate. Indeed, the bigger the specific surface area is (small particle size), the more enhanced the emanation will be, as a larger proportion of the radium atoms will be closer to the particles surface. Morawska and Philips (1993), calculated that for a spherical sand grain (r=0.5 mm) without any inner porosity, the radon emanation coefficient is 8000 times higher with a surface radium distribution than with a homogeneous one within the grain. The soil moisture content may also increase the emanation by slowing down radon atoms in the

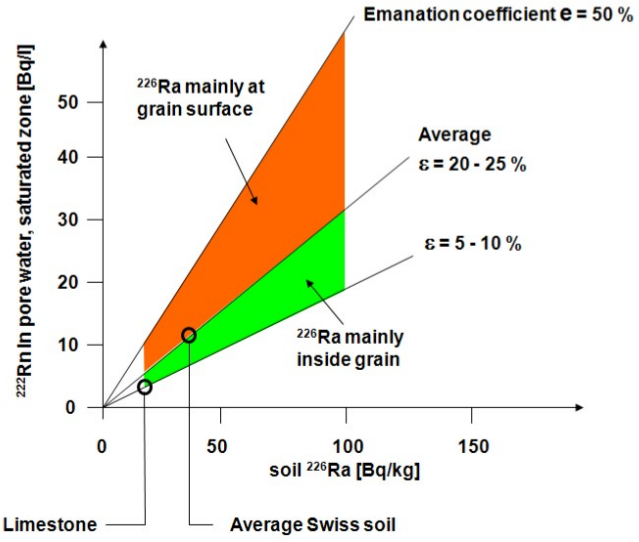

Fig. 2: Radon emanation coefficient and expected concentrations (Surbeck, 2005)

pore space. The porosity affects it as well, as larger pores diminish the number of radon atoms to enter adjacent grains.

1.3.1.2 Radon in soil

Radon production in soil is far more important than in a heavily fractured limestone, where radium is present in the bulk and not on the surface, and atmospheric radon concentrations are several orders of magnitude below soil gas radon levels (Surbeck, 2005). Well developed soils, where adsorption processes and dissolution phenomenons permit secondary radium accumulation on the surface of soil grains, lead to high radon concentrations. Indeed, several studies underlined the tendency of radium to be adsorbed on iron- and manganese-oxyhydroxides (Ames *et al.*, 1983; Scott and Wiegand, 2003). Moreover, Schwertman (1985) pointed out that these oxides reflect soil pedogenenis and weathering degree. The action of vegetation plays a significant role as well. Radium is cycled by vegetation, as it is retained in the soil and bound in humidified organic matter (Greeman *et al.*, 1990). This means that plants favour high radon concentration in soil gas by maintaining radium concentration in a readily emanating form.
Radon concentrations in soil are also affected by degassing to the atmosphere by diffusion (Climent, 1996). A diminishing of radon levels are thus observed towards the surface, whereas they increase downwards through the soil. These observations were corroborated by Savoy (2007) who, in addition, observed the highest concentrations at the soil/epikarst interface.
Even though some radon from deep down could be involved in soil overhanging uranium rich igneous rock (Grolander, 2009), this is not really probable, especially over a karst system. Indeed, limestone is a poor radon source, as low radium concentrations were measured in Swiss Jura Mountains samples (10 Bq/Kg), with radium present in the bulk and not at the surface (Surbeck, 2005). That implies a very low production and emanation coefficient.

1.3.2 Carbon dioxide

Carbon dioxide (CO_2) is mainly produced in soil. It is accounts for more than 20% of total carbon dioxide emissions to the atmosphere (Rastogi *et al.*, 2002). According to Surbeck (2005), the mean CO_2 concentration in soil is twenty times higher than the one measured in

the atmosphere, respectively 1%Vol and 0.04%Vol. It is released from soil through soil respiration, which involves three biological processes: microbial, root and faunal respiration. These three processes principally occur at the soil surface or within the upper layers where the bulk of plant residual matter is concentrated. Soil microbial population contributes up to 99% of total CO_2 resulting of the decomposition of organic matter. About 50 % of this microbial CO_2 production happens within the plant roots system (Macfadyen, 1970). As for faunal respiration, it only contributes to less than 1% of total soil emissions.

1.3.2.1 Factors influencing CO_2 emission from soil

Temperature noticeably influences CO_2 emission. A strong correlation between mean daily litter temperature and CO_2 evolution was observed (Edward, 1975). Indeed, seasonal CO_2 flux is highest in spring and summer, as the biological activity is high and organic decomposition efficient.

Soil moisture content affects soil respiration and therefore CO_2 evolution as well. An increasing soil moisture content intensifies CO_2 release up to an optimum level, above which it diminishes (Johnson *et al.*, 1994). Besides, following a dry period, a newly remoistened soil increases microbial activity and is accompanied by release of air in the soil pores contributing to CO_2 variation. Furthermore, under dry soil conditions, soil microbial respiration is stronger during the day than at night, while day and night respiration is very similar when soil is wet, which involves a reduction of soil temperature variability under wet conditions (Grahammer *et al.*, 1991).

Atmospheric pressure change also plays a noticeable role controlling CO_2 emission from soil. On the one hand, it was observed that atmospheric pressure is inversely related to CO_2 release from soil to the atmosphere (Moore and Dalva, 1993). On the other hand, CO_2 dissolution in water is directly linked to atmospheric pressure, as high pressure allows more gas to be dissolved.

Nonetheless, these statements are not true, especially in karst systems flows outside the soil zone, where limestone dissolution by CO_2 and degassing involves a diminishing of this gas concentration in percolating water from the soil down to the system outlet. The dissolution of calcite can be expressed by the following equation:

$$CaCO_3 + CO_2 + H_2O \leftrightarrow Ca^{2+} + 2HCO_3^-$$

1.3.3 Supersaturation

TDGP (total dissolved gas pressure) represents water vapour pressure in addition to the individual dissolved gases partial pressures. As oxygen and nitrogen are the dominant components in outside air and are well soluble, they mostly contribute to the TDGP in percolating water. When TDGP in water exceeds the atmospheric pressure, supersaturation occurs. This phenomenon is also known as “excess air”. It is measured by subtracting the atmospheric pressure to the TDGP in water and is expressed as [mbar].

The formation of excess air is usually linked to the complete or partial dissolution of entrapped air bubbles in the soil under the influence of the hydrostatic pressure (Heaton and Vogel, 1981). Except for air naturally present within soil pore space, air entrapment may occur following water level fluctuations (Faybishenko, 1995).

Holocher *et al.* (2002) studied the formation of supersaturation in quasi-saturated media by analysing dissolved noble gas concentrations in laboratory column experiments. Two types of experiment were set up. The first one simulated groundwater recharge by a vertical water flow through the column, whereas the second one tried to reproduce the behaviour of groundwater level fluctuations. Several physical constraints controlling the formation of excess air were identified.
The dominant parameter is the pressure, as the hydrostatic pressure in combination with the capillary pressure force a new equilibrium condition between air in the pore space and water. Growing hydrostatic pressure leads to higher dissolution of gas in water. Moreover, the remanent hydrostatic pressure makes degassing of an initial dissolved gas excess far less efficient. Therefore, a newly hydrostatic pressure constrained by a precipitation event and water table level fluctuations are of significant importance regarding excess air formation in soil. Indeed, a head of 1 m would lead to a pressure in the air pocket 10% above atmospheric pressure.
The flow regime plays a sizeable role as well, as dominant vertical advective flow improves the complete dissolution of air trapped within pore space and thus the formation of supersaturation (Holocher *et al.*, 2002). During no-flow conditions, regarding for instance poorly drained soil, the entrapped air is generally not totally dissolved.
Other noticeable parameters are the total volume of initially entrapped air and the air bubble distribution size. The former limits the maximum amount of excess air being potentially produced, the latter influences it, as small bubbles show a propensity to be

more efficiently and completely dissolved. Both these factors are affected by soil porosity and permeability.
Supersaturation can also be generated following a temperature contrast (0.6 °C/100m) between the infiltration area and the source (Surbeck, 2005), as O_2 and N_2 solubilities diminish with temperature at a rate of 2% / °C.

1.3.4 Use of dissolved gases as natural tracers

Radon and carbon dioxide are two gases produced in soil. They are both characterized by good solubilities and can be dissolved in percolating water and transported to system outlets (Surbeck, 2005; Savoy *et al.*, 2011). Even tough originating from the same "production" area, these gases have different chemical and physical properties.
On the one hand, radon is a radioactive noble gas produced through α-decay of radium present in soil and is characterized by a half-life of 3.82 days. It can be used to assess fast transport processes only, as its concentrations pass under detection limits after 20 days. An inert gas such as radon shows a conservative behaviour and doesn't interact with its environment. Radon concentrations in water are constrained by radioactive decay and degassing to the atmosphere (Mullinger *et al.*, 2007).
On the other hand, carbon dioxide isn't an inert gas. In addition to degassing, it reacts with carbonates on its way down to the saturated zone.
Consequently, both these gases characterized by good solubility, different chemical and physical properties and naturally and abundantly produced in soil, are suitable to use as natural tracers. The temporal variations of their respective concentrations in underground rivers or in springs not only permit gaining valuable information about fast transport processes in karst systems, but also to identify the different water reservoirs contributing to the discharge at the sources. This allows to put forward the following premises (Surbeck, 2005):

(i) high radon and CO_2 concentrations are typical for water originating from the soil,

(ii) low radon and high CO_2 levels for the epikarst,

(iii) low radon and CO_2 concentrations along with high eC values are representative of the saturated zone,

(iv) whereas freshly infiltrated rainwater shows low levels of eC, radon and CO_2.

Gas supersaturation allows to gain insight into transport processes in karst systems. It emphasizes the “activation” of aquifers following a rainfall event. Indeed, during a precipitation event, the air in the soil pore space undergoes a newly applied hydrostatic pressure, allowing more gas to be dissolved. The identification of this gas enriched water signal at aquifer systems outlets or sampling points permits obtaining the transit time of water following a specific meteorological perturbation (Surbeck, 2005). Nevertheless, it is important to point out that a supersaturation signal only assesses the transit time of water infiltrated and gas enriched in the soil, as direct infiltrations of rain in fissures are characterized by high flow velocities and turbulent behaviour resulting in efficient degassing.

1.4 Study area

1.4.1 Gorges de l'Areuse

The Gorges de l'Areuse study area is situated some 20 km east of the city of Neuchâtel (Fig. 3) in the Neuchâtel administrative district (Switzerland). This valley is crossed by the Areuse river whose watercourse starts west in Saint-Sulpice village and discharges 30 km east from the source into the Neuchâtel Lake.

Fig. 3: Localisation of the Gorges de l'Areuse study area.

1.4.1.1 Climate

Average annual rainfall in the Gorges de l'Areuse area is about 1075 mm with an average yearly temperature of 10.3°C (Neuchâtel City weather station). Due to the area steep slopes, the study site is characterized by a high humidity level and low sunshine. As a result, snow cover can be persistent up to June.

1.4.1.2 Geology

The Gorges de l'Areuse valley is situated within the two first major folds of the folded Jura Mountains north of the Molasse Basin. In the area, the lithological stratification of rocks shown on the surface following the Jura Mountains folding (Miocene), started during the middle Jurassic with limestone of Callovian age and went on up to the Hauterivien age. These marls and hard rock limestone were subsequently covered by lateral and ground moraines, originating from the Rhône glacier (Riss and Würm ice age), that can be found up to 750 m. During some periods a local glacier (Creux du Van) contributed with autochthonous limestone moraines. The glacier withdrawal played an important part in local erosion; indeed, landslides, rock slides and solifluction are directly linked to rock decompression of the mountain.

1.4.2 Prédernier artificial drainage gallery

1.4.2.1 Geology and hydrogeology

The Areuse river started to erode, as soon as the Tertiary Period, a narrow and deep valley within the geological layouts of the folded Jura Mountains (Fig. 4). As a result, the Gorges de l'Areuse valley became an important discharge area for groundwater. Indeed, in the region, Argovian marls circumscribe regional Dogger and Malm aquifers. Moreover, Bathonian, Purbeckian and Hauterivian marls isolate local aquifers in the overhanging limestones. Several sources discharges either along the Areuse river level or above on the valley slopes. These sources have been used for more than a century to provide drinking water to the cities of Neuchâtel and La Chaux-de-Fonds.

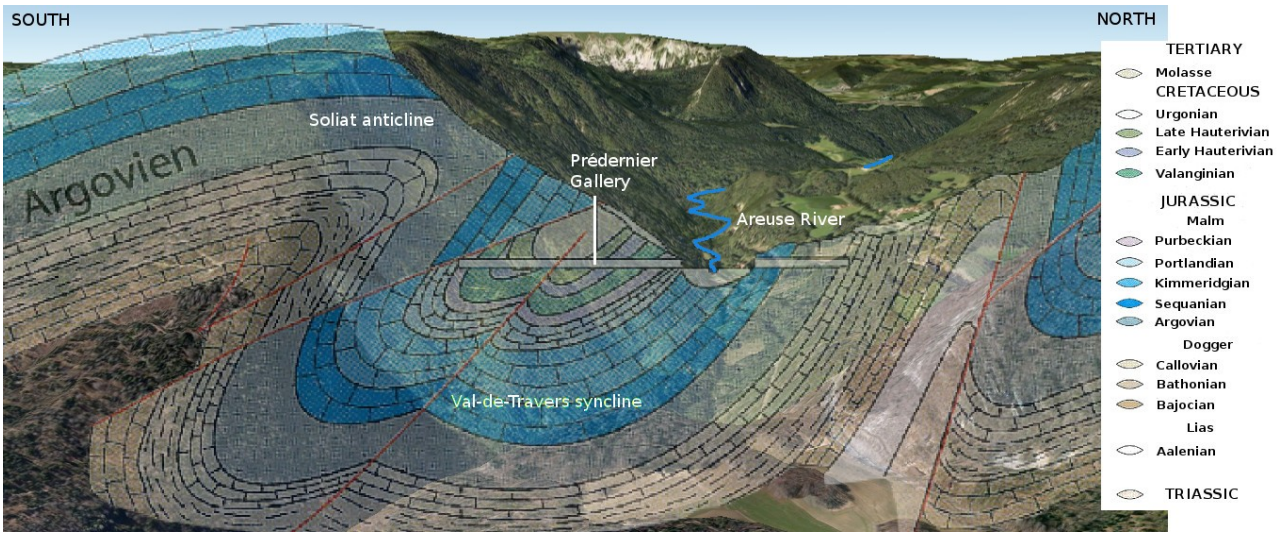

Fig. 4: Cross section of the Gorges de l'Areuse valley (modified after Meia 1986).

The Prédernier artificial drainage gallery, which brings water to the city of Neuchâtel, is located on the southern slope of the valley. The gallery was dug in 1934 at an altitude of 630 m. It begins in the Cretaceous limestones and continues through the Tertiary Molasse. Both these entities characterise the Tertiary hinge of the Val-de-Travers syncline. The gallery ends some 700 meters south in the Jurassic reverse sequence of the Soliat anticline. The main exploited aquifer, ranging from Portlandian to Sequanian limestones, is confined on the one hand by the Argovian marls and on the other hand by the Tertiary Molasse. A dam in the gallery within the Tertiary Molasse allows to “control” water production from the aquifer. During high-flow conditions, the manometric pressure can reach 110 meters. During low-flow conditions, the pressure drops down to zero. This feature can be attributed to the aquifer having a drainage base level at an altitude inferior to the 630 meters characterising the gallery (Burger, 1987). This base level could be the Combe-Garot source, discharging from Sequanian limestones, and situated some two kilometers east down the valley at an altitude of 535 m.

Just above the gallery entrance a dozen meters of unsaturated zone sits on top of it, whereas at the other end several hundred meters of unsaturated zone overhang the gallery.

1.4.2.2 Soil

Jacot (2010) highlighted different soil types over the Prédernier drainage gallery. Just above the gallery entrance and limited to low altitude Eutric Brunisoil (a kind of braun soil) can be found. It is undersaturated with respect to carbonate and poorly drained. Alpine moraines allowed that kind of soil to develop. All others soil types found higher in the area are highly linked to the underlying limestone and marls rocks. Even though a lot of different soil types can be found, they can mostly be referred to as Calco soil (humo-calcic soil). Calco soil found on marls in this particular area is usually undersaturated with respect to carbonate and poorly drained, whereas when found on limestone it is carbonate rich and well drained.

Moreover, soil average thickness above the gallery entrance, where the slop is steep, was estimated to 0.2 to 0.3 meters. Whereas, when the steepness is not so marked, farther above the gallery, the average thickness is around 1 meter (Fig. 5)

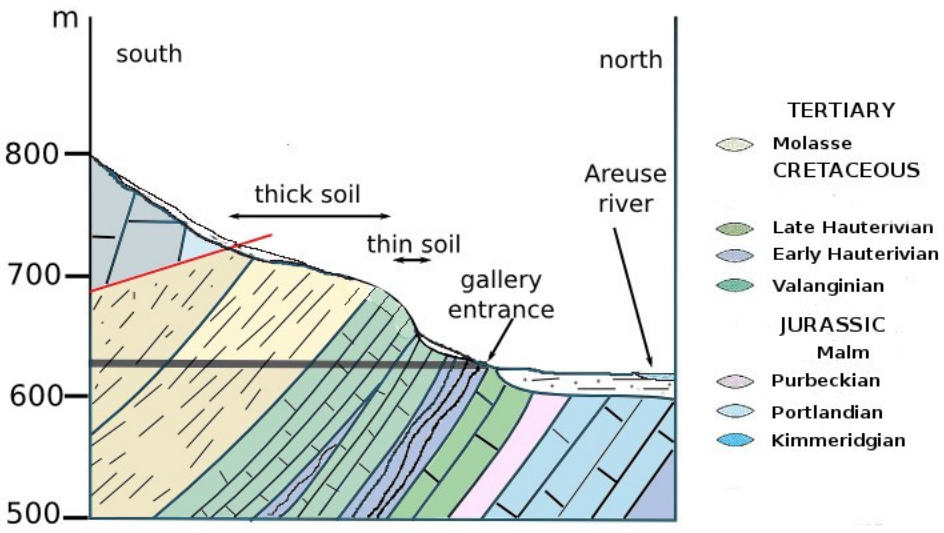

Fig. 5: Soil thickness above the drainage gallery.

1.4.2.3 The Prédernier gallery watershed

The watersheds of the Prédernier drainage gallery and its followed seepages (A1, A2 and C3) and spillways (Dev and G4) (c.f 1.5.1) were estimated (Fig. 6). As Macropores can greatly increase infiltration and are created by soil fauna and root channels (Mukhtar *et al.* 1985; Radke and Berry 1993), the commonly used distribution of run-off, evapotranspiration and infiltration (respectively 33, 33 and 33%) in Switzerland was slightly adapted. The three contributions were estimated to: 27% for run-off, 33% for evapotranspiration and 40% regarding effective infiltration (Taylor *et al.*, 2009).

The theoretical watershed area were calculated based on the average annual discharge of the gallery, the three seepages and the two spillways; and on the average annual precipitations in the Prédernier gallery area of 1075 mm (MeteoSwiss Combe-Garot meteorological station n°: 6240). The following equation was used:

$$A\ [m^2] = \frac{Q_m\ [m^3 \cdot year^{-1}]}{R\ [m \cdot year^{-1}]}$$

A: watershed surface area [m^2]
Q_m: average annual discharge [m^3/year]
R: effective recharge [m/year]

	Q_m [m^3/year]	R [m/year]	Surface area [m^2]
Dev spillway	44700	0.43	103954
A1 seepage	1183	0.43	2751
A2 seepage	539	0.43	1253
C3 seepage	1445	0.43	3360
G4 seepage	16820	0.43	39117

Table 2: Watershed estimated surface area for the Dev and G4 spillways, and for the A1, A2 andC3 seepages.

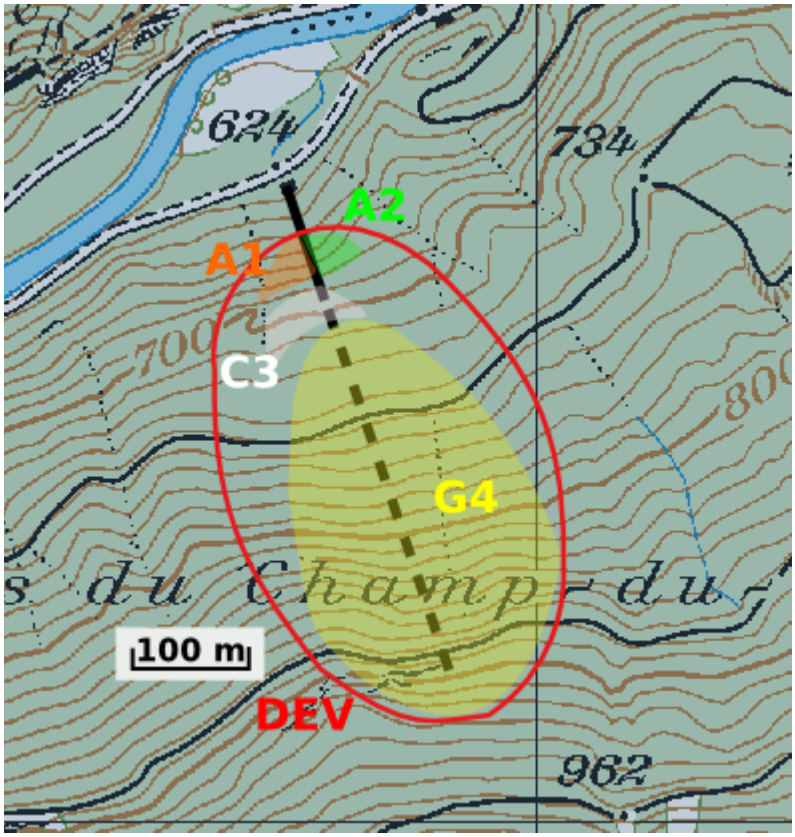

Fig. 6: Estimated watersheds for the A1, A2, and C3 seepages, and for the Dev and G4 spillways.

1.5 Measurement methods, sampling and data acquisition

1.5.1 Prédernier artificial drainage gallery

The Prédernier artificial drainage gallery is located on the southern slope of the Gorges de l'Areuse valley. The gallery was dug at an altitude of 630 m above see level through the Cretaceous and Tertiary hinge of the Val-de-Travers syncline. It ends some 700 m south in the Jurassic reverse sequence of the Soliat anticline (Fig. 7). Just above the entrance a dozen meters of unsaturated zone sits on top of it, whereas at the other end several hundred meters of unsaturated zone overhang the gallery. Even tough the gallery is 700 m

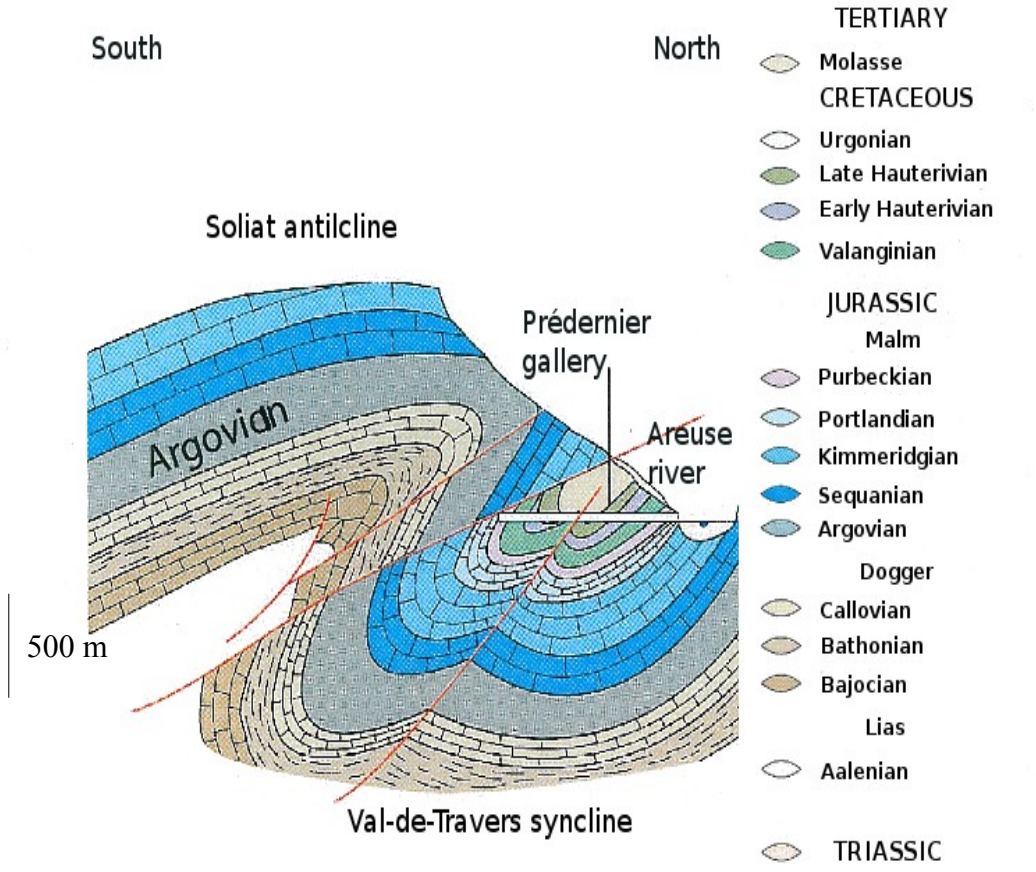

Fig. 7: Geology of the southern slope of the Gorges de l'Areuse valley and Prédernier gallery localisation (modified after Meia, 1986)

long, only 50 m are available for monitoring facilities (Fig. 8). Indeed, the first 50 m from the entrance are covered with concrete casing and so are the remaining 350 m, before reaching the exploited Malm aquifer. The latter concrete casing underwent some serious

damages through time, as many parts collapsed causing significant water infiltrations. Water originating from the Malm aquifer never reaches the monitored area. Indeed, a pipe brings it directly to distributing facilities for the city of Neuchâtel.

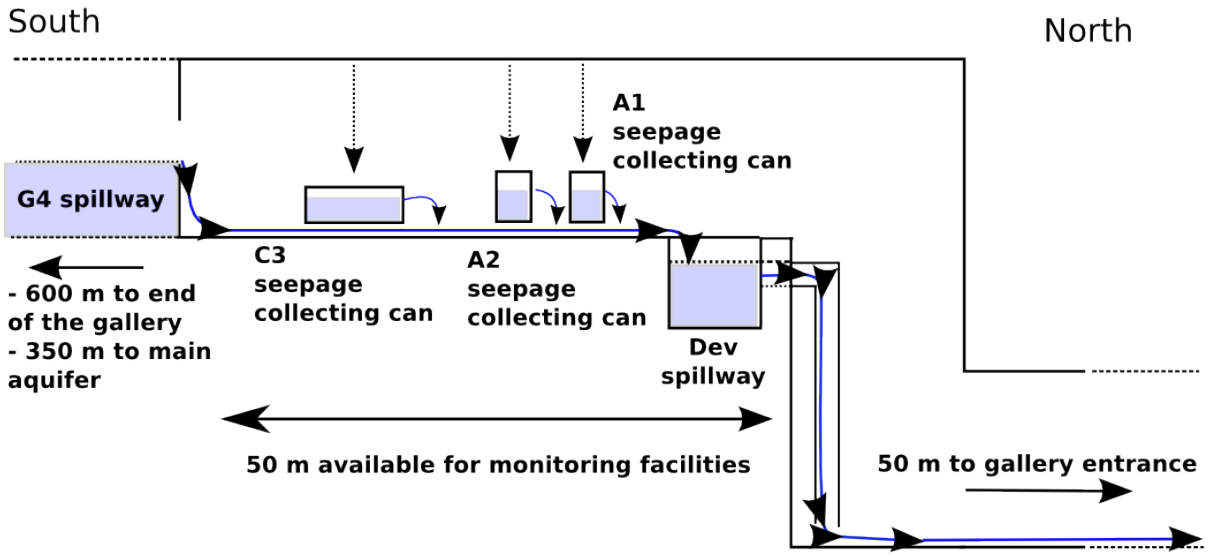

Fig. 8: Prédernier artificial drainage gallery general survey.

In order to get insight into the travel time, the storage location and the quality of water, three seepages (A1, A2 and C3) and two spillways (Dev and G4) were investigated (Fig. 8) from October 2009 to August 2012. Discharge and electrical conductivity (EC) were manually measured at the three seepages and in the two spillways. These five sampling points were also followed from April 2010 to August 2012 by means of automatic electrical conductivity survey. Continuous discharge monitoring was carried out as well, in the A1, A2 and C3 seepages. For continuous monitoring of TOC (total organic carbon) and turbidity, two field fluorometers (GGUN-FL30), were in use in the Dev spillway and in the A1 seepage from December 2009. Uninterrupted radon, CO_2 and total dissolved gas pressure monitoring in percolating water was carried out from March 2010 to August 2012 in the A1, A2, C3 seepages collecting cans and in the Dev spillway (Table 3).

	Dev spillway	A1 seepage	A2 seepage	C3 seepage	G4 spillway
Turbidity	Continuous	Continuous		Continuous	
Total organic carbon	Continuous	Continuous			
Electrical conductivity	Continuous and manual	Continuous and manual	Continuous and manual	Continuous and manual	Continuous and manual
Discharge	Manual	Continuous and manual	Continuous and manual	Continuous and manual	Manual
Radon	Continuous	Continuous	Continuous	Continuous	
CO_2	Continuous	Continuous	Continuous	Continuous	
Total dissolved gas pressure	Continuous	Continuous	Continuous	Continuous	

Table 3: Overview of the monitoring program in the Prédernier artificial drainage gallery.

1.5.2 Turbidity and total organic carbon

For continuous monitoring of total organic carbon (TOC) and turbidity, two flow-through field fluorometers GGUN-FL30, initially developed by the Group of Geomagnetism of the University of Neuchâtel for continuous monitoring of artificial dyes (Schnegg and Costa, 2003; Schnegg, 2003), were used in the Dev spillway and in the A1 seepage from December 2009.

Organic matter fluorescence occurs following the excitation of a loosely held electron in a molecule to a higher energy level by the absorption of energy, e.g. a photon. Fluorescence occurs as the electron returns to its ground state energy level. Each molecule is characterized by a wavelength at which absorption (excitation) and emission take place (Wicklow, 1999).

Four excitation and detection units are integrated in the field fluorometer allowing the successive measurements of three fluorescent dyes and an independent turbidity signal. Each unit is composed of an excitation LED (light emitting diode) mounted on one axis, and of a photodetector on another axis at 90° which measures the intensity of the emitted tracer fluorescence. The fluorescence measured by the photodetector is filtered by an optical filter. The emission-absorption spectra of the followed dye defines the implemented features of each excitation – detection unit (Fig. 9).

The turbidity signal is obtained by measuring the scattered light from the excitation LED set at 660 nm. The turbidity sensors were calibrated with formazine standards (ISO 7027)

of respectively 0, 1, 10 and 100 NTU (Nephelometric Turbidity Unit). The accuracy of turbidity measurements is on the order of 10%.

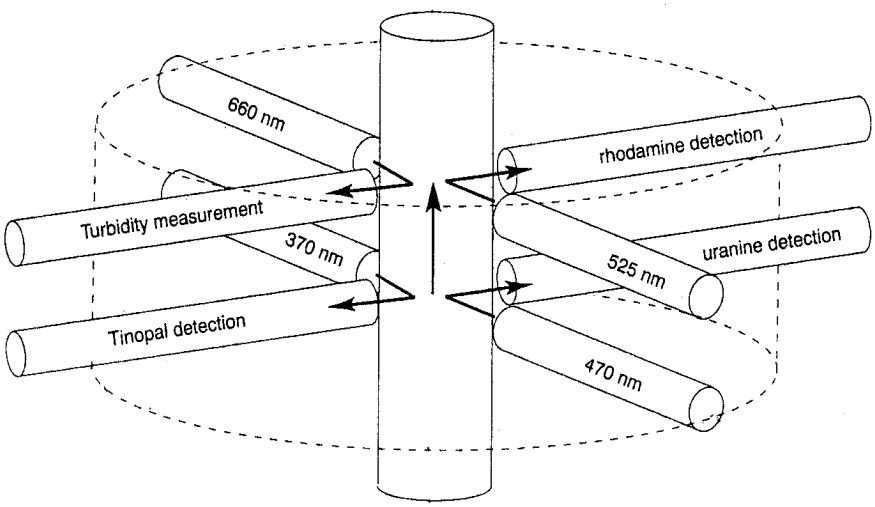

Fig. 9: Excitation and detection units integrated in the GGUN-FL30 field fluorometer (Schnegg, 2003)

Organic matter intrinsic fluorescence has been used extensively in the last 50 years in the water sciences. It allowed the study of the composition, dynamics and distribution of organic matter from different sources in various aquatic environments (Batiot, 2002; Hudson *et al.*, 2007; MacCraith *et al.*, 1993; Savoy, 2007). Total organic carbon emission wavelength ranges from 350 to 500 nm, whereas excitation varies from 250 to 425 nm. The maximum intensity measured for excitation and emission ranges respectively from 320 to 350 nm and from 420 to 450 nm. The tinopal detection system integrated in the field fluorometer, is characterized by an excitation diode set at about 370 nm and emission is detected between 420 and 550 nm. These wavelengths are close to the optimum signals intensity produced by organic matter, enabling the use of the tinopal detection unit as a surrogate for total organic carbon monitoring.

Water samples from the Dev spillway and from the A1 seepage in the Prédernier artificial drainage gallery were taken in various discharge conditions. These samples were analysed by 680° catalyst-aided combustion and non-dispersive infrared detection method. The TOC results of the batch samples were used in order to calibrate the field fluorometers immersed in the Dev and A1 sampling points (Fig. 10).

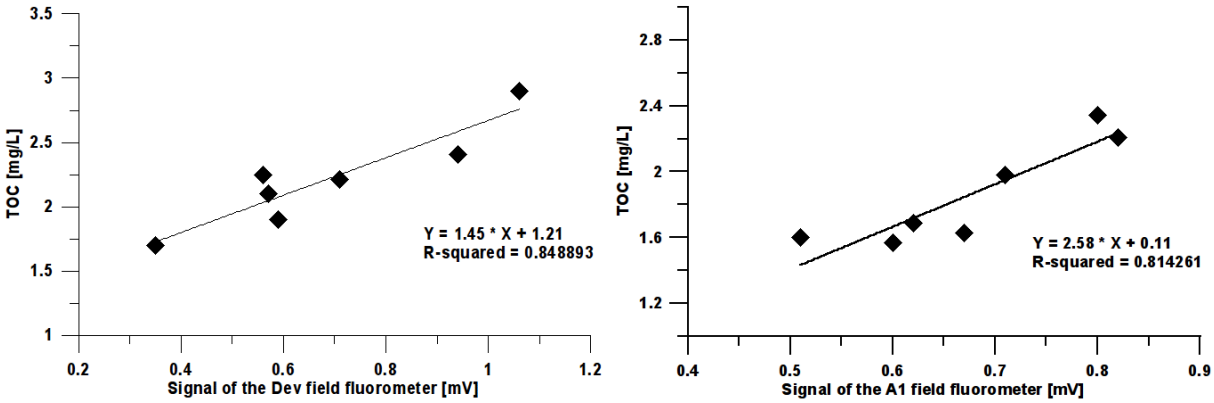

Fig. 10: Fluorometer mV signal vs TOC [mg/L] in respectively the Dev spillway and the A1 seepage.

1.5.3 Electrical conductivity and temperature

Manual measurements of temperature and electrical conductivity were carried out by a WTW 340i conductimeter (WTW, Weilheim, Germany) in the Dev and G4 spillways and in the A1, A2 and C3 seepages. According to the manufacturer, the device accuracy of the measurements is 0.1 °C for the temperature and 10 µS/cm for the electrical conductivity.
A multisampling conductimeter and data logger, specially designed by the Group of Geomagnetism of the University of Neuchâtel, allowed continuous measurements of electrical conductivity in the three seepages collecting cans and in the two spillways. The multisampling conductimeter was calibrated in order to fit the WTW 340i field conductimeter data.

1.5.4 Discharge

Continuous discharge measurements were carried out at the A1, A2 and C3 seepages. Data was gained by means of pressure probes. An STS (DL/N 64, Sirnach, Switzerland) pressure probe was used in the C3 seepage collecting can, whereas the A1 an A2 seepages were monitored with Keller (46X, Winterthur, Switzerland) pressure transducers coupled with a data logger (DT50, DataTaker, Victoria, Australia). Pressure probes data were calibrated to fit manual discharge measurements performed at the three seepage collecting containers (Fig. 53- 59, Appendix I)

Manual measurements of discharge were carried at all sampling points as well, i.e. the Dev and G4 spillways, and at the A1, A2 and C3 seepages.

1.5.5 Rainfall

The MeteoSwiss Combe-Garot meteorological station (station n°: 6240) provided daily rainfall data. It is situated about 2 km down the Gorges de l'Areuse valley at an altitude of 532 m. A field pluviometer was considered at some point, but its setting up was abandoned as the area of the Prédernier artificial drainage gallery is totally covered by well developed and thick forests.

1.5.6 Radon, carbon dioxide and total dissolved gas pressure

For uninterrupted radon monitoring in percolating water, a closed circuit of air-filled semipermeable polypropylene tubing was immersed directly into the A1, A2, C3 seepages collecting buckets and into the Dev spillway (Fig. 11). Thanks to switching valves, gas in equilibrium with water was successively pumped through a detector. A Lucas-cell coupled to a photomultiplier detector was used to measure the radon concentration in the air circuit. CO_2 determination was obtained in the same closed air circuit by IR absorption (Fig. 12). Radon and CO_2 sensors were enclosed together with the pump and electronics in a watertight box on a dry platform inside the drainage gallery (Fig. 13). As for the measurement of the total dissolved gas pressure, a thin-walled silicone tube, closed at one end and connected at the other end to a pressure sensor was placed into the three collecting buckets and in the Dev spillway. Ten minutes are needed to reach a steady state regarding the pressure inside the tube being equal to the sum of partial pressures of the dissolved gases plus water vapour pressure. Ra_don, CO_2 and TDGP were monitored hourly and measures were transmitted daily (GPRS protocol) to a data server through a Tetraedre TRMC-5 data logger/transmitter. Because of the one hour sampling interval, the obtained signals are likely to show periodic oscillation features. Soil radon concentrations and CO_2 content are affected by various seasonal and daily changes, such as precipitations, atmospheric pressure and temperature (Edsfeldt, 2001), leading to complex time series. To obtain manageable data, non relevant components needed to be removed. A Fourier transform low pass filter (FFT low pass filter) was applied on the radon and CO_2 time series. It allowed to remove high frequencies from the radon an CO_2 signal, the cut-off frequency

being 1/4hours. The same low pass filtered was applied to total dissolved gas pressure data.

It is relevant to point out that due to the radon radioactive feature and as gas in equilibrium with water was successively pumped through the same detector, each radon concentration measure in the air circuit undergoes the influence of the previous measure. Therefore, radon data set had to be deconvoluted according to the equation:

$$d_i = c_i - 0.4 \cdot c_{i-1} - 0.2 \cdot c_{i-2}$$ (H. Surbeck personal communication)

where d_i [Bq/L] is the radon concentration after deconvolution at a specific time i, c_i the untreated radon concentration at this same specific moment and c_{i-1} and c_{i-2}, the radon level one and two hours before, respectively.

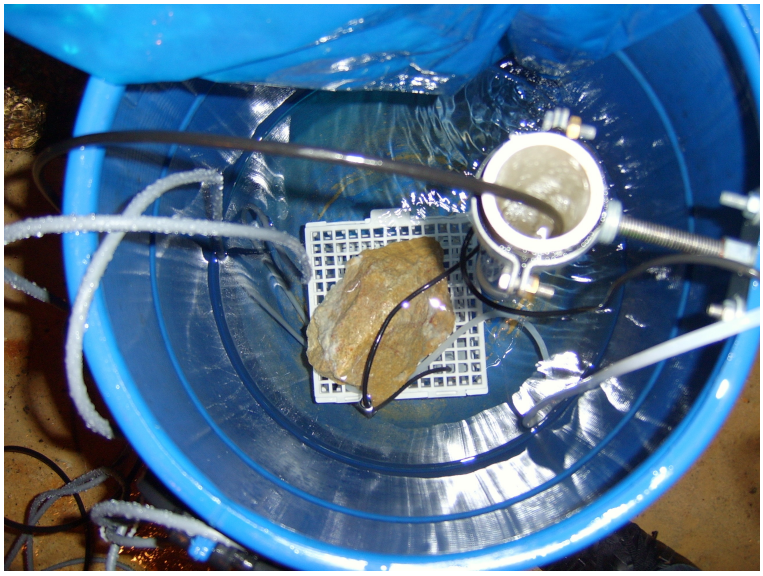

Fig. 11: Closed circuit air-filled semipermeable polypropylene tubing immersed into a collecting can.

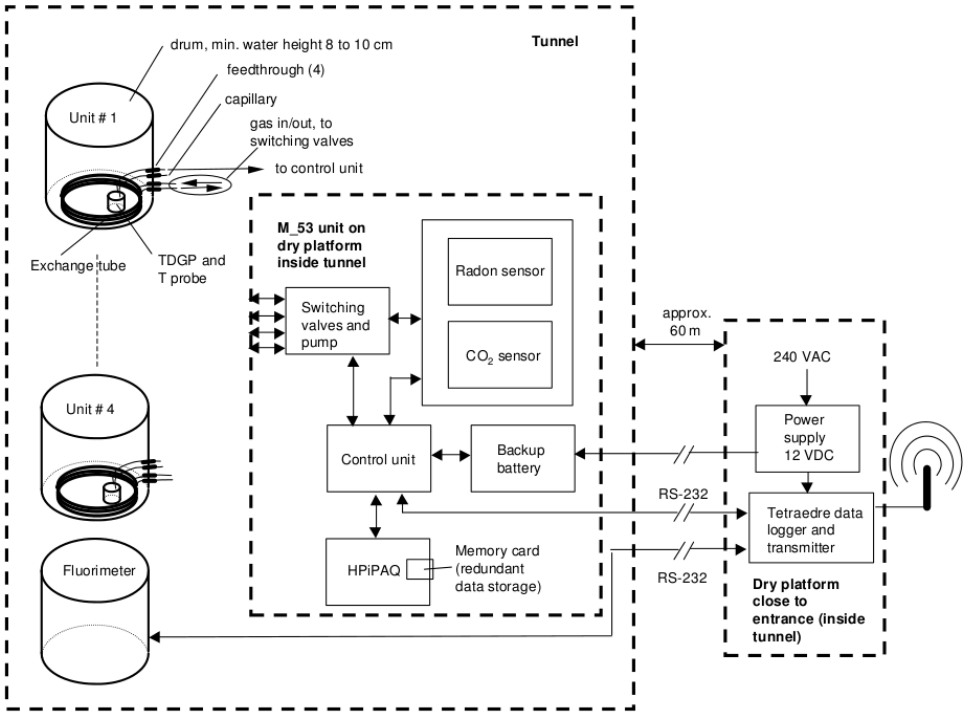

Fig. 12: Radon, CO_2 and total dissolved gas pressure monitoring facilities at the Prédernier drainage gallery (Surbeck, 2005).

Fig. 13: Radon and CO_2 sensors enclosed together with the pump and electronics in a watertight box.

1.5.7 Major ions

The analysis of major ion chemistry followed the same procedure. Water was gathered in 500 mL plastic bottles and transported to the laboratory in cooling boxes. Each water samples, except those intended to assess TOC content and stable isotopes ratio, were filtered through a 0.45 µm pore size membranes. In order to insure cation preservation, water samples were acidified to pH<2 with HNO_3. Bicarbonate contents were determined within 6 h following the sampling by titration (HCl 0.1 M to a pH of 4.3). Major ions concentrations were determined by ion chromatography (IC DX-120, Dionex, USA) within weeks following the water sampling. Measurements accuracy for ions and bicarbonate is respectively 0.5 and 10 mg/L.

Total organic samples were acidified with HCl and were analysed by 680° catalyst-aided combustion and non-dispersive infrared detection method.

In order to assess the quality of major ion analysis, the charge balance error equation was used. If the error is less than 5%, the analysis can be considered relevant (Table 4, Appendix I).

2 Results and interpretations

2.1 Watershed of the artificial drainage gallery

The manual monitoring of discharge and electrical conductivity (eC) in the Dev spillway, which collects all the seepages throughout the Prédernier drainage gallery, along with continuous monitoring of turbidity and total organic carbon (TOC), allowed, as a first step, some general conclusions to be drawn on the processes governing the hydrodynamics of the test site (Fig. 60, Appendix II). As the G4 spillway highly influences the gallery general dynamics, it was also followed by use of manual discharge, eC and partial continuous eC measurements.
It is relevant to point out two different phenomenons structuring the following description of the hydrogeological evolution of the gallery. The first one is a succession of classical high-flow and low-flow periods. The second one is the contribution (entire watershed contribution) or not (restricted watershed contribution) to the total discharge of the gallery from the G4 spillway, which collects water infiltrating in the last 350 m.

2.1.1 Low-flow conditions from August 2010 to December 2010

From August to the end of November 2010 (Fig. 14) low-flow conditions prevail in the drainage gallery. The mean discharge is about 15 [L/min], with a maximum of 30 [L/min] measured on August 19th in reaction to a precipitation event of 67 [mm] between August 14th and 16th. Until August 31st the entire gallery watershed contributes to the dynamics of the Dev spillway, as beyond this date the G4 spillway totally dried up. The G4 spillway noticeably influences the dynamics of both the total gallery discharge and electrical conductivity. It collects water infiltrating in the last 350 meters of the gallery. As this part of the gallery is covered by an unsaturated zone thickness ranging from 75 to as much as 300 meters, the G4 sampling point is less prone to nervous discharge variations. Before drying up, the total G4 discharge is stable and contributes to around 30% of the gallery flow. The G4 electrical conductivity is characterized by a higher mineralization compared with the Dev spillway, whether it is low-flow or high-flow conditions. Indeed, it could potentially present a Tertiary Molasse influenced chemical signature (e.g. Thüler (2010)

measured on November 7th 2009 a 63 mg/l SO4 and 6 mg/l Na+K content, respectively 5 mg/l and 1 mg/l in the Dev spillway, and a higher Mg/Ca ratio).

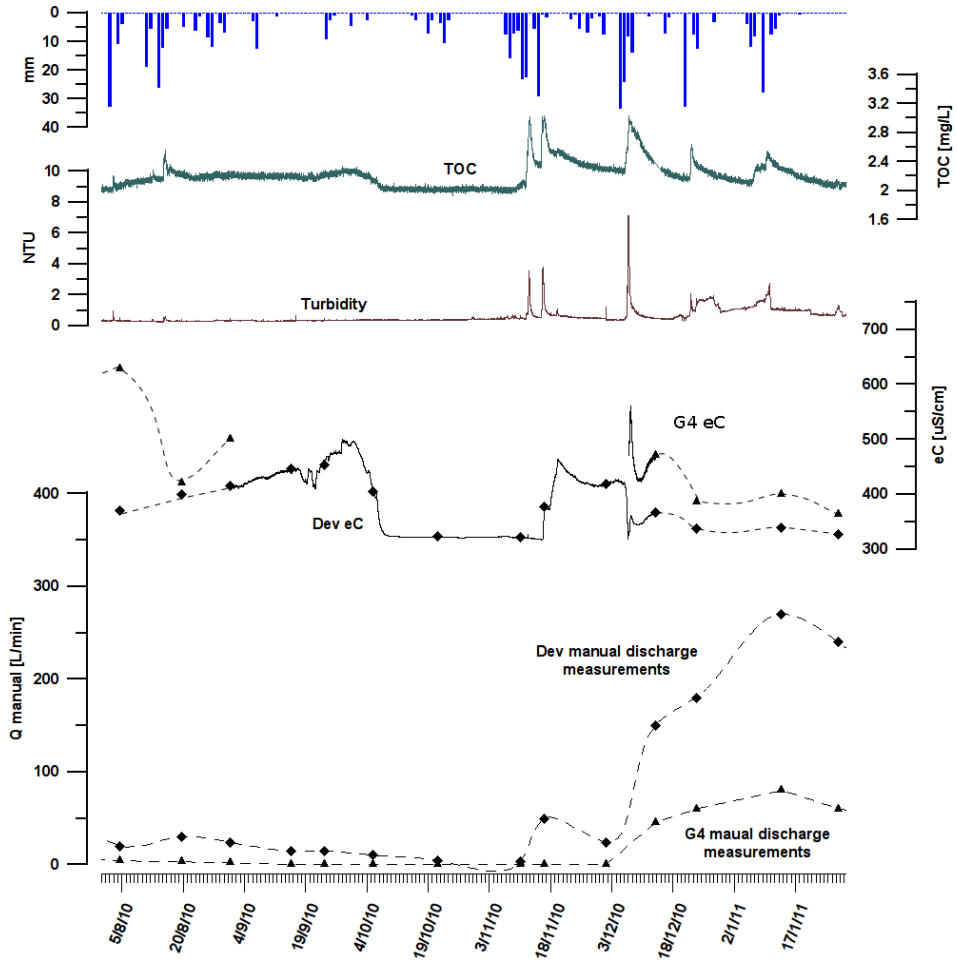

Fig. 14: Manual discharge and eC in the Dev and G4 spillway, along with turbidity and TOC in the G4 sampling point from December 2010 to January 2011.

The electrical conductivity continues to raise progressively in the Dev spillway and reaches 500 [µS/cm] at the end of September 2010. Some negative peaks of eC following precipitations between August 6th and 8th, as between August 24th and 26th of respectively 15 and 13 [mm] indicate that freshly infiltrated water bypassed soil storage, as field capacity threshold was reached. This long term eC increase can be attributed to the contribution of remaining seepages influenced by a Tertiary Molasse signature close to the G4 spillway (totally dried up). These highly mineralized seepages were active until October 10th, when a noticeable drop of electrical conductivity values was measured to remain stable until mid-November 2010 around 325 [µS/cm].

Starting from the beginning of August 2010 (Fig. 15), the first evolution of total organic carbon content are measured. A rainfall of 33[mm] on August 2nd induced the first TOC peak of 2.2 [mg/L], followed by a second and third noticeable one on August 13th and 15th of respectively 2.3 and 2.6 [mg/L] in reaction to rainfalls occurring on August 11th (19 [mm]) and between August 14th to 16th (67 [mm]). Meanwhile turbidity shows reactions to the above mentioned precipitation events.

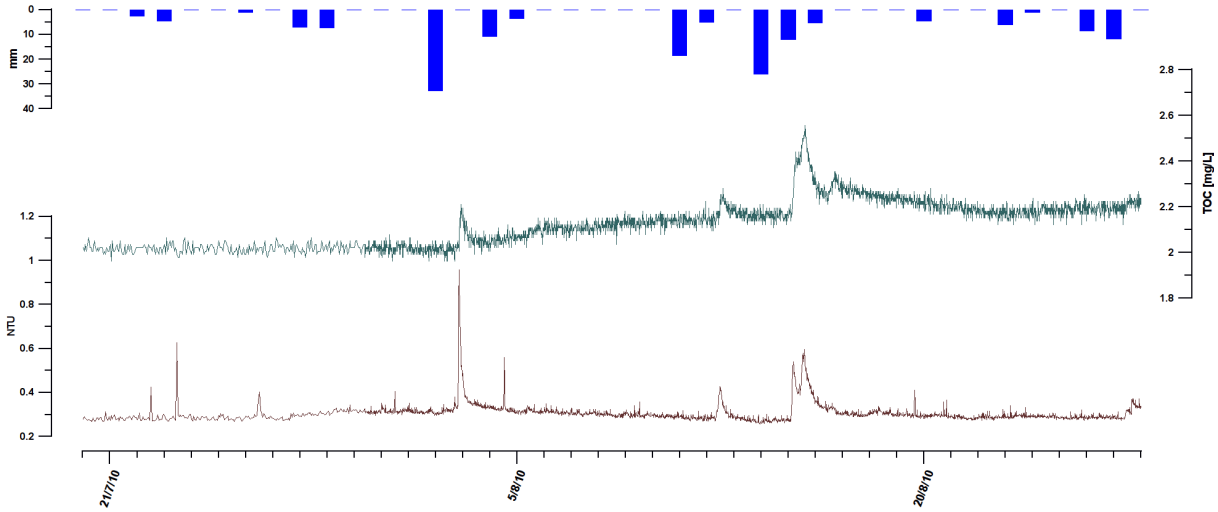

Fig. 15: TOC and turbidity in August 2010 in the Dev spillway.

On August 3rd a 0.9 [NTU] allochthonous turbidity peak is narrower, precedes and occurs during the rising limb of the TOC signal. It is accompanied by a very slight autochthonous turbidity pulse on August 2nd. The same pattern is observed on August 15th, when a more noticeable autochthonous peak precedes allochthonous turbidity. This behaviour is consistent with findings from Bradford *et al.* (2003), Keller *et al.* (2004) and Pronk (2007), which enhanced faster transport of colloids with respect to solute due to exclusion processes, i.e. particles move along the fastest flow lines, whereas solutes use the entire fluid volume.

Nevertheless, even though some turbidity and TOC pulses were observed during this low-flow condition period, their concentrations remain very low and quite stable. Moreover, between August and mid-October 2010, TOC concentrations seem to be highly influenced by the G4 spillway and its adjacent highly mineralized seepages. Indeed, during this period, TOC levels are above the base concentration of 2 [mg/L] which is reached as soon as the G4 related seepages stop to contribute to gallery discharge.

From September to November 2010 total cumulated precipitations only reached 40 [mm]. Thus, a consequent rainfall event of 82 [mm] between November 7th and 12th was needed to reactivate the system (Fig. 16) and to allow soil water content to exceed field capacity.

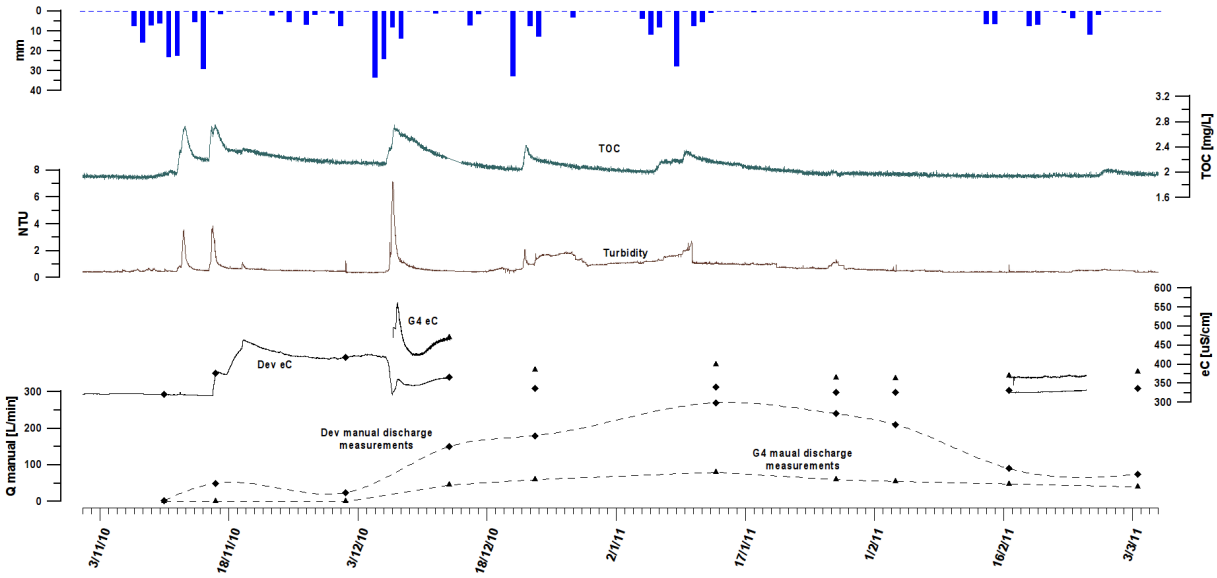

Fig. 16: Discharge, eC, turbidity and TOC in the Dev spillway from November 2010 to March 2011.

A first allochthonous turbidity peak of 3.8 [NTU] preceded by a small autochthonous turbidity pulse occurs on November 13th. It accompanies the rising limb of the TOC signal which reaches 2.8 [mg/L]. This suspended matter variation is the contribution of the restricted gallery watershed only, as the G4 spillway and its related seepages are not active yet. Following another rainfall event of 36 [mm] taking place on November 14th and 15th, a second coupled Turbidty-TOC peak takes place. It coincides with the reactivation of the G4 related seepages, as can be seen by the sudden eC increase in the Dev spillway.

2.1.2 High-flow conditions from December 2010 to April 2011

A noticeable rainfall event of 80 [mm] between December 5th to 8th marks the transition to high-flow conditions and the contribution of the entire watershed as the G4 spillway is active again. It is characterized by an allochthonous turbidity peak reaching 7 [NTU], preceded by a slight autochthonous pulse and an associated TOC pulse of 2.8 [mg/L] which trails behind and a well marked eC drop, pointing out to a considerable freshly infiltrated water contribution (Fig. 17). The precipitation event of the beginning of December

influences the G4 spillway as well. Following the spillway renewed contribution to the total discharge in the gallery, the eC measured in the G4 sampling point rises to 550 [µS/cm],

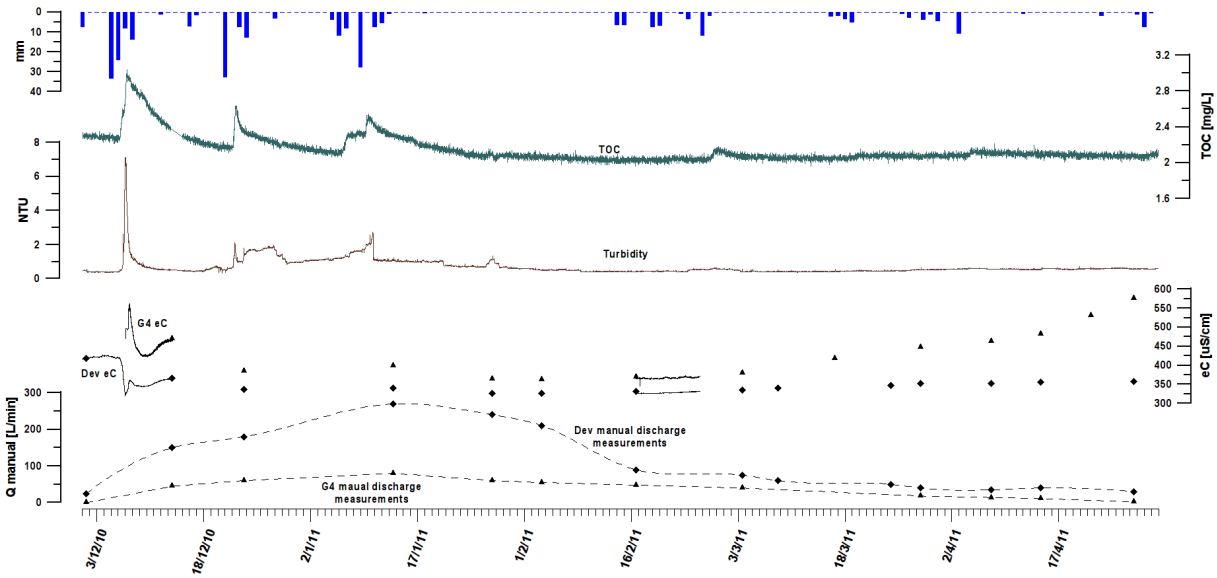

Fig. 17: Discharge, eC, turbidity and TOC in the Dev spillway from December 2010 to April 2011.

reflecting the arrival of mineralized water stagnating behind the structure. Then it drops to 425 [µS/cm] in relation to the above mentioned rainfalls. The lag between the minimum eC values in the Dev and G4 spillway of two days, respectively December 7th and 9th, can be explained on the one hand by the thickness of unsaturated zone covering the gallery above the G4 area, ranging from 75 to 300 meters, and on the other hand by the time needed to replenish the 500 [m^3] behind the spillway allowing it to flow again.

Discharge increases progressively to reach 250 [L/min] on January 14th, following rainfalls happening at the end of December 2010 and at the beginning of January 2011. Then it gradually diminishes to 30 [L/min] at the end of April 2011. The G4 spillway contributes to around 30% of the total discharge.

Two noticeable turbidity and TOC peaks are observed on December 22nd and on January 9th, as a reaction to rainfalls of 33 [mm] on December 21st and of cumulated 50 [mm] occurring between January 5th and 9th 2011. Starting from February 2011, discharge remains stable at about 40 [L/min] and eC increases to reach 350 [µS/cm] in the Dev and 580[µS/cm] in the G4 spillway on April 27th, enhancing the role of the latter on the gallery dynamics.

Between January 14th and April 29th 2011 only 80 [mm] of cumulated precipitations were recorded leading to extreme low-flow conditions.

2.1.3 Low-flow conditions from May to December 2011

The low-flow conditions from May to December 2011 can be characterized as extreme (Fig. 18). Indeed, total gallery discharge was under 10[L/min] to even reach 3[L/min] on July 7th. Meanwhile, electrical conductivity continual increase in both the Dev and G4 spillway, reflects seepage-flows from the low permeability volume, with longer transit times, which characterize the base-flow regime.

The G4 spillway contribution stopped on April 27th, and the last G4 related seepages flowed until May 22nd when a noticeable drop in eC values is measured in the Dev Spillway.

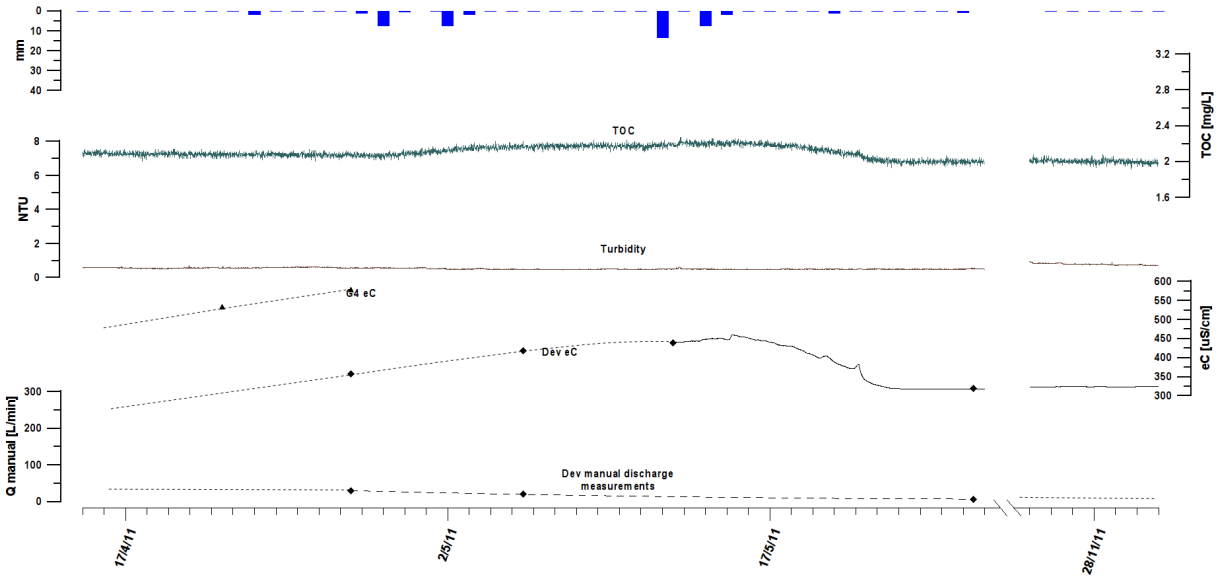

Fig. 18: Low-flow conditions in the Dev spillway from April to November 2011.

2.1.4 High-flow conditions from December 2011 to April 2012

The transition to high-flow condition in December 2011 is characterized by a succession of significant precipitation events (Fig. 19). The first one of 100 [mm] occurs between December 2nd and 7th, the second one of 132 [mm] from December 10th to 23rd, with a maximum 29 [mm] measured on December 16th and the third one of 146 [mm] spreads out

from December 28th 2011 to January 8th 2012. In reaction to the above mentioned first rainfall event, four TOC peaks are reached on respectively December 3rd, 4th, 6th and 8th with 2.1, 2.5, 3 and 3.2 [mg/L]. They are accompanied by turbidity pulses of 0.6, 0.9, 1.9 and 6.2 [NTU] occurring during the rising limb of TOC content. The two last turbidity signals allow to discriminate between autochthonous turbidity, resulting from the remobilisation of intrakarstic material and allochthonous turbidity originating from the soil.

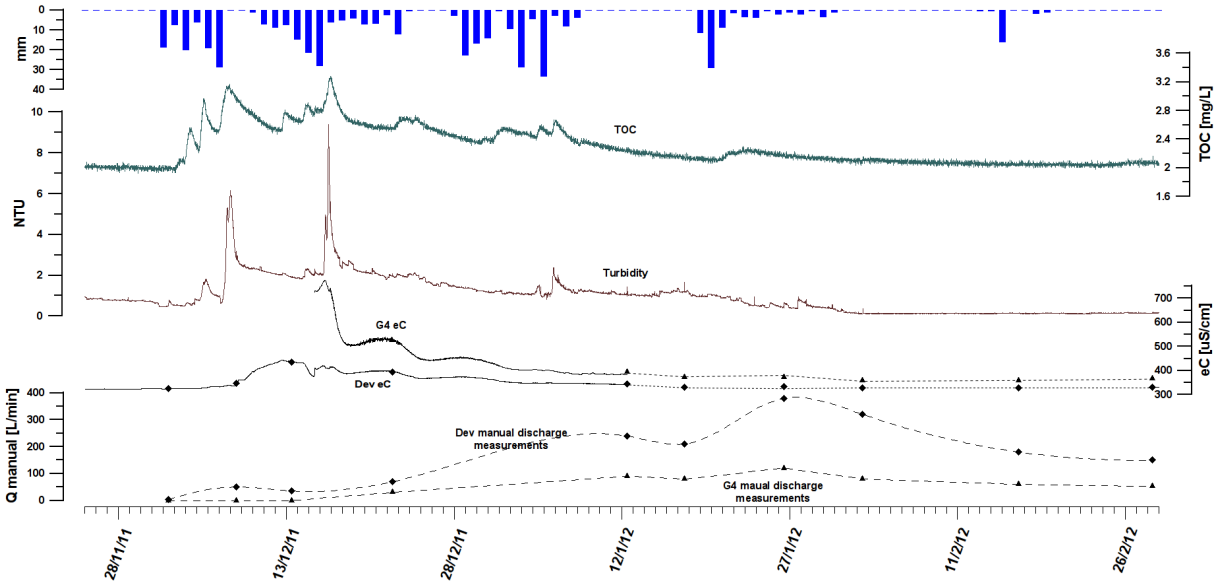

Fig. 19: Discharge, eC, turbidity and TOC in the Dev spillway from December 2011 to February 2012.

Such a succession of combined turbidity and TOC pulses can be observed following the second and third precipitation events, even if it is not as sharply defined, except for the one happening on December 17th, in reaction to a maximum rainfall of 29 [mm] on December 16th. As mentioned for the previous major pulse, autochthonous and allochthonous turbidity can be identified, the latter reaching 9.5 [NTU].

Discharge progressively increases to reach 240 [L/min] on January 12th, and even 380 [L/min] on January 26th. Meanwhile G4 spillway discharge follows the same evolution, but as previously said, not showing a nervous reaction. It contributes to about 30% of total discharge in the gallery.

Electrical conductivity starts to rise on December 9th, as the G4 related seepages contribute to gallery discharge. As for the G4 spillway, reactivated on December 16th, it undergoes the same phenomenon which happened during the previous transition to high-flow condition, i.e. the eC reaches 760 [µS/cm], enhancing the arrival of mineralized water stagnating behind the spillway structure, then dropping to 500 [µS/cm] in reaction to the

second rainfall event of 132 [mm]. From January 2012, snow covers the watershed of the drainage gallery, noticeably attenuating TOC or turbidity responses, which reach base level concentrations by the end of February.

2.1.5 Low-flow conditions from May 2012 to September 2012

On the contrary to low flow conditions, from May to December 2011, which could be described as extremely dry, the period betwwen May and September 2012 is characterized by a high discharge (Fig. 20). As recharge of the system was effective during the last high-flow period, it is less affected by the resumption of biological activities and plant growth, as it remains stable around 80 [L/min] until mid-July, when it progressively diminishes to reach 35 [L/min] on September 11th. Base-flow characterizing eC is slightly increasing to reach 360 [µS/cm] at mid-September under the influence of a predominant seepage-flow, the rising mineralization and contribution of water originating from the G4 spillway which never dries out.

As rainfall is homogeneously distributed throughout this period, soil water content is more than field capacity, allowing noticeable influences from the soil to be observed. Indeed, turbidity peaks, preceding linked TOC pulses were monitored on several occasions, e.g. on May 23rd, June 9th and 22nd, July 6th and even on August 30th.

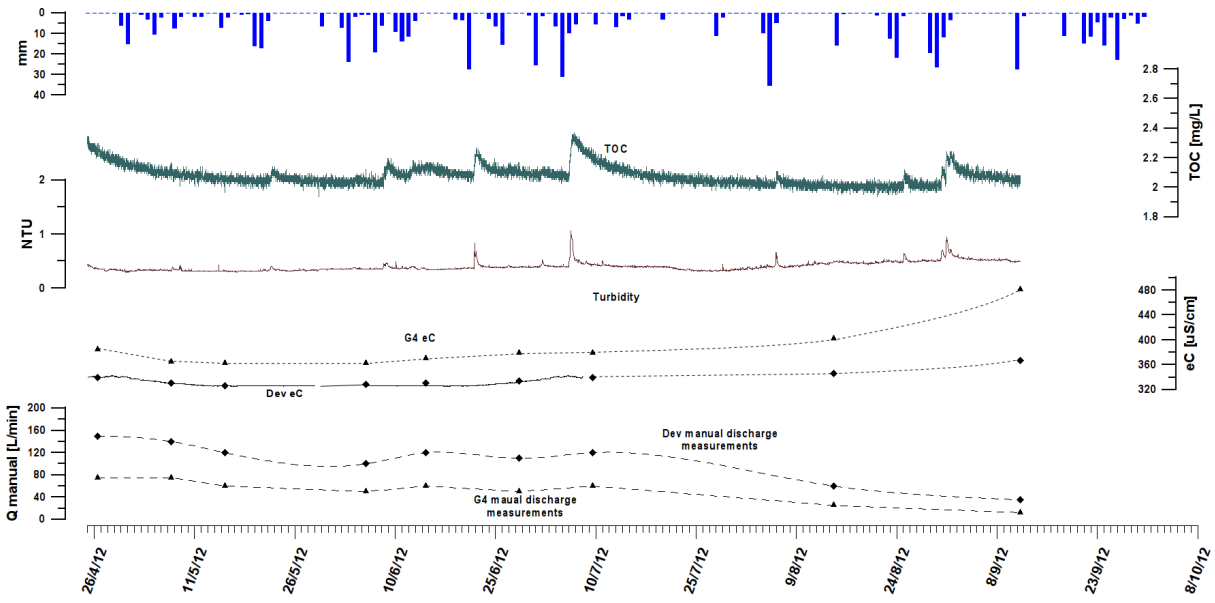

Fig. 20: Discharge, eC, turbidity and TOC in the Dev spillway during low-flow conditions from May to September 2012.

2.1.6 General characteristics of the Prédernier artificial drainage gallery

Chemical and physical data recovered from the 2 year monitoring period allowed to infer some preliminary statements regarding the processes governing the hydrodynamics of the Prédernier drainage gallery, mainly focusing on the relations between the Dev and the G4 spillways. Indeed, the Dev spillway collects water originating from all the seepages distributed throughout the gallery, including G4 related water during high-flow conditions. As such, it reflects an average of all their miscellaneous contributions to the total gallery flow. A typical hydrological year would be described as follows.

During low-flow conditions the Dev spillway reveals the contributions of seepages spread out throughout the 50 meters available for monitoring facilities, i.e. between the Dev and the G4 spillway, referred to as restricted gallery watershed. It is characterized by a steady discharge averaging around 15 [L/min] and showing no reaction to any rainfall or precipitation event. Indeed, during a major part of this period, from circa April to September, biological activities and plant growth highly intercept rainfalls. Moreover, as release of water to the system depends on the degree of saturation of the soil, i.e. if the soil water content is more or less than field capacity, total organic matter concentrations and turbidity content remain very low and stable at respectively around 2 [mg/L] and 0.5 [NTU]. Though some variations can be observed following remarkable storm events, the concentrations remain very low. Meanwhile, electrical conductivity is characterized by progressively increasing values. The combined absence of discharge, TOC or turbidity variations, points out to a base-flow, being defined by a predominant seepage-flow component from the low permeability volume.

The transition to high-flow conditions is highlighted by the resumption of discharge from the G4 related seepages. It is characterized by an increase of both electrical conductivity and discharge in the Dev spillway. Perrin (2003) suggested that a piston-flow phase starts at the moment of discharge increase and lasts until the arrival of freshly infiltrated water. He states that water discharging during this phase, showing no change in eC, originates from the epikarst, released by a pressure pulsed induced by increasing hydraulic head. It also implies that during steady-state low-flow conditions, the system is fed by water stored in the epikarst. Nevertheless, this conceptual model can not be applied on the Prédernier gallery dynamics. Indeed, on the one hand, even though some discharge increases were monitored during pre-high-flow periods, it is attributed to the G4 related seepages, as eC

increases as well. On the other hand, when discharge reaches a state when it can be influenced by fresh water infiltrations (eC negative pulses), it is clearly under the influence of water originating from the soil reservoir, as remarkable TOC and turbidity pulses were monitored. Therefore a piston-flow phase, as described by Perrin, can not be implied, as it was never recorded, regarding the Prédernier gallery hydrodynamics and more importantly the base-flow can not be linked to epikarst water but rather to seepage-flow from the low permeability volume.

High-flow conditions are characterized by discharge ranging from 50 to as much as 380 [L/min]. It can be described as a mixed-flow phase, where water discharging at the outlet implies soil water, rainwater and epiphreatic water, each of them accounting for a predominant influence at some point. During this period biological and plant activity is at its lowest level, allowing recharge of the system by precipitation events and snow melt. Indeed, water content in soil is more than field capacity, thus soil water can reach the outlets and storm event water can bypass the soil reservoir to contribute as well. This features are highlighted by noticeable TOC and turbidity pulses, along with negative eC peaks. This period coincides with the reactivation of the G4 spillway (entire gallery watershed), whose discharge and highly mineralized water, contribute to total gallery flow. Following a succession of remarkable rainfall events, usually happening between November and January, TOC and turbidity pulses occured. Usually, the turbidity pulse precedes to corresponding TOC signal, as it occurs during the rising limb of the TOC curve, although both turbidity and TOC originate from the soil. These observations are in agreement with findings from other studies highlighting faster transport of particles with respect to solutes in karstic conduits due to exclusion phenomenons (e.g. Göppert and Goldscheider, 2008). At the end of the soil signature, i.e. TOC and turbidity pulses, discharge reaches its maximum (Fig. 21). This highlights the predominant role of soil water regarding the recharge of the system during high-flow conditions, as discharge then drops down to reach a base level and is mainly sustained by epiphreatic flow. The resumption of biological activity and plant growth intercepts rainfalls. As a result, discharge progressively diminishes to reach low-flow conditions sustained by seepage-flow from the low permeability volume.

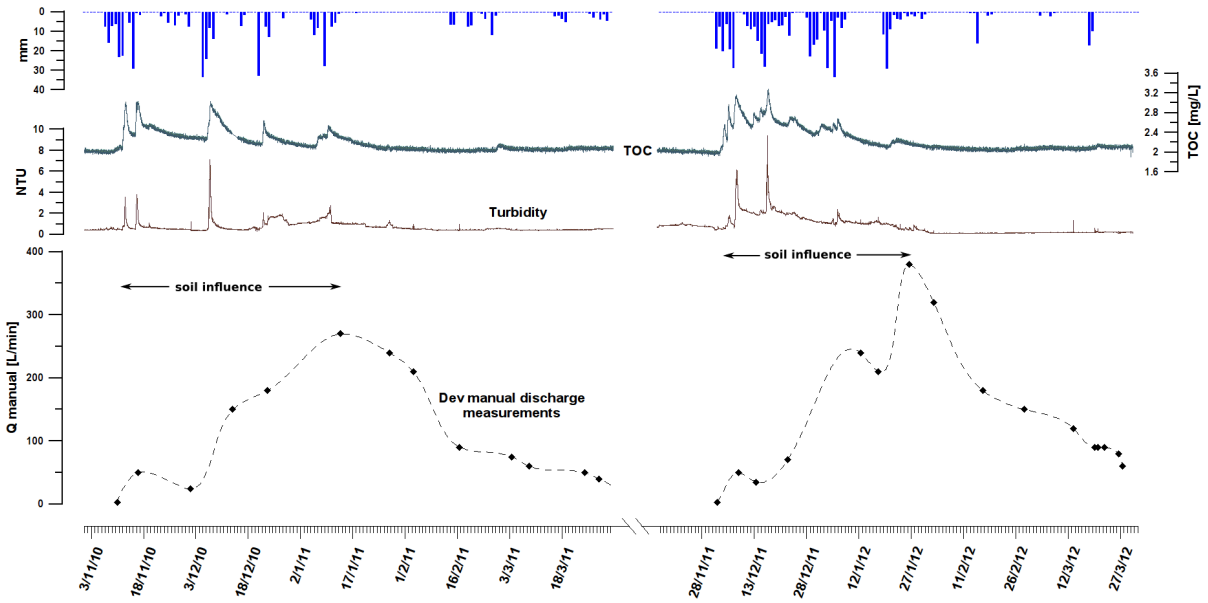

Fig. 21: Discharge apex in the Dev spillway in reaction to soil influence.

2.1.7 Chemical properties of water in the Dev spillway

Water in the Dev spillway was sampled between November 2011 to April 2012 for the analysis of major ion chemistry. It allowed to follow the chemical evolution from low to high-flow conditions. The typology of groundwater characterizing the Dev spillway, which represents the entire watershed signature, was further analysed through ternary piper plots. As expected, samples exhibited a general pattern characteristics of Ca^{2+} and CO_3+HCO_3^- waters, typical of karst aquifers. Nevertheless, water originating from the G4 spillway or G4 related seepages, especially during the transition to high-flow conditions, show a Tertiary Molasse signature (Fig. 22), with higher SO_4 and Na+Cl content. As can be seen from samples taken on December 13th and 22nd 2011 (Fig. 23), G4 related water noticeably influences the chemistry of the Dev spillway.

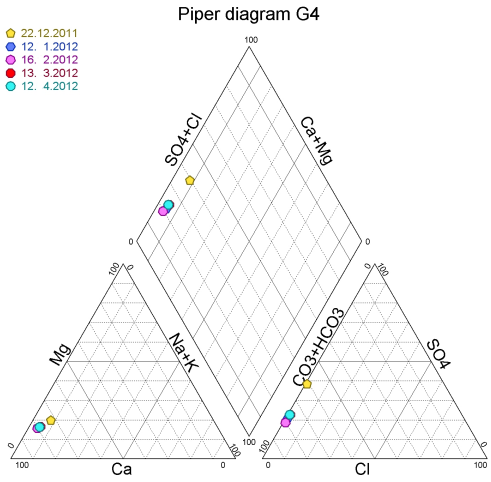

Fig. 22: Piper diagram of samples taken in the G4 spillway between November 11th 2011 and April 12th 2012.

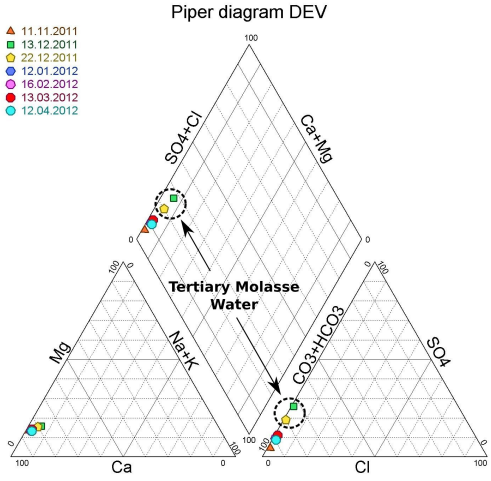

Fig. 23: Piper diagram of samples taken in the Dev spillway between November 11th 2011 and April 12th 2012.

2.2 Dissolved gases

2.2.1 C3 seepage survey

The monitoring of the C3 seepage by means of discharge, electrical conductivity, turbidity, radon, carbon dioxide and supersaturation offered the unique opportunity to characterize the flow regime following extreme drought periods. Indeed, between July 27th to December 7th 2010, and between April 7th to December 17th 2011, the C3 seepage was totally dried up and deactivated. As such, no contributions from neither seepage-flow through the low permeability volume nor the soil reservoir could be involved regarding the hydrodynamic of the sampling point during these extreme low-flow conditions. Moreover, the resumption of the discharge in the C3 seepage allowed to discriminate the origin of water during the reactivation of the system and the transition to high-flow periods. For the following discussion it is relevant to point out that during very low discharge rates, even more regarding total drought occurrences, total dissolved gas pressure in infiltrating water, if any, reaches equilibrium with the atmosphere. Therefore, the radon, carbon dioxide and supersaturation levels monitored during these periods only reflect the gas content in the air of the gallery and cannot be used for further interpretation (Fig. 61, Appendix II). As a result the following description is based on transitions to high-flow conditions, and high-flow periods themselves when discharge is sufficient not allowing the gas phase in the percolating water to reach equilibrium with the atmosphere (Fig. 62, Appendix II).

2.2.1.1 Transition to high-flow conditions of December 2010

As mentioned above, before December 7th 2010, the C3 seepage was totally dried up (Fig. 24). A precipitation event of 80 [mm] between December 5th and 8th was needed in order to permit fresh rainwater bypassing the soil reservoir through preferential flow paths or direct infiltrations and reactivating the seepage. On December 7th the discharge starts to increase and reaches 4 [L/min] on December 9th. The first water arrival is characterized by a massive turbidity pulse of 2.2 [NTU] occurring during the rising limb of the discharge increase. It can be referred to as autochthonous turbidity, resulting from the remobilisation of intrakarstic material, as it is accompanied by a first available minimal eC value of 305 [µS/cm]. It is followed by an allochthonous

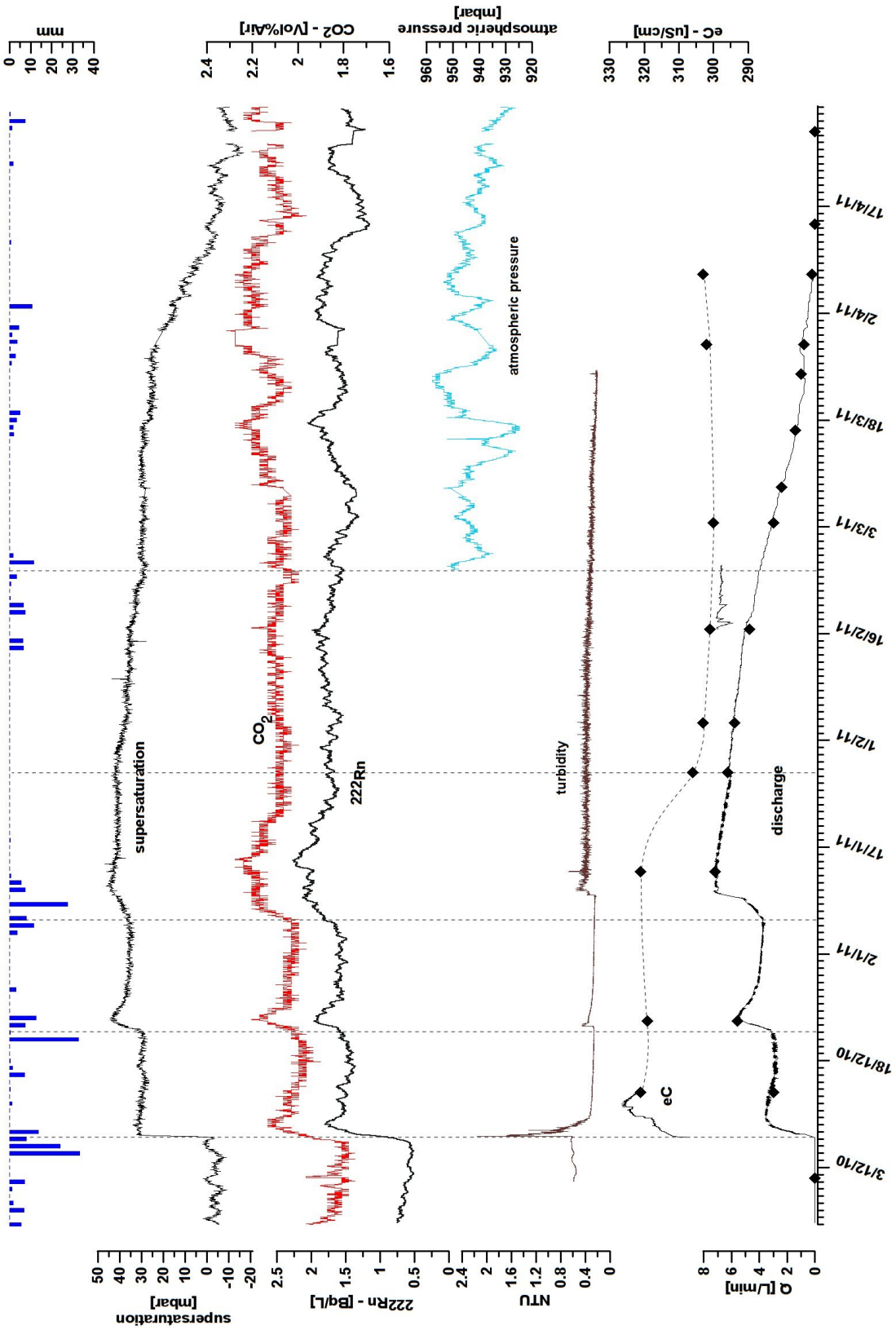

Fig. 24: Monitoring of discharge, eC, turbidity, radon, CO_2 and supersaturation in the C3 seepage from December 2010 to April 2011. Measurement uncertainties : Rn:~3%, CO_2:~7%, supersaturation:~3%.

turbidity event of lower amplitude. The rather non classical behaviour regarding the autochthonous and allochthonous turbidity event, can be explained by a limited contribution from the soil surface following the drought period that occurred in the C3 seepage system. The electrical conductivity rises then to 325 [µS/cm] reflecting soil water mineralization, as it was stored for a consequent time before release. Another premise pointing out to an important soil reservoir contribution, is the synchronous radon and CO_2 increase occurring as soon as the seepage is active again. Their respective peak concentrations are 1.7 [Bq/L] and 2.1 [Vol%Air] and are reached at the same moment as the fist maximum discharge event, i.e. on December 9th.
The first supersaturation data deserves to be treated carefully. Even though it is characterized by a level of around 30 [mbar] it should not be considered as a typical peak but rather as a base level, as all data obtained before December 7th regarding dissolved gases are irrelevant. This observation implies that water contributing to the first discharge increase in the C3 seepage originates from deeper part of the saturated soil, pushed down the system under the influence of a newly applied hydraulic stress, had enough time to degas to the atmosphere. Water stored in the upper part of the soil which is directly affected by precipitation events, and is thus prone to develop supersaturation peak features, doesn't reach the seepage following the first December rainfalls, as no real pulse was monitored. This affirmation is enhanced by the lag observed between the first supersaturation data (December 7th) which remains very stable (degassing to the atmosphere) and the synchronous radon-CO_2 peak monitored on December 9th. These first three dissolved gas signals reflect deeper soil pre-event water signature. The radon-CO_2 synchronous peak, two days after first water arrival, can be considered as the average transit time from the deeper soil reservoir to the C3 system outlet.

The second precipitation event, mainly characterized by a rainfall of 33 [mm] on December 21st, results in another behaviour regarding soil contribution to the C3 discharge. On the contrary to the previous rainfalls which induced discharging from the deeper part of the soil reservoir, the following description implies contributions from the whole soil sub-system. Indeed, as discharge starts to increase on December 22nd to reach 6 [L/min] on December 24th, so do radon and CO_2 concentrations which are respectively of 2 [Bq/L] and 2.2 [Vol%Air] on December 24th. They are accompanied by a synchronous allochthonous turbidity pulse with no evidence of any autochthonous peak, all intrakarstic pre-event may have been flushed, pointing out to superficial soil contribution. This upper part soil influence is enhanced by the presence of a typical supersaturation increase reaching 45 [mbar].

The third rainfall event of 51 [mm] taking place between January 5th to 9th 2011 (29 [mm] on January 9th), induced a similar behaviour implying the entire soil reservoir contributing to the discharge. Indeed, a synchronous increase of discharge, turbidity, radon, CO_2 concentrations and supersaturation levels is monitored as soon as January 7th and their peak values are reached on January 11th, with respectively 7 [L/min], 0.5 [NTU], 2.3 [Bq/L], 2.2 [Vol%Air] and 45 [mbar]. A secondary radon-CO_2 peak occurring on January 15th enhances the reactivity of the system once sufficient soil water saturation is reached, as it follows a small rainfall event of only 12 [mm] that happened from January 11th to 13th.
Maximum discharge rate was reached at the end of the January 2011 precipitation event, coinciding with the progressive diminishing of soil stored water influence on the hydrodynamics of the C3 seepage. As no more rainfalls were recorded until a slight succession of precipitations spreading out from February 14th to 27th (43 [mm]), the C3 discharge diminishes. The resulting drop of eC between January 13th to 27th, from 323 to 305 [µS/cm] points out to an epiphreatic flow increasing influence. January 27th marks the end of the recession limb of the third radon-CO_2 event. Until the beginning of March 2011, radon and CO_2 concentrations remain stable around respectively 1.6 [Bq/L] and 2.1 [Vol %Air], implying that soil stored water still contribute to the C3 seepage discharge by continuous and regular release to the system. At the beginning of March 2011 the supersaturation curve reaches its base level of 30 [mbar] and lasts until the end of the month. As by this period only scarce precipitations occurred and the resumption of biological activity and plant growth is initiated, only deep soil water, that underwent significant degassing to the atmosphere contributes to the discharge, as it is revealed by its flat base-level episode. As discharge rate is low (e.g. less than 2 [L/min] on March 8th) radon and CO_2 concentrations start to be inversely related to the atmospheric pressure and can be considered increasingly non relevant. Consequently, on April 7th 2010, the C3 seepage being totally dried up, the measured gas data reflects the equilibrium of the gas phase in remaining water within the C3 seepage collecting can with the atmosphere of the gallery.

2.2.1.2 Transition to high-flow conditions of December 2011

The transition to high-flow conditions in mid-December 2011 follows an extremely dry low-flow period (Fig. 25). Indeed, from April to December 2011, total rainfalls accounted for only 540 [mm]. A remarkable succession of precipitations of 188 [mm] spread out from

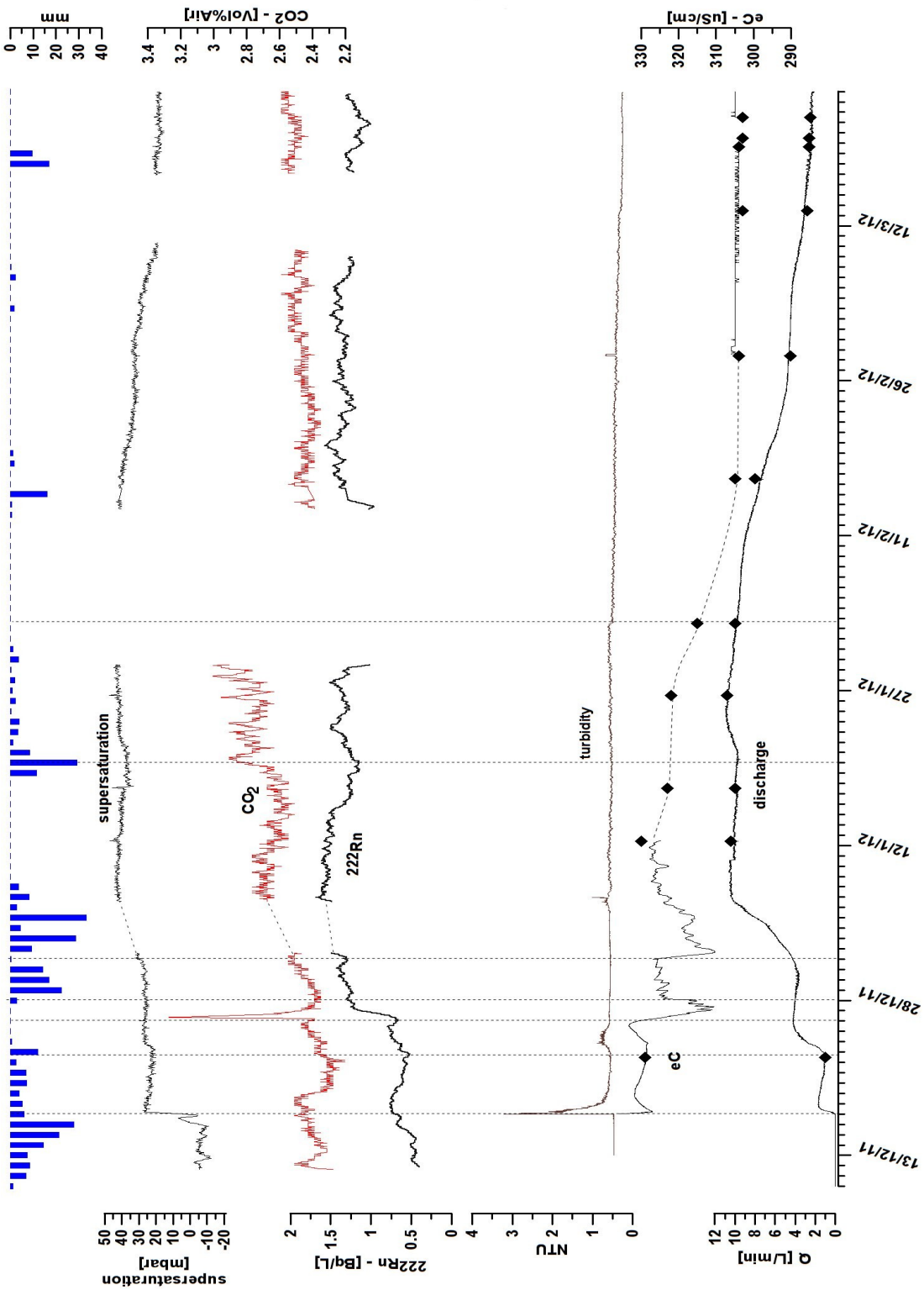

Fig. 25: Monitoring of discharge, eC, turbidity, radon, CO_2 and supersaturation in the C3 seepage from December 2011 to March 2012. Measurement uncertainties : Rn:~3%, CO_2:~7%, supersaturation:~3%.

December 2nd to 16th were needed in order to replenish the soil water deficit to reactivate the seepage. As such, on December 17th, freshly infiltrated water could bypass the soil reservoir and contribute to the discharge resumption in the C3 seepage. This phase is highlighted by an autochthonous turbidity peak of 2.9 [NTU] resulting from significant flow variation in intrakarstic conduits and sediments remobilisation and by a synchronous negative shift of eC values. It is followed by a very slight allochthonous turbidity event. On December 18th, discharge reaches a first maximum of 2 [L/min]. It is accompanied by a slight eC increase, along with radon and CO_2 first pulses. These features point out to an increasing but still limited soil water contribution to the discharge of the seepage. Nevertheless, as mentioned for the first high-flow transition, water mostly originating from deeper parts of the soil reservoir reaches the outlet, as the supersaturation signal remains quite stable around 30 [mbar] (pre-event water degassing to the atmosphere) and precedes the radon-CO_2 pulse (main deep soil contribution), as both these gases are continuously produced in soil and dissolved in water if soil saturation is sufficient.

In reaction to a rainfall of 13 [mm] on December 23rd, the entire soil sub-system starts to contribute to C3 seepage flow. Indeed, as discharge reaches 4 [L/min] on December 25th, it is accompanied by an eC increase, an allochthonous turbidity pulse and a combined slight supersaturation, CO_2 and radon signal. This behaviour reflects a combined dominant pre-event water stored in the soil (eC increase) contribution, along with the first influences of water from the upper part of the soil reservoir (radon, CO_2, supersaturation and allochthonous turbidity pulse).

On December 27th, five days after the last rainfall, a significant negative eC pulse is recorded, evolving from 335 (on December 26th) to 310 [µS/cm]. It is accompanied by remarkable radon and CO_2 peaks, reaching respectively 1.5 [Bq/L] and 3.3 [Vol%Air], whereas the supersaturation signal remains stable. These characteristics can be explained by the massive arrival of deep soil water in reaction to a piston flow, constrained by the newly water column formed in the upper part of the soil. Indeed, the supersaturation level remains stable, pointing out that rainfalls are used to replenish the soil water deficit. The low eC negative peak implies that in combination with this piston flow, considerable volume of fresh rain water bypass the soil reservoir through preferential flow paths.

From December 24th to 27th no rainfalls were recorded. The lack of fresh rainwater supply allowed deep soil water to predominantly contribute to the system, as can be seen by the eC curve gaining higher values from December 28th.

Another remarkable precipitation event of 147 [mm] distributed between December 28th and January 8th, marks the most significant discharge increase in the C3 seepage, as it reaches 10.5 [L/min] on January 7th. This discharge evolution along with radon, CO_2 and

supersaturation positive trends, with diminishing eC values, clearly enhances the contribution of fresh low mineralized water stored in the soil during the precipitation event. Moreover, the monitored increasing supersaturation signal points out to the system being more reactive, not allowing degassing to happen to the atmosphere. Such an influence is also monitored in reaction to rainfalls occurring between January 19th to 21st.
Beyond this last rainfall event, upper soil impact on the dynamic of the C3 seepage weakens (very low turbidity level), but still contributes through its deeper part, as can be seen by rather stable radon and CO_2 values, in combination with a progressively diminishing supersaturation which, is nonetheless still above its base level. Discharge along with electrical conductivity are progressively reduced, to reach respectively 2.5 [L/min] and 302 [L/min] on March 13th, reflecting the progressive predominance of epiphreatic flow. Supersaturation values returning to a base level of 30 [mbar] points out to the very end of soil stored, gas enriched water contribution.

2.2.1.3 General characteristics of the C3 seepage and conceptual model

The monitoring by means of continuous measurements of dissolved gases, electrical conductivity and turbidity allowed some conclusions to be drawn regarding the processes governing the hydrodynamics of the C3 seepage. This monitored sampling point only reflects one contribution, among others, to the general flow regime of the Prédernier artificial gallery. It offered the unique opportunity to characterize the flow regime following extreme drought periods, as between July 27th to December 7th 2010, and between April 7th to December 17th 2011, the seepage was totally deactivated. Moreover, the resumption of the discharge in the C3 seepage allowed to discriminate the origin of water during the reactivation of this pristine system.
Even though the watershed drained by the C3 seepage is characterized by a relatively small surface area (chapter 1.5.2.3), it can certainly provide valuable indications, with regards to karst system covered with thick and well developed soil. Indeed, its average thickness is estimated to 1 [m] (Jacot, 2011).

A typical response to precipitation events leading to the resumption of the discharge in the C3 seepage may be synthesised in the following phases.

The first phase referred to as a lag phase, is characterized by significant rainfalls on the watershed. Nonetheless, the seepage shows no reaction, remaining totally dried up. The

degree of water saturation in the soil highly influences this period, i.e. if soil water content is more or less than field capacity. All precipitations are stored in the soil.

The second step, which could be described as a soil phase, or piston phase implies two end members. On the one hand, once field capacity is reached, part of fresh rainwater can bypass the soil reservoir and contribute to discharge resumption in the C3 seepage. This event is characterized by a significant autochthonous turbidity pulse accompanied by a drop of eC values. On the other hand, it marks the beginning of soil, more specifically deep soil, contributions to the discharge (Fig. 26). Indeed, this pre-event water, following a significant rainfall, undergoes a newly applied hydrostatic pressure and is pushed down the system. A typical response at the sampling point following the autochthonous turbidity peak consists in the combination of a constant supersaturation level, which can be considered as base level, and of a codependent radon and carbon dioxide pulse. Indeed, water stored in the soil before a rainfall event is characterized by a remanent level of supersaturation, as it is prone to degassing in order to reach equilibrium with the atmosphere. Concerning radon and carbon dioxide, both these gases are continuously produced in the soil and available for dissolution in the matrix and percolating water.

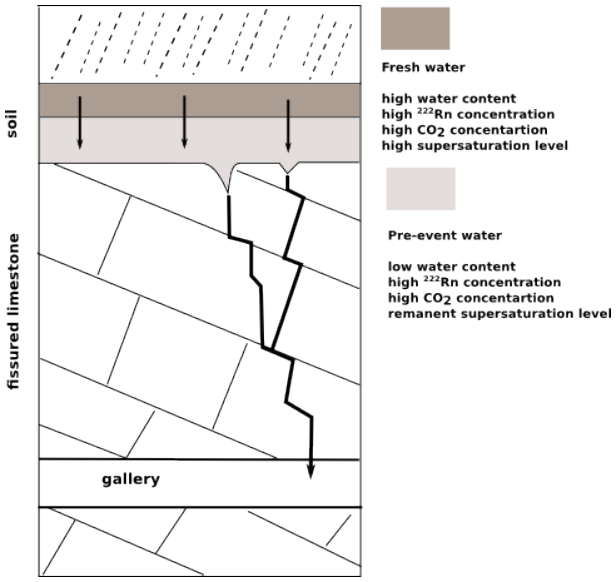

Fig. 26: Conceptual flow model of the deep soil contribution to the discharge.

The next sequence of this phase (Fig. 27), is responsible for a noticeable discharge increase. It is initiated, in the C3 seepage, by the first arrival of gas enriched water stored in the soil and the last contributions of pre-event water from the deeper soil reservoir to the seepage. It is followed by a dominant fresh soil water signature. The activation of this phase depends on the time needed for fresh water to replenish the soil reservoir and to migrate down by percolation to the system outlet. Thus total amount of precipitations, storage time, soil thickness and its intrinsic properties influence the transfer time. A typical reaction to this phase at the C3 seepage is characterized by a simultaneous radon, carbon dioxide, supersaturation increase and an allochthonous turbidity event. Depending on how

long the rainfall event water has been stored in the soil before release, it constrains conductivity values.

Following the efficient recharge of the system through soil and freshly infiltrated water, a maximal recharge rate is reached and electrical conductivity diminishes pointing out to a progressively predominant epiphreatic sustained flow, with contribution from continuous release from the soil reservoir and fresh storm water, describing the mixed phase

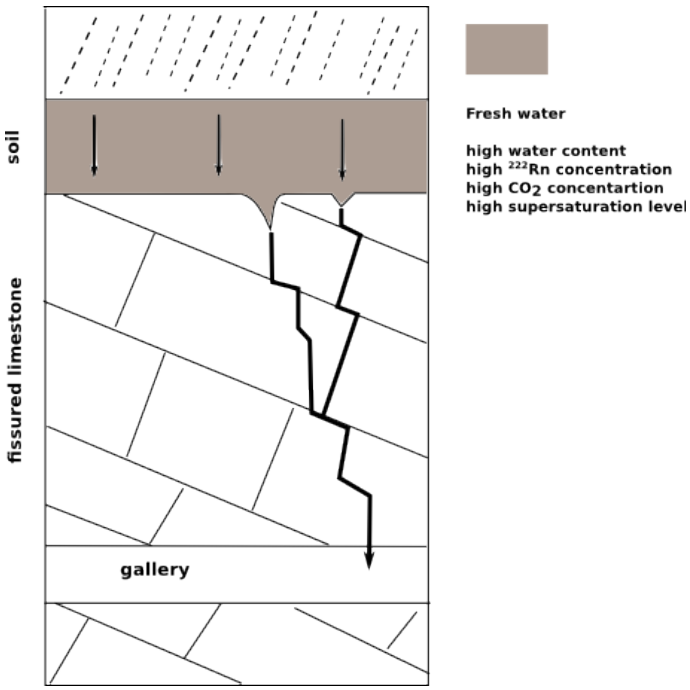

Fig. 27: Conceptual flow model of the entire soil contribution to the discharge.

It is relevant to notice that none of the above mentioned phases implies the contribution of an epikarst storage. No evidence was observed regarding its influence on the flow regime of the C3 seepage. Indeed, based on radon and CO_2 monitoring, a typical epikarst storage signature would imply a constant radon level (because it is not a production area) and increasing CO_2 values.

2.2.1.4 March 2010 tracing test

Thüler (2010) carried out a tracing experiment above the Prédernier drainage gallery on March 19th 2010, coinciding with a slight precipitation event of 9 [mm] between March 19th to 21st. The early stages of the monitoring of the seepage by means of radon, CO_2 and supersaturation took place at the same period as well.

The injection point is situated some 80 meters above the C3 seepage and around 40 meters west (Fig. 28), resulting in a straight line distance of approximately 90 meters. The tracing experiment involved the injection of 0.2 [kg] of fluorescein directly in the soil in a specifically dug pit characterized by a surface area of 0.5 [m^2]. In order to enhance the infiltration of the tracer, 1 [m^3] was applied on the pit, resulting in the simulation of an

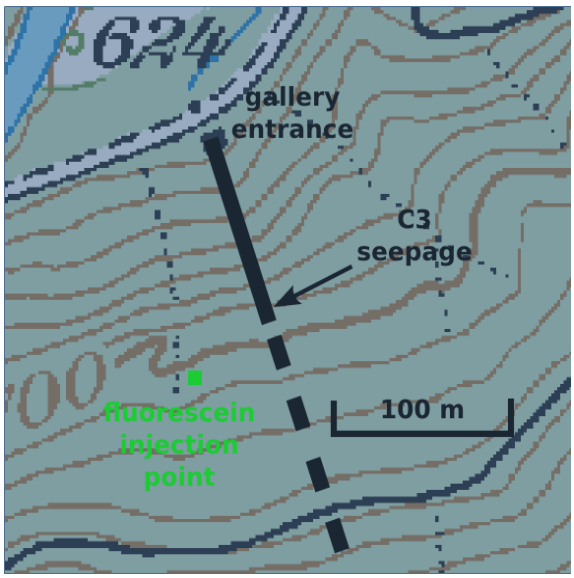

Fig. 28: March 2010 tracing experiment settings.

exceptional 2000 [mm] precipitation event. All seepages were followed by means of manual sampling. In addition, a field fluorometer was use in the Dev spillway in order to obtain continuous measurements.

The first detection time of fluorescein in the C3 seepage, corresponding to fastest flow velocities was monitored on March 29th, ten days after the injection (Fig. 29). As for the highest concentrations, 5.5 [µg/L], representing dominating flow velocities, they were recorded on April 7th. Manual sampling continued until the end of April. Thüler considered an average discharge of 5.6 [L/min] in the C3 seepage, resulting in a tracer recovery rate of 0.38%.

The A1 seepage is characterized by a very low peak value of 0.35 [µg/L] on March 29th. Based on an average discharge of 2 [L/min], fluorescein recovery rate reaches 0.0031%.

The temporal evolution of the fluorescein signal in the G4 spillway is very similar to the one observed in the C3 seepage. Indeed, highest concentrations of 3.6 [µg/L] were reached on March 7th as well, and first detection time was monitored on March 29th. The only noticeable difference is depicted by a recovery rate of 2.12% (average discharge 60 [L/min]). Total tracer recovery rate of the gallery, the Dev spillway being monitored as well, reached only 3.77% with an average discharge of 150 [L/min]. March 27th marks the first detection time.

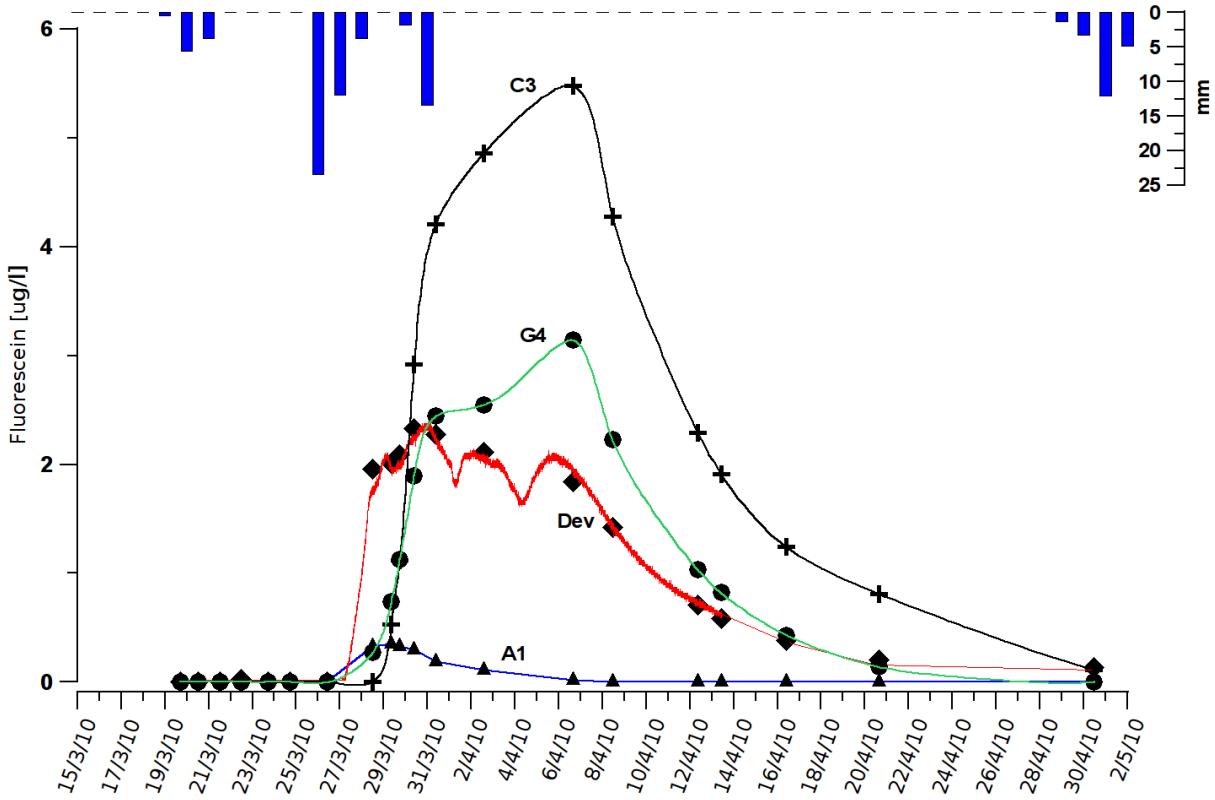

Fig. 29: Fluorescein restitution curves in the A1, C3 seepages and in the Dev and G4 spillways.

This very low recovery rate suggests a significant buffer capacity in the unsaturated zone, that can be explained on the one hand by the thickness of the low permeability volume overhanging the gallery (80 meters) and on the other hand by the high storage capacity of the soil. A part of the dye could also have bypassed the gallery and be transported east.

Based on recovery rates characterizing the different sampling points, a conceptual flow model can be designed, showing the most important underground flow paths (Fig. 30). The Late Hauterivian strata dip in the gallery area points towards south, as such it constrains flows. This could explain the higher recovery rates being observed in the G4 spillway and in the C3 seepage in comparison with the A1 seepage.

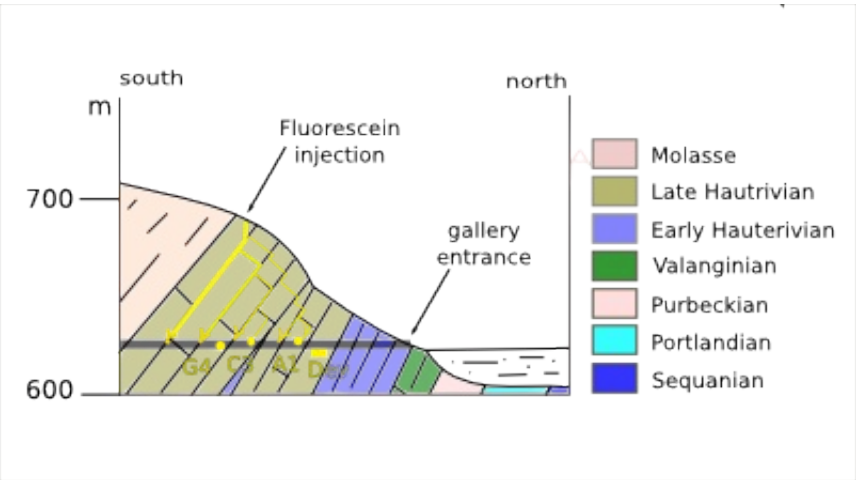

Fig. 30: Conceptual model showing underground flow paths.

2.2.1.5 C3 seepage conceptual model versus tracing test

During the tracing experiment, discharge in the C3 seepage reached a high-flow condition constant low point with less than 4 [L/min]. Besides, the entire month of April was extremely dry, as no rainfall events were monitored until April 29th. As such, even though the C3 seepage was not totally dried up, the lack of any precipitations before March 19th and after March 31st, allowed to compare processes during the tracing experiment with the reactivation of the C3 seepage, and its derived phases, of December 2011 following an extreme low-flow period. The comparison of the tracing experiment with the dissolved gas monitoring is synthesised by the following figure (Fig. 31).

The injection of 0.2 [kg] of fluorescein occurred during the soil phase, in the middle of the so called deep-soil episode. Discharge is stable around 4 [L/min] and pre-event water characterized this period. Indeed, this remanent pre-event water is depicted at the outlet by a combination of a constant supersaturation level and of a codependent radon and carbon dioxide evolution. Following a precipitation event of 39 [mm] between March 26th to 28th fresh rainwater bypasses the soil reservoir and to contribute to a slight discharge increase. This feature is enhanced by a noticeable codependent drop of radon and CO_2 levels as soon as March 26th.

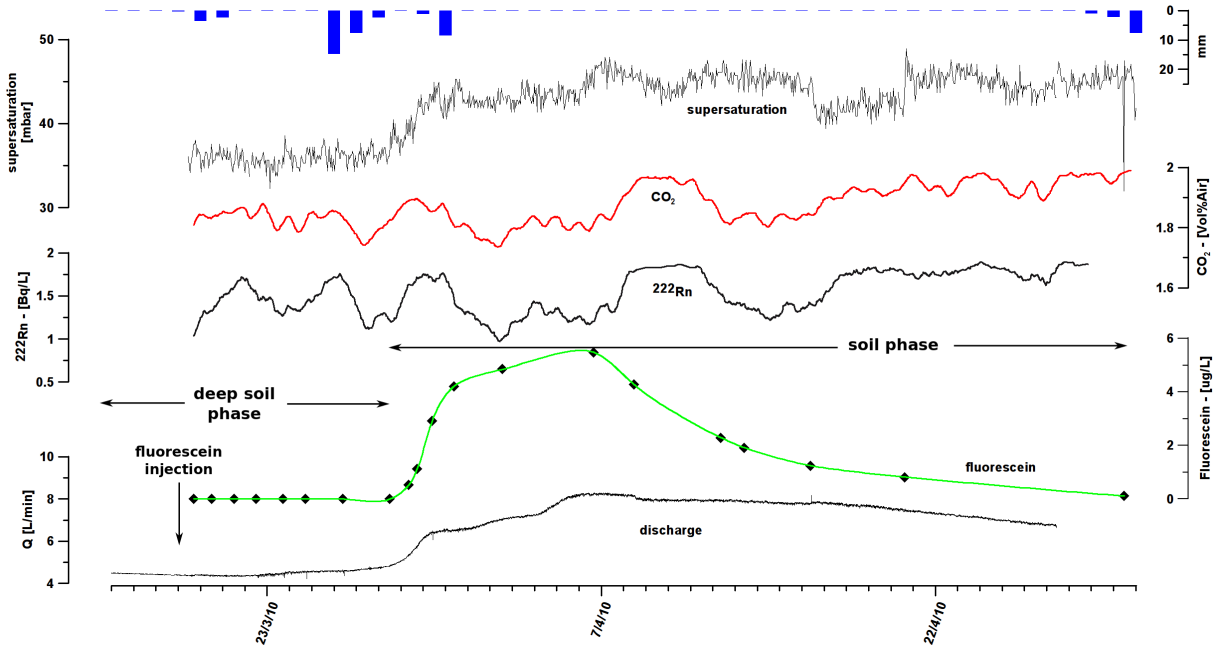

Fig. 31: Comparison of dissolved gases temporal evolution with regards to the March 2010 tracing experiment. Measurement uncertainties : Rn:~3%, CO_2:~7%, supersaturation:~3%.

March 29th marks the beginning of another sequence. Indeed, a codependent and synchronous radon, CO_2 and supersaturation increase is monitored in the C3 seepage. It is responsible for a noticeable discharge increase and is initiated by the first arrival of gas enriched water stored in the soil, which is confirmed by the first detection of fluorescein. The next remarkable event happened on April 7th. Another well defined radon, CO_2 and supersaturation pulse is initiated and coincides with dominant flow velocities as fluorescein highest concentrations were measured.

Soil thickness and high storage capacity, governing the time needed for event soil water to leave the soil reservoir is enhanced by the supersaturation curve. Indeed, its flattened shape, rather than a pulse like appearance, points out to a significant soil thickness and degassing to the atmosphere.

Moreover, the fluorescein breakthrough curve clearly permitted linking radon, carbon dioxide and supersaturation rises to gas enriched water stored in the soil before release to the system.

2.2.1.6 Chemical properties of water in the C3 seepage

Water in the C3 seepage was also sampled between December 2011 to April 2012 for the analysis of major ion chemistry. As it followed extreme low-flow conditions, the chemical evolution was assessed only for high-flow conditions.

The typology of groundwater characterizing the C3 seepage (Fig. 32), which represents a contribution to the entire watershed signature, was analysed through a ternary piper plot. As expected, samples exhibited patterns characteristics of Ca^{2+} and CO_3+HCO_3^- waters, with no noticeable differences during the high-flow sampling.

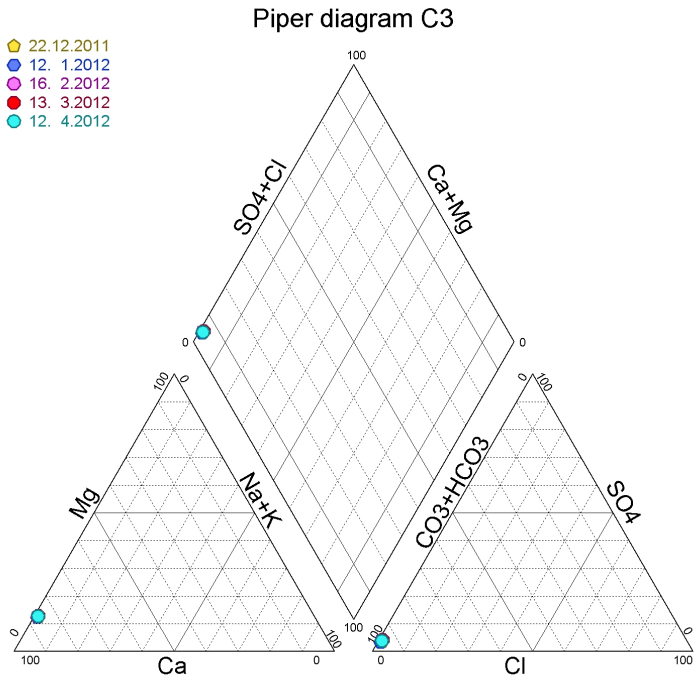

Fig. 32: Piper diagram of samples taken in the C3 seepage between December 2011 and April 2012.

2.2.2 A1 and A2 seepages survey

The A1 and A2 seepages were followed by means of continuous discharge, electrical conductivity, radon, carbon dioxide and supersaturation measurements. Continuous turbidity and total organic carbon monitoring was undertaken in the A1 seepage collecting can only. It appears that for the shared followed parameters, the A1 ans A2 seepages behave in a similar way. The only noticeable differences were observed regarding the intensity of discharge and supersaturation. Nevertheless, for all parameters the measured variations between both sampling points are synchronous (Fig. 63, Appendix II).
Moreover, dissolved gases data in the C3 seepage revealed that during extreme low-flow conditions, total dissolved gas pressure in remanent water in collecting can, if any, reaches equilibrium with the atmosphere. Therefore, the radon, carbon dioxide and supersaturation levels monitored during these periods only reflect the gas content in the air of the gallery and couldn't be used for further interpretation. Consequently dissolved gases measurements in the C3 seepage during drought periods (i.e. between July 27th to December 7th 2010 and between April 7th to December 17th 2011) were compared with radon and CO_2 data characterizing low-flow conditions in the A1 and A2 seepages, when discharge didn't exceed 0.5 [L/min] (Fig. 64-67, Appendix II). It appears that radon and carbon dioxide levels monitored in the C3 seepage are linearly related to data obtained in the A1 and A2 seepages, extremely close to an ideal relation expressed by Y = X. Radon linear regressions are characterized by R-squared values of 0.98 and standard error of the regression is less than 1%. As for CO_2 level comparisons, R-squared is 0.81 and standard error of the regression is around 5%.
Thus, as corollary to similarities between the A1 an A2 seepages and the complete set of data available in the A1 sampling point, as turbidity and TOC concentrations were followed, only the A1 seepage will be described. Moreover, due to dissolved gases non-relevancy during noticeable low-flow conditions radon, $C0_2$ and supersaturation will be discussed during the transition to high-flow conditions of December 2010. As for the following low-flow period, it will only be assessed through classical physical and chemical parameters.

2.2.2.1 Transition to high-flow conditions of December 2010

High-flow conditions in the A1 seepage started on December 6th (Fig. 33) They were initiated by a cumulated precipitation event of 79 [mm] between December 5th to 8th, which induced a discharge increase, from less than 0.5 [L/min] on December 6th to 6.2 [L/min] on

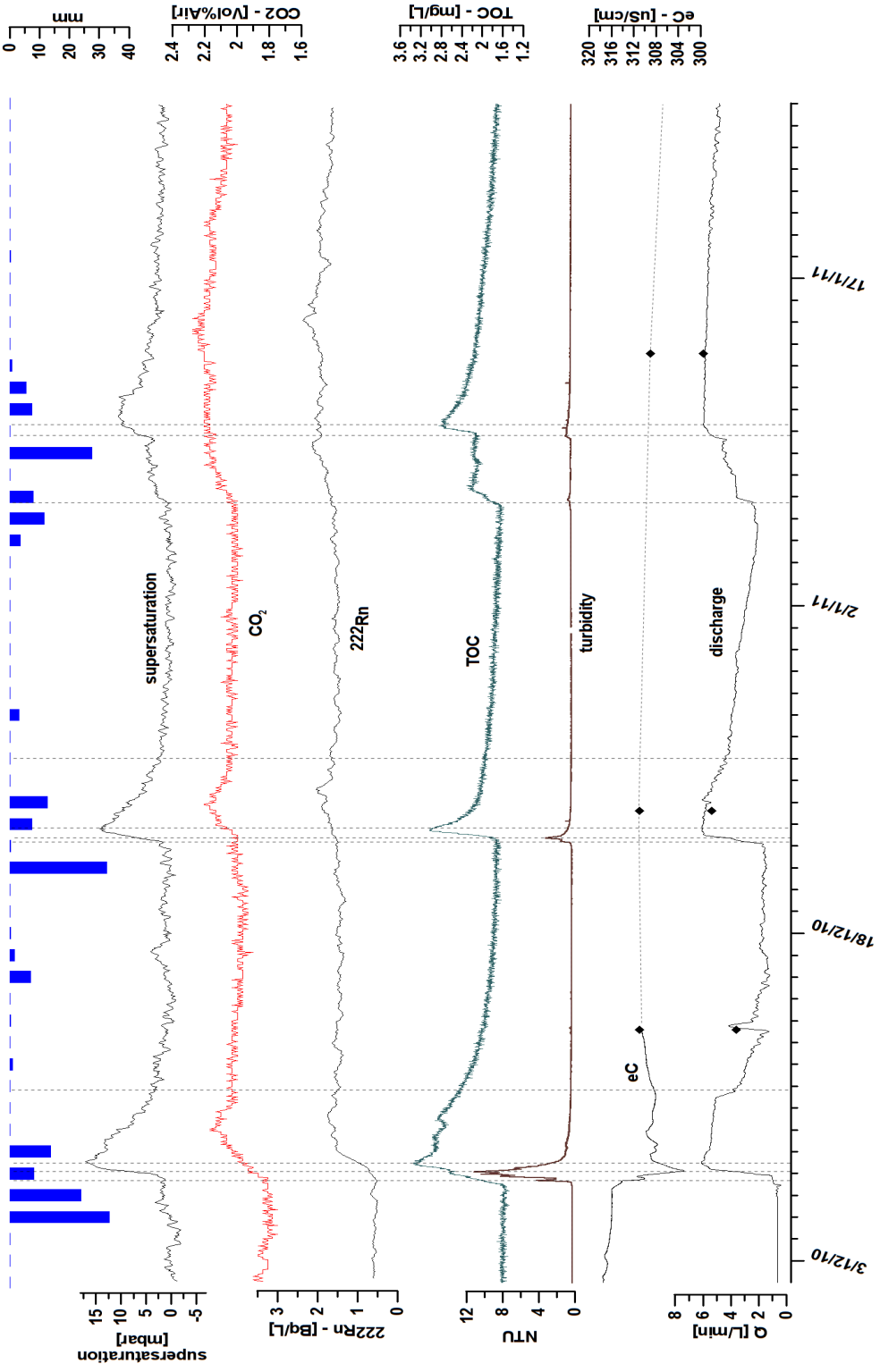

Fig. 33: Discharge, eC, turbidity, TOC, radon, CO_2 and supersaturation during high-flow conditions in December 2012. Measurement uncertainties : Rn:~3%, CO_2:~7%, supersaturation:~3%.

December 7th. Fresh rainwater bypassing the soil reservoir and reaching the outlet, is enhanced by a noticeable first drop of electrical conductivity which evolves from 320 to 310 [µS/cm] during the last hours of Dec 6th. It coincides with a well defined autochthonous turbidity pulse of 4 [NTU]. The reactivity of the seepage is underlined, as it is quickly followed, from December 7th, by a remarkable allochthonous turbidity increase (11[NTU]), pointing out to the arrival of fresh storm water transiting through the soil, which can be seen by another diminishing of eC values reaching 301 [µS/cm]. It is accompanied by the simultaneous and progressive increase of total organic carbon, radon, CO_2 and supersaturation, which corroborate the increasing soil reservoir influences. Dominating flow velocities following the rainfall event are reached on December 7th. One can see that thanks to the simultaneous peak maximum of both TOC and supersaturation, reaching respectively 3.3 [mg/L] and 16 [mbar]. As radon and CO_2 are continuously produced in the soil, they are more efficiently dissolved in percolating water when the flow rate is lower. This explains their maximum level being reached on December 9th. December 11th marks the diminishing influence of dissolved gas enriched precipitation water, as supersaturation reaches a base-level around 0 [mbar] and no more rainfalls were recorded. Following this date, discharge decreases underlining soil influence on the recharge of the system. Nevertheless, soil still contributes to the dynamics of the seepage by constant water release, as shown by the constant levels of both CO_2 and radon. The lack of precipitations allows water stored in the soil to acquire higher mineralization, as can be noticed from the eC increase reaching 310 [µS/cm].

Constant levels of discharge, dissolved gases, turbidity and TOC remain until December 22nd. Indeed, a remarkable rainfall of 33 [mm] occurs on December 21st. It induced a discharge increase which reaches 6 [L/min] on December 23rd. The rising limb of the hydrograph is accompanied by an autochthonous turbidity pulse of 2 [NTU], quickly followed by an allochthonous turbidity increase which reaches 4 [NTU]. It coincides with the synchronous TOC and supersaturation rise. Their maximum values of respectively 3 [mg/L] and 13 [mbar] are recorded during the early hours of December 23rd. As mentioned above, radon and CO_2 levels reach their maximum with a lag compared to supersaturation and TOC as higher concentrations are made possible during a lower and steadier flow rate, i.e. post-storm conditions. When dissolved gas enriched water stop its contribution to A1 seepage dynamics on December 26th, as supersaturation base-level is observed, discharge decreases less drastically than during the previous rainfall period. As a matter of fact, recharge of the system is progressively achieved enhancing a new epiphreatic contribution. The epiphreatic zone contribution is even more obvious following constant conditions

being reached after the precipitation event spread out from January 5th to 12th. Even though discharge diminishes, it does so on a rather attenuated and progressive way, as it reaches 1[L/min] only at the beginning of March 2010. This last meteorological event induced a similar signature regarding discharge, dissolved gases, turbidity and TOC. Indeed, supersaturation and TOC maximal levels were monitored simultaneously (January 10th) and radon and CO_2 concentrations trails behind.

2.2.2.2 Low-flow conditions from April to December 2011

The period between March and December 2011 can be characterized as extremely dry. Indeed, biological activities and plant growth, highly intercept rainfalls. Nevertheless, unlike the C3 seepage, the A1 sampling point never dried up. Measured discharge ranges between 0.1 to 0.6 [L/min] (Fig. 34). Continuous electrical conductivity increase during these months (310 [µS/cm] during mid-April and 335 [µS/cm] in mid-September) points out to a base-flow regime under strong seepage-flow influence. This seepage-flow signature is enhanced by the Mg/Ca ratio in the A1 and A2 seepages. Indeed, December 2011 low-flow and high-flow conditions are characterized by ratios of respectively 0.09 and 0.08.

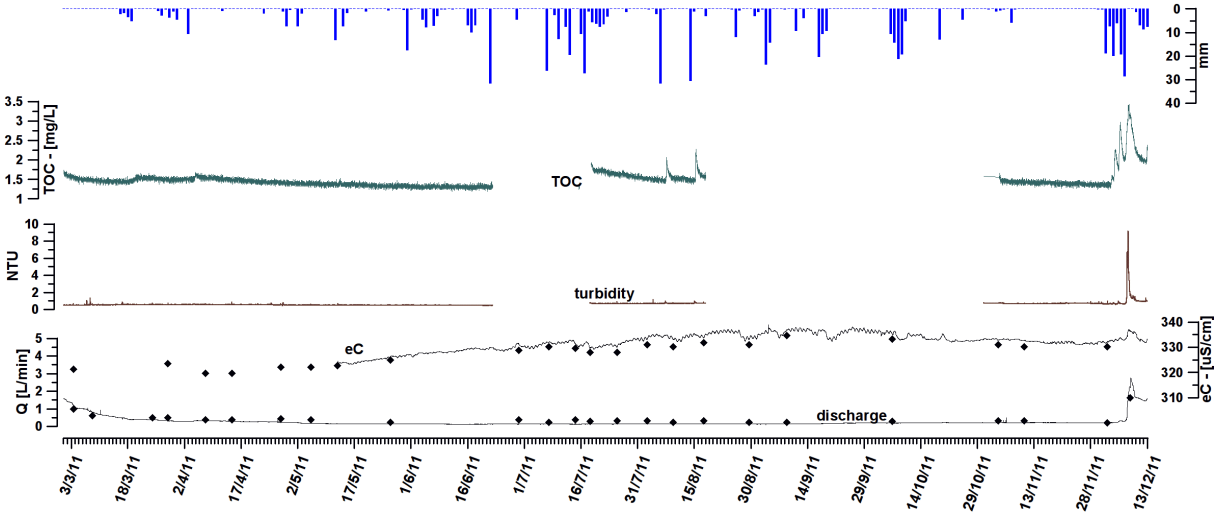

Fig. 34: Discharge, eC, turbidity and TOC in the A1 seepage during low-flow conditions from March to December 2011.

Turbidity and TOC levels are very low around respectively 1 [mg/l] and 0.3 [NTU]. Some contribution from fresh water percolating through the soil was monitored, in reaction to

remarkable precipitation events, as seen from very slight eC drops and associated turbidity-TOC pulses (e.g. on August 6th and 14th).

2.2.2.3 General characteristics of the A1 seepage and conceptual model

The monitoring of the A1 seepage by means of dissolved gases and classical parameters such as turbidity and total organic carbon, allowed to assess hydrogeological processes governing the dynamic of this size reduced system. Indeed, its discharge rate is order of magnitude smaller than the entire gallery one. Even though being a small contribution to the average flow regime, it emphasizes the behaviour of a karst system covered by a moderate thickness of unsaturated zone of circa 20 to 30 meters. Moreover, it is characterized by a thin soil cover of 0.2 to 0.3 meters (Jacot, 2011).

A typical response to a precipitation event can be summarized by the following phases.

Similarly to the C3 seepage, the first monitored phase can be referred to as a lag phase. A very low and stable discharge is measured, along with no variation regarding neither dissolved gas content, nor classical parameters such as turbidity, total organic carbon and electrical conductivity. Discharge is mainly sustained by seepage-flow from the low permeability volume.

Following a rainfall event and sufficient soil water storage, the soil phase is initiated. Indeed, fresh water contributes to the discharge increase. It is emphasized by a synchronous autochthonous turbidity peak, resulting from the remobilisation of intrakarstic material and a negative eC pulse.
It is quickly followed by a significant contribution of fresh water transiting through the soil. It coincides with maximal discharge levels, a remarkable allochthonous turbidity pulse, even lower eC values and the beginning of the rise of other soil related parameters such as TOC, supersaturation, radon and CO_2. Dominating flow velocities of water resulting from the rainfall event are reached afterwords, which is underlined by simultaneous maximum levels of both TOC and supersaturation. Main soil stored water contribution is enhanced by the codependent radon and carbon dioxide maximal levels, which trail behind the supersaturation and TOC peak. Indeed, as radon and CO_2 are constantly produced, higher concentrations are measured in percolating water once lower flow velocities prevail and

partial water storage occurs in the soil reservoir, as a more efficient dissolution is made possible.

Once the influence of gas enriched water originating from the soil diminishes, supersaturation reaches a base level, CO_2 and radon values remain stable and discharge undergoes a noticeable drop, implying that it is mainly sustained by leakage from the soil and seepage flow. This discharge lowering is less pronounced following the next rainfall events. As a matter of fact, sufficient recharge of the system is progressively achieved through significant contributions from soil stored and freshly infiltrated water. This leads to the progressive resumption of an epiphreatic flow component and depict the mixed phase.

Soil continues to influence the A1 seepage discharge as underlined by constant levels of both CO_2 and radon.

It is interesting to underline that unlike the C3 seepage, characterized by a thick soil cover, which revealed the contribution of deep soil pre-event water during the piston phase (constant supersaturation level along with a CO_2 and radon peak), such a signature was not monitored during the A1 survey. Indeed, soil covering the presumed A1 watershed is thinner (0.2 to 0.3 meters). As such, pre-event water stored in the soil reservoir, even though it certainly underwent significant degassing to the atmosphere, doesn't account for a sufficient volume to influence the noticeable supersaturation content of fresh rainfall event water. As a result, supersaturation, radon and carbon dioxide concentrations increase simultaneously.

2.2.2.4 Chemical properties of water in the A1 and A2 seepages

Water in the A1 and A2 seepages was also sampled between December 2011 to April 2012 for the analysis of major ion chemistry.

The typology of groundwater characterizing both seepages (Fig. 35 and 36), was analysed through a ternary piper plot. Samples exhibited a general shift towards the apex characteristics of Ca^{2+} and CO_3+HCO_3^- waters, with no noticeable differences between the high-flow and low-flow sampling.

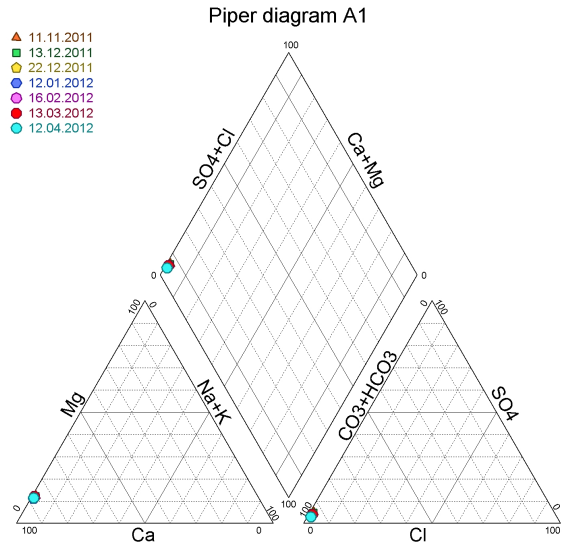

Fig. 35: Piper diagram of samples taken in the A1 seepage between November 11th 2011 and April 12th 2012.

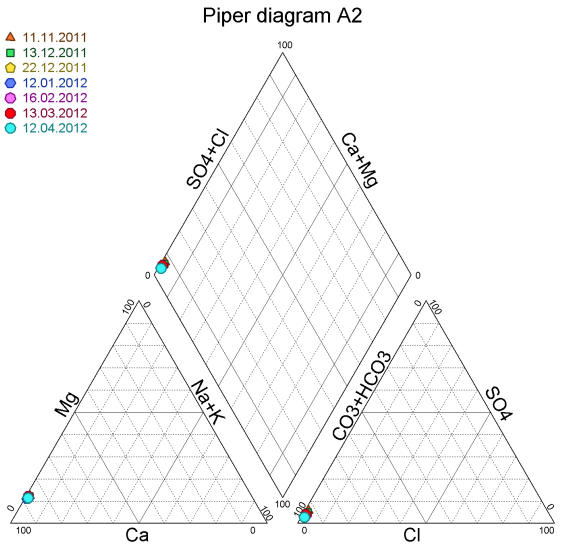

Fig. 36: Piper diagram of samples taken in the A2 seepage between November 11th 2011 and April 12th 2012.

2.3 Discussion

The monitoring of the Prédernier artificial drainage gallery offers a unique feature allowing to compare the dynamics of natural parameters characterized by different storage origin, transit time and watershed scales. Thus the Dev spillway reflects the influence of the entire watershed during high-flow conditions, whereas during low-flow periods it characterizes the restricted watershed limited to the 50 meters separating the Dev sampling point and the G4 spillway. The A1, A2 and C3 seepages are contributions among others.

Total gallery dynamic is governed by the cumulated contributions of two end members. The first one is depicted by the C3 seepage influence. It is characterized by thick non saturated zone of around 80 meters and covered by a noticeable soil cover of circa 1 meter. The second one, represented by the A1 seepage, is overhanged by a moderate non saturated zone ranging from 20 to 30 meters covered by thinner soil of 0.2 to 0.3 meters. These structural characteristics lead to contrasted signatures regarding water storage time in the soil sub-system, and reactivity of flows in sampling points following precipitation events.

In order to asses these features classical parameters, such as turbidity, total organic carbon and electrical conductivity were monitored in combination with soil related gases. Indeed, radon and carbon dioxide are continuously produced in the soil and are well soluble, allowing them to be constantly dissolved in soil water and to be transported to system outlets depending on hydrogeological conditions. As for supersaturation, another soil typical parameter, it is characterized by the formation of excess air linked to the complete or partial dissolution of entrapped air naturally present within soil pore space under the influence of a newly applied hydrostatic pressure. Thus, it reflects gas enriched water in the soil sub-system during rainfall events. The following discussion is based on a precipitation event of 79 [mm] spread from December 5th to 8th.

2.3.1 The lag phase

In both the A1 and C3 systems, the lag phase is characterized by stable and low discharge rates (Fig. 37 and 38). During extreme low-flow conditions the C3 seepage even totally dries up. Rainfall events have already occurred, and as the duration of this phase highly depends on soil water saturation and if it has reached its specific field capacity, no reaction

are monitored in the outlets. Rainfall water is essentially used to replenish the soil water deficit. Higher

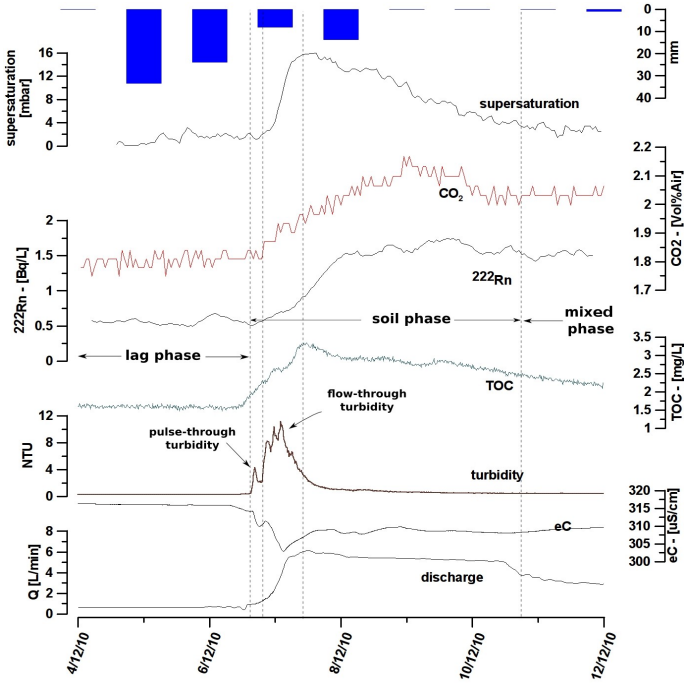

Fig. 37: Lag, soil and mixed phases in the A1 seepage during high-flow conditions in December 2010.

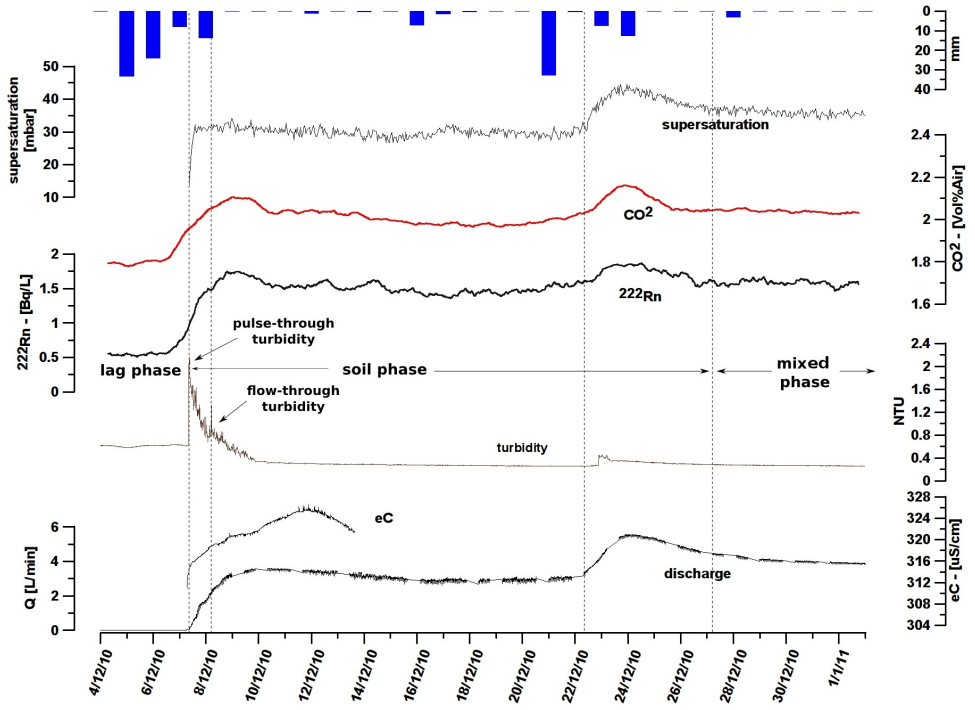

Fig. 38: Lag, soil and mixed phases in the C3 seepage during high-flow conditions in December 2010.

electrical conductivities, very low turbidity and total organic carbon levels enhance a base-flow regime mainly sustained by seepage flow through the low permeability volume. During this period, if discharge is not sufficient, allowing the gas phase in the seepage collecting cans to reach an equilibrium with air in the gallery, radon, CO_2 and supersaturation measured concentrations can be considered as irrelevant.

2.3.2 The soil phase

The soil phase is initiated when the soil sub-system reaches its field capacity. It allows fresh rainwater to bypass the soil reservoir through preferential flow paths and to contribute to the increase of discharge. It is generally accompanied with a eC drop and by an autochthonous turbidity peak, known as pulse-through turbidity, resulting from the remobilisation on pre-existant intrakarstic material in the conduits. As rainfall data is monitored on a daily basis, this episode only allows to estimate an approximative transit time for first fresh water arrival.

Fastest flow velocity

In reaction to the first rainy day of December 5th (to allow an easier interpretation the rainfall is set at 12 AM) first storm water arrival in the A1 seepage is monitored from December 6th at 2PM, resulting in an approximative transit time of 26 hours for the fastest flow velocity. First discharge increase in the C3 seepage occurred at the same time. Autochthonous turbidity peaks along with eC drops were observed in both the A1 and C3 seepages. They respectively reach 4 and 2.2 [NTU]. The A1 pulse-through event is well defined, finishing in a matter of hours, and precedes the upcoming allochthonous turbidity episode. Conversely, the C3 event consists in a massive pulse, in comparison with the yet to come flow-through turbidity pulse, and lasts for around 20 hours. This feature can be explained by the significant remobilisation of intrakarstic material following the drought period that occurred in the C3 seepage.
The pulse-through event marks the very beginning of the influence of soil stored water, as showed by the synchronous slight increase of TOC, radon, CO_2 and supersaturation levels in the A1 seepage. In the C3 seepage, the soil contribution rather stands for the deep soil reservoir, as only radon and CO_2 values increase, whereas supersaturation remains stable.

Dominating flow velocity

Dominating storm water flow velocity is underlined by the allochthonous turbidity pulse event, known as flow-through turbidity, and by a more pronounced eC negative shift, depicting the first arrival of fresh water from the soil surface. Its thickness noticeably influences this episode regarding the comparison between the A1 and C3 seepages. Indeed, the main difference resides in the intensity and in the duration of the recession episode of the allochthonous turbidity curve.

The A1 seepage watershed is characterized by a thin soil cover. Thus, soil water replenishing can quickly be achieved, resulting in a remarkable contribution from the soil surface. It reaches 11 [NTU] on December 6th, and in about 20 hours the main flow-through turbidity peak is passed and a base level is already reached on December 7th.
As for the C3 seepage, characterized by a thick soil and unsaturated zone, the allochthonous turbidity event is depicted by a very slight pulse of 1 [NTU] on December 8th, which is significantly less than the preceding pulse-through turbidity event. A base level is

reached on December 10th. These characteristics point out to a moderate contribution from the soil surface, due to soil cover thickness.

In the A1 seepage, the flow-through turbidity event occurs during the rising limb of both TOC and supersaturation, which enhances faster transport of colloids with respect to solutes due to exclusion processes in karstic media (Göppert and Goldscheider, 2008; Savoy, 2007). Simultaneous peak values of both TOC and supersaturation on December 7th around 12 AM results in a transit time on the order of 48 hours. The presence of the supersaturation peak implies the influence of fresh, gas enriched, storm water from the entire soil reservoir. The entire soil affecting the dynamic of the seepage is underlined by noticeable increase of both radon and CO_2, with maximum levels being reached once the dominating flow velocity is passed. Indeed, as both these gases are continuously produced in the soil, they are more efficiently dissolved in water when a steady-state flow conditions with a high level of water saturation in the soil is reached. The progressive transition to a steady-state flow regime is accompanied by an eC increase, as it allows higher mineralization in soil stored water. In reaction to the soil phase, discharge reaches its maximum with 6 [L/min].
The C3 seepage reveals a drastically different behaviour regarding soil water contribution. As mentioned above, water originating from the soil surface doesn't play any significant role (very slight allochthonous turbidity peak). The monitored radon, CO_2 and supersaturation concentrations rather point out to a deeper soil reservoir contribution, attributed to a newly applied hydrostatic pressure from the upper soil-water column, resulting in a piston type flow. As radon and CO_2 reach their peak values on December 9th, implying a transfer time of circa 84 hours, eC rises pointing out to mineralized, pre-event, deep soil stored water, while discharge is around 4 [L/min]. Supersaturation remaining stable during this period reveals that water arriving at the outlet has undergone significant degassing to the atmosphere before release to the system. Only pre-event water stored long enough in the soil can develop that kind of supersaturation signature. Gas enriched water never reach the C3 seepage, and rainfall replenishes the thick soil reservoir. Contribution from the entire soil sub-system only occurred following a rainfall event of 33[mm] on December 21st, resulting in the synchronous peak affecting supersaturation, CO_2 and radon on December 24th. The deducted transfer time is around 60 hours. It is accompanied by a slight flow-through turbidity signal which precedes the supersaturation peak level and results in a significant discharge increase reaching 6 [L/min].

2.3.3 The mixed phase

Supersaturation concentrations reaching a base level, respectively around 30 [mbar] for the C3 seepage and 0 [mbar] for the A1 sampling point, mark the beginning of the mixed phase. Water discharging at outlets is a mixture of soil leakage water, as underlined from the constant CO_2 and radon levels, rainwater and epiphreatic flow. Following an effective recharge of the system the epiphreatic zone is progressively replenished, contributing increasingly to the flow of each seepage.

2.3.4 Supersaturation base level

The monitoring of dissolved gases in the A1 and C3 seepages and in the Dev spillway (Fig. 39) revealed a particular feature: the supersaturation base level. The following discussion is based on a period the period from December 2010 to June 2011 and mainly corresponds to high-flow conditions when discharge rates were sufficient in the followed sampling points not allowing degassing to the atmosphere of the gallery, i.e. more than 1[L/min] in the A1 and C3 seepage, and at least 30[L/min] in the Dev spillway.

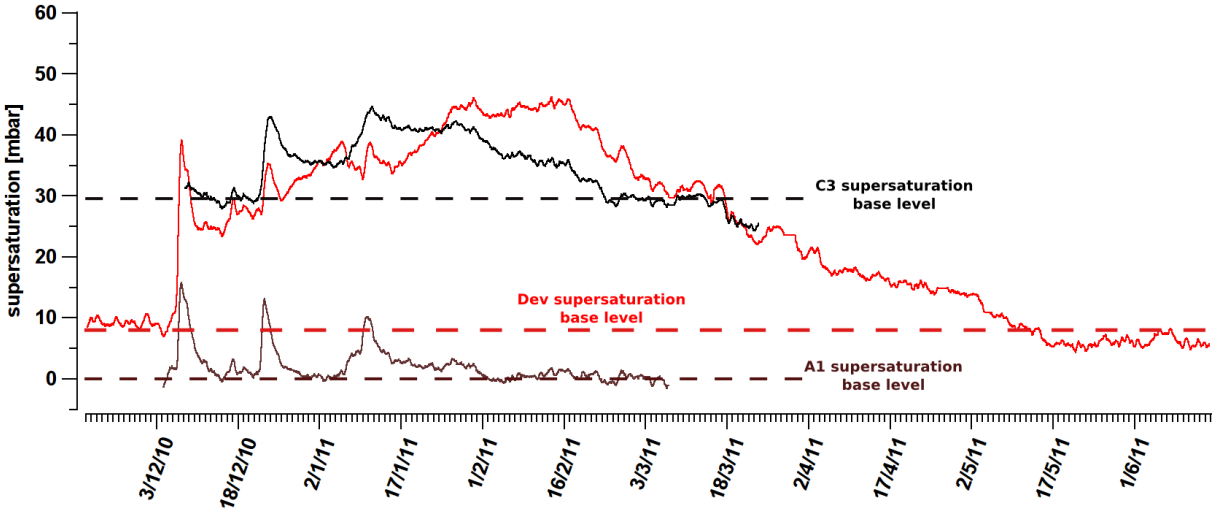

Fig. 39: Supersaturation base level in the A1, C3 seepages and in the Dev spillway.

As mentioned in the previous chapters, supersaturation pulses allow to discriminate gas enriched rainfall/storm water at systems outlets and can assess dominating flow velocities,

as TOC peak values are reached synchronously. It doesn't permit entirely describing the time extent of the contribution of the soil stored water, which is more efficiently apprehended through analysis of the supersaturation base level.

The A1 seepage, among all sampling points, is characterized by a more noticeable reactivity and smallest flow rate. Indeed, its discharge ranges from 0.1 to 7 [L/min]. Between recorded supersaturation events, a base level around 0 [mbar] is reached. The C3 seepage and the Dev spillway, respective discharge rates range from 0 to 9 [L/min] and 1.5 to 380 [L/min]. The C3 supersaturation base level is situated around 30 [mbar], as for the Dev spillway it oscillates around 10 [mbar].

These specific base level signatures can be linked to a distinctive feature characterizing each sampling point: soil thickness. Soil covering the watershed of the C3 seepage is characterized by a 1 meter thickness. As such, the replenishing of the soil reservoir following precipitation events can store a significant volume of water and produce a noticeable supersaturation level. The total volume of initially entrapped air limits the maximum amount of excess air being potentially produced (Holocher, 2002). Even though degassing to the atmosphere occurs between rainfall events, as gases will migrate from points of higher to those of lower pressure (Scanlon *et al.*, 2002), significant amount of excess air remains in the soil. Indeed, the hydrostatic pressure applied by residual soil stored water, makes degassing of an initial dissolved gas excess difficult. It results in a supersaturation gradient, with lower concentrations toward the surface. When the soil water content is sufficient to allow release of this water to the system, the average remanent supersaturation content, i.e. the supersaturation base level is acquired and is soil specific, explaining the 30 [mbar] monitored in the C3 seepage. As the extent of each seepage watershed evolves throughout the hydrological year, depending on high and low-flow conditions, the supersaturation base level may adapt to the intrinsic properties of newly contributing soil layers.

As for the A1 seepage watershed, with a soil cover of 0.2 to 0.3 meters, total initial amount of air present in pore space is far less important. Soil water storage is also limited. This implies a more efficient and quick degassing to the atmosphere and results in a supersaturation base level of 0 [mbar].

As the Dev spillway represents the cumulated contributions of all seepages spread out through the drainage gallery, which two end members are represented by the A1 and C3

seepages, its base level is observed at circa 10 [mbar]. The resulting average soil thickness of the restricted watershed is estimated to 0.45 meters.

The thickness of the vadose zone overhanging the A1 and the C3 seepage could also have been involved at some point. Indeed, high supersaturation levels can be reached due to the clogging of parts of the unsaturated zone conduits during high-flow periods. Thus, entrapped air undergoes compression by the water column above, leading to more gas being dissolved (Surbeck, 2005). The ticker the vadose zone is, the more gas can potentially be dissolved. Nevertheless, this hypothesis has to be ignored, as that kind of phenomenon would result in sharp well isolated peaks, and cannot in any case explain the constant base level values.

2.3.4.1 Implication regarding the contribution of a thick soil

The C3 seepage, as previously mentioned, is characterized by a thick soil cover. As such, noticeable amount of excess air can be produced, its peak values goes up to 45 [mbar] and its specific supersaturation base level reaches approximately 30 [mbar] (Fig. 40).

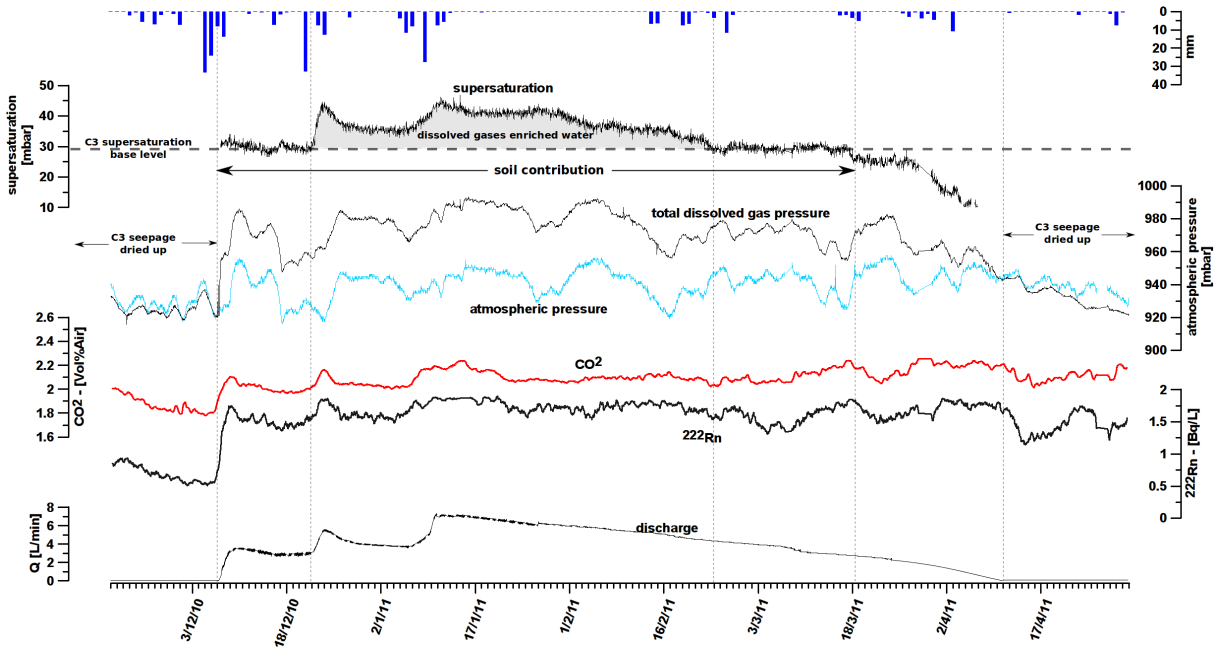

Fig. 40: Soil contribution to the C3 seepage from December 2010 to April 2011.

Thus, the assessment of soil contribution to the hydrodynamic of the seepage heavily depends on the previously mentioned base level. Indeed, when supersaturation is above its base level, it enhances the signature of rainfall/storm water at systems outlets, as seen between December 22nd 2010 and February 24th 2011. Between precipitation events, steady-state flow conditions with a high level of water saturation in the soil and well-organised flow routes through the vadose zone, allow a continuous and regular release, which is enhanced by constant levels of both radon and CO_2 and by the absence of noticeable supersaturation peaks. Radon and CO_2 concentrations only increase in reaction to rainfalls, as pre-event water is pushed down the system by the newly formed water column. It can be described as a piston flow. When supersaturation reaches its base level, water arriving at the outlet is not any more under the influence of fresh, gas enriched, storm water, but rather reflects the contribution of soil water that has been stored for a sufficiently long time to undergo degassing to the atmosphere. This base-level signed water is constantly released from the soil to the unsaturated zone, and contributes to the flow regime in combination with the epiphreatic reservoir. Two scenarios can be observed. On the one hand, at the beginning of December 2010, coinciding with the resumption of the discharge in the C3 seepage, deep soil pre-event water arrives at the outlet through a piston effect, as radon and CO_2 reach peak levels and supersaturation is stable. On the other hand, between February 24th 2011 and March 18th, soil contributes to the dynamic of the seepage by constant release, as depicted by the supersaturation base level, and the quite stable radon and CO_2 concentrations. The slight drop observed regarding the radon curve around March 7th, is linked to the shorter half-life of radon compared with the one characterizing the CO_2. Indeed, as low-flow conditions are progressively prevailing, the transit time through the vadose zone increases. Discharge is diminishing further, and radon concentration in water tends to equilibrate with radon level in the air. Air radon content is affected by the atmospheric pressure, as low pressures allow radon release from limestone and residual seepages, by a suction phenomenon. Starting from March 18th, the progressive equilibrium being reached, is enhanced, as the difference between total dissolved gas pressure in water and atmospheric pressure decreases further more. This is depicted by the supersaturation values passing under the base level. From this moment, data assessing dissolved gas content in water of the collecting bucket, doesn't permit to identify any soil contribution, and the flow, is mainly sustained by seepage-flow from the low permeability volume. Moreover, the remarkable difference measured regarding radon concentrations, during low discharge episodes (before December 7th and after March 18th) depending on seasons, may be explained by a ventilation effect (Nagy *et al.*, 2012). The temperature gradient, which affect air density, between the gallery and outside air is

involved. Indeed, when the outdoor air temperature is lower than the gallery air temperature, which is the case in December 2010, the cold air flows from outside into the gallery, and the radon concentration decreases in the gallery and remains low. However, when the outdoor air temperature is higher than the gallery air temperature, the denser gallery air is stuck, minimising the ventilation. Therefore, radon concentrations increase or stay high, which were monitored starting from March 18th when the discharge is low or non existent.

Thus, the contribution of the soil reservoir to the C3 seepage, revealed by the supersaturation base level maximal extension, spreads out from December 7th to March 18th. It noticeable contribute to the system recharge, as discharge undergoes significant variations.

2.3.4.2 Implication regarding the contribution of a thin soil

As the watershed drained by the A1 seepage is characterized by a thin soil cover, less air in the pore space is available for dissolution, resulting in supersaturation peaks not exceeding 16 [mbar]. A thin soil also enables more efficient degassing which results in a supersaturation base level close to 0 [mbar], which is also close to a non-relevancy level. Indeed, when comparing total dissolved gas pressure in the A1 sampling point with the atmospheric pressure, it is obvious how closely related they are (Fig. 41). The only noticeable differences occur during supersaturation sharp peaks in reaction to precipitation events. As such, in order to identify soil contribution periods, discharge plays a discriminant role. As mentioned above, if discharge is low the gas phase in water is prone to equilibrate with the air in the gallery. Thus the low-flow periods before December 7th 2010 and after March 14th 2011, are typical of a no-soil contribution signature. The difference, with regards to low and higher radon concentrations, reflects the previously mentioned seasonal ventilation effect. As discharge is sufficient, from December 7th 2010 to Mar 14th 2011, dissolved gas content is relevant. As such the codependent supersaturation, radon and CO_2 pulses, reflect the contribution of rainfall, gas enriched water originating from the soil. The in between supersaturation base-level, and stable radon and CO_2 concentrations, depict the continuous release of water from the soil reservoir.

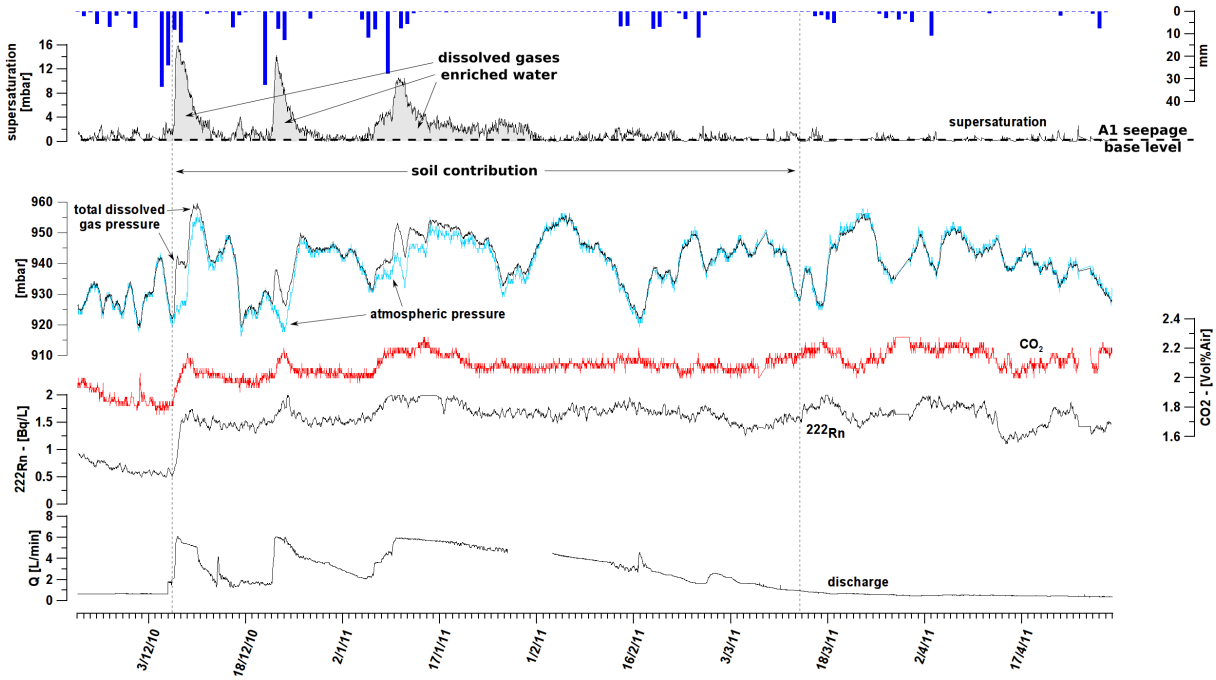

Fig. 41: Soil contribution to the A1 seepage from December 2010 to April 2011.

2.3.4.3 The Dev spillway survey

On the contrary to the C3 and A1 seepages which represent karst systems of a rather limited extension, the Dev spillway depicts the contributions of all seepage distributed throughout the drainage gallery. As such its base level supersaturation of circa 10 [mbar] represents the weighted average of all water inflows (Fig. 42). Maximum supersaturation values around 50 [mbar] are influenced by thicker soil contribution, whereas excess air sharp peaks rather points out to a thinner soil related reactivity. Based on the supersaturation base-level of 10 [mbar], the soil thickness of the system was estimated to 0.45 meters. During the following discussed period, i.e. from November 2010 to July 2011, the Dev spillway monitoring reveals that soil contribution to the gallery dynamics is constant. Indeed, from November 16th 2010 to March 17th, soil stored water discharging in the gallery is characterized by a dissolved gas enriched signature, as can be seen by supersaturation being above its base level. Between November 2010 and mid-January 2011, the system reveals a noticeable reactivity, as following precipitation events, codependent supersaturation, radon and CO_2 pulses are monitored, pointing out to the arrival of fresh, gas enriched water stored in the soil.

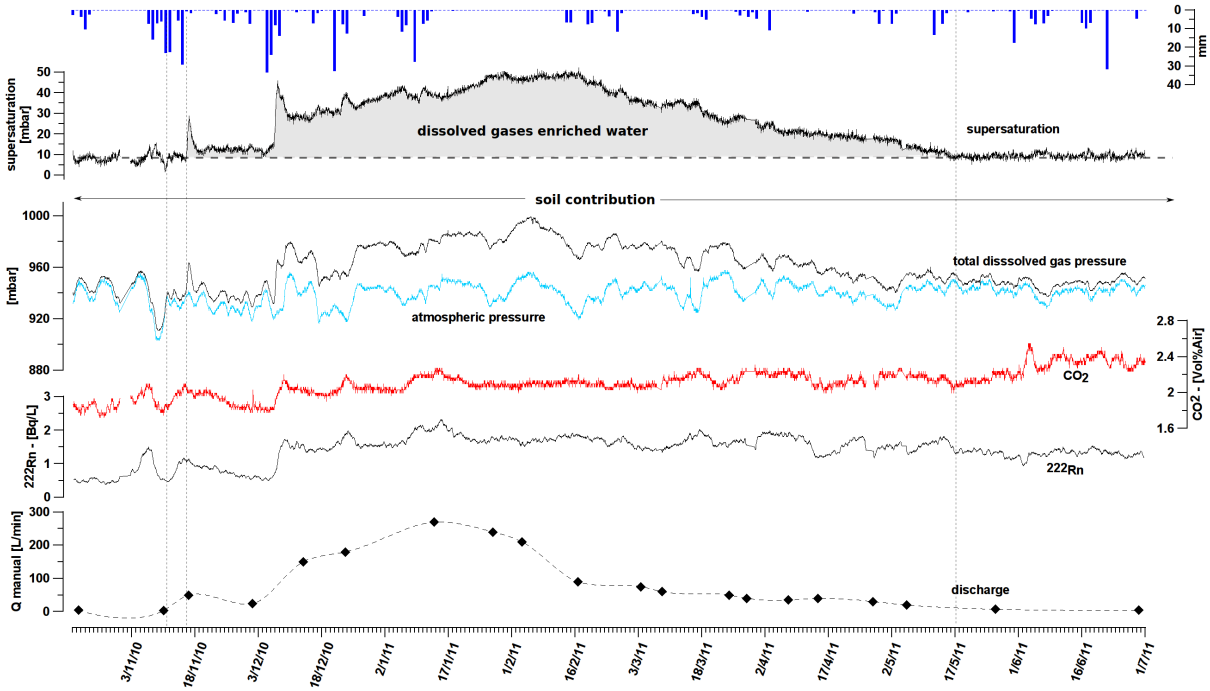

Fig. 42: Soil contribution to the Dev spillway from December 2010 to July 2011.

The first noticeable discharge decrease reaching a low point of 85 [L/min] measured on February 16th, is the result of very scarce rainfall events. Even though the flow rate is gradually diminishing, gas enriched water is still released to the system and will be monitored until May 17th, when discharge only accounts for 8 [L/min]. After May 17th, the supersaturation content meets its base level, it characterizes the constant contribution of residual water stored in the soil for a sufficient time to undergo degassing to the atmosphere and acquire the base level signature. The continuous release of soil stored water to the system outlet is also enhanced by quite high and stable radon and CO_2 values. The increasing CO_2 content in June 2011 reflects an intense biological activity.

2.3.5 The dissolved gases approach in a selected porous media aquifer

It is noteworthy that during the survey of the artificial drainage gallery, no contribution from the epikarst sub-system was monitored. Indeed, an epikarst storage signal would have been theoretically revealed by low radon concentrations and increasing CO_2 levels. This characteristic could involve a poor development of the epikarst which would only act as flow concentrating media.

In order to confirm the codependent evolution of both radon and carbon dioxide, reflecting only a typical soil water signature, excluding any epikarst contribution, Martini (2012) used the dissolved gases approach in a porous media aquifer.

2.3.5.1 The Mont Gibloux study area

The Mont Gibloux (Fribourg, Switzerland) is a hill situated a couple of kilometers west of the Gruyère Lake in the Sorens district (Fig. 43). Its altitude ranges from 1000 to 1200 m.

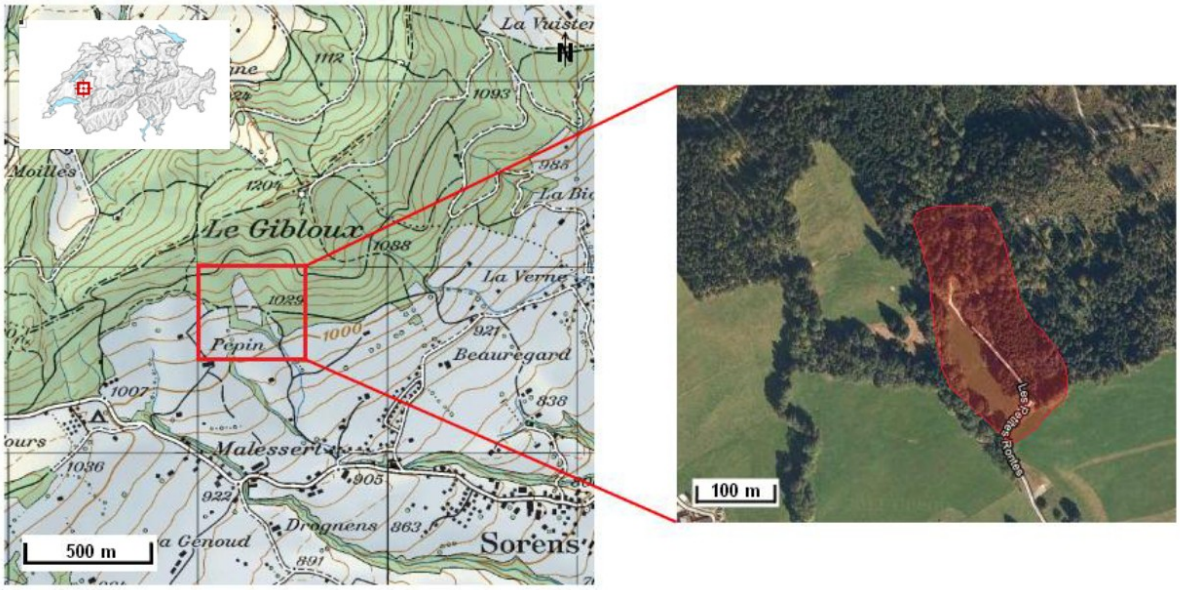

Fig. 43: Localisation of the Mont Gibloux study area (modified afted Martini 2012).

2.3.5.1.1 Climate

Average annual rainfall in the Mont Gibloux area is about 1250 mm with an average yearly temperature of 6°C (Mététosuisse weather station, Planfayon).

2.3.5.1.2 Geology

The Mont Gibloux hill is situated on the northern margin of the Subalpine Molasse overlap over the Molasse Basin, which is the northern foreland basin of the Alps and formed during the Oligocene and Miocene. The study area is depicted as an antycline structure, whose dip points towards the north-east. It is manly composed of Tertiary Molasse covered by alpine moraines. Braun soil overhangs the previously mentioned moraines.

2.3.5.1.3 Local hydrogeology

The Mont Gibloux aquifers are characterized by two end members (Martini, 2012). On the one hand a deeper molassic aquifer component, depicted by a significant residence time. Water contributing to the discharge is a combination between regional and local groundwater flows. On the other hand, sub-surface moraine aquifers which show noticeable physico-chemical variations and are prone to be noticeably influenced by meteorological events.

2.3.5.1.4 Description of the followed outlets

Between November 2011 and July 2012, Martini applied the dissolved gases approach on several outlets, consisting in drains, used to provide drinkable water to the Sorens district (Fig. 44). Water originating from all these outlets discharges in a “water collecting facility”. They are located on the souther slope of the hill within sub-surface moraine aquifers. The following description will only focus on two outlets, the 123 and 40 drains, whose watersheds are homogeneously covered by brown soil (Sottas, 2010) and overhanged respectively by forest and pasture land. According to Gobat *et al.* (1998), as the soil is a rather an old component, it is not unusual to find the same soil type under forests and pasture when situated in the same area. The only noticeable difference consists in the

humus, which is prone to develop specific features if situated under forests or pasture land.

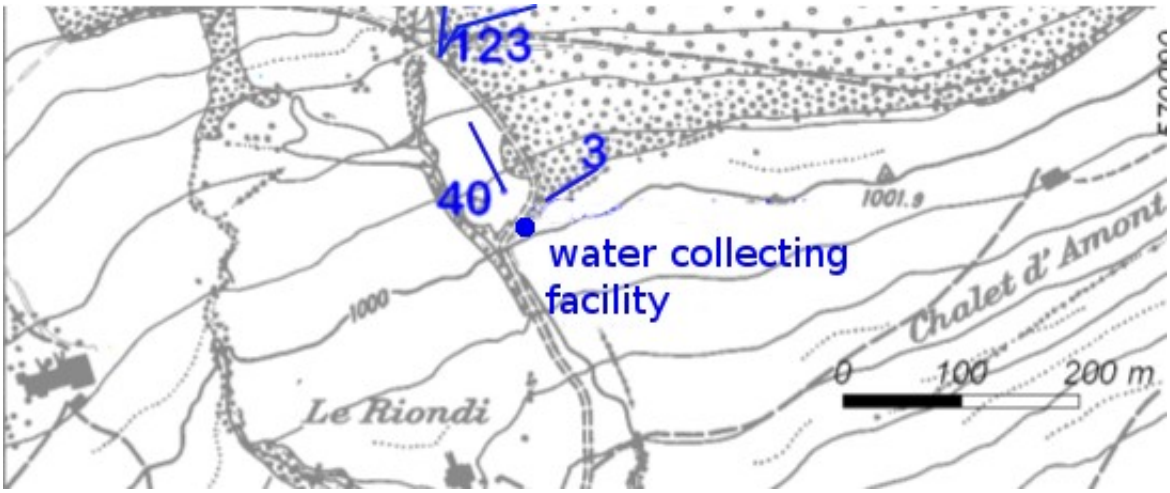

Fig. 44: Localisation of selected drains (123 and 40) on the southern slope of the Mont Gibloux hill (modified after ABA-GEOL SA, 2006).

2.3.5.1.5 Results and interpretations

Outlet 40 under pasture land in April 2012

Until April 7th discharge in the 40 drain is sustained by the moraine aquifer (Fig. 45). Indeed, the discharge and electrical conductivity are stable around respectively 8 [L/min] and 530 [µS/cm] (Fig. 46). Nevertheless, in reaction to the 32 [mm] precipitation event between April 3rd to 5th, some soil stored water contributes to the system, which is enhanced by a synchronous radon, CO_2 and supersaturation increase. This contribution, even though limited, is instantaneous, as it happens with rainfalls (i.e. on April 3rd) and could imply a piston effect.

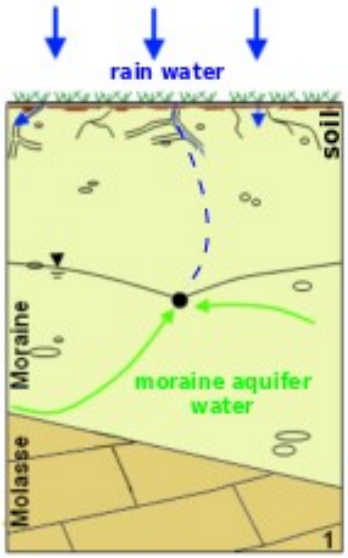

Fig. 45: Conceptual flow model during moraine aquifer predominant contribution (modified after Martini, 2012).

A noticeable rainfall of 36 [mm] on April 7th initiates the first massive arrival of soil water. Indeed, an 18 [mbar] supersaturation pulse, along with a radon and CO_2 increase is observed. The discharge synchronously reaches 85 [L/min], accompanied by a remarkable eC negative pulse. The negative evolution of eC values doesn't necessarily reflect direct rain water infiltrations, but rather underlines the reactivity of the system and poor soil storage capacity. The soil layer is quickly saturated with fresh water which isn't stored long enough in soil before release to acquire a noticeable mineralisation.

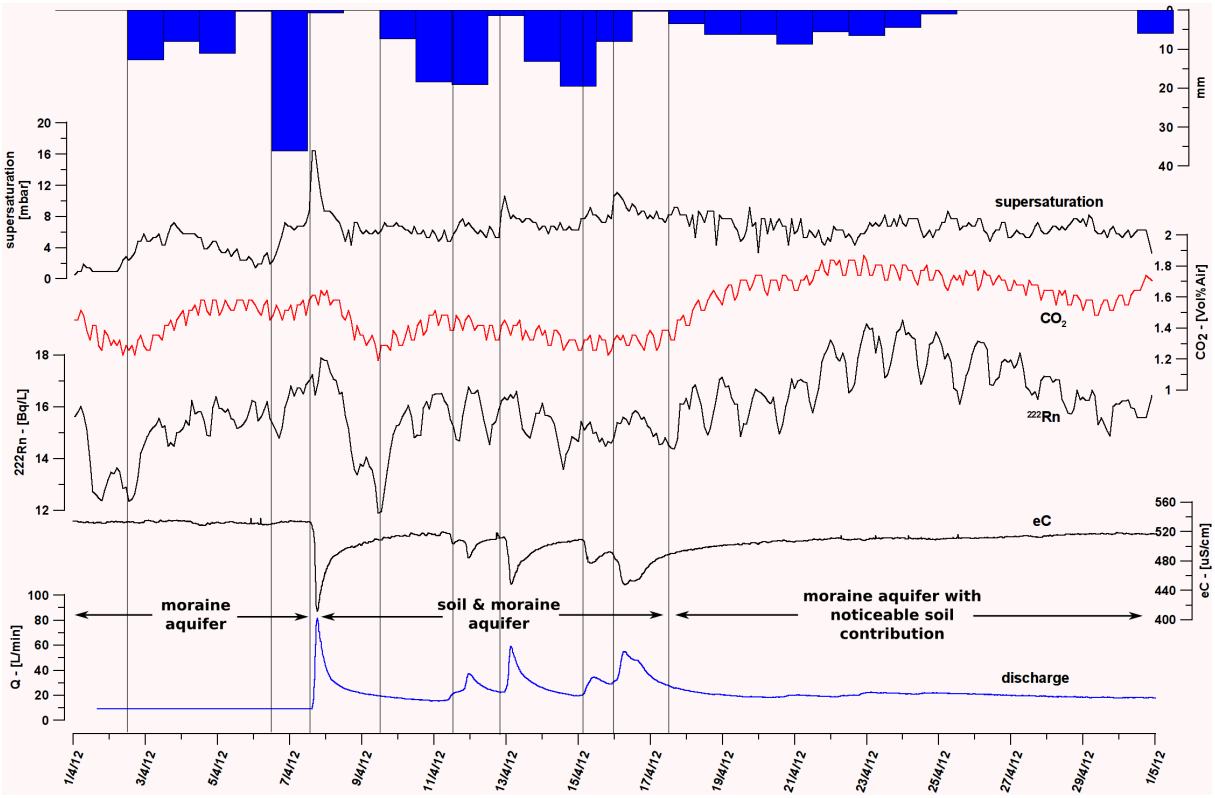

Fig. 46: Dissoved gases in the 40 drain in April 2012. Measurement uncertainties : Rn:~3%, CO_2:~7%, supersaturation:~3%.

Following this event, discharge quickly diminishes along with radon and CO_2 values while eC levels increase. These features imply a renewed dominant influence of the moraine aquifer which attenuates the soil water signature.

The moderate and continuous rainfall event of 85 [mm] between April 10th to 16th is enhanced by a succession of discharge increases and eC negative pulses, accompanied every time by supersaturation peaks of limited amplitude. Once again, a piston effect is involved as radon and CO_2 levels codependently increase with rainfalls from April 10th to remain stable until April 17th. These characteristics reveal an alternate contribution on the

hydrodynamic of the system, between water originating from the moraine aquifer and a noticeable poorly mineralized soil water component (Fig. 47).

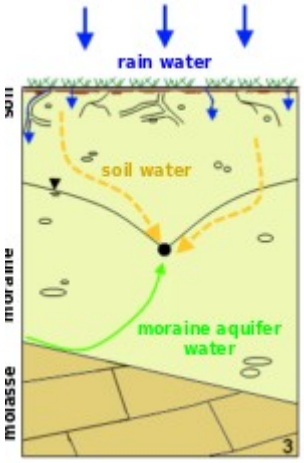

Fig. 47: Conceptual flow model during moraine aquifer and soil alternate contributions (modified after Martini, 2012).

The last slight precipitation event of 42 [mm] between April 18th to 25th doesn't result in any significant discharge increase. Indeed, the flow is mainly sustained by the moraine aquifer as depicted by the stable discharge rate end eC level. Nevertheless, the soil plays a noticeable role by continuously releasing water to the system, which is enhanced by ever growing radon and CO_2 contents. Moreover, eC levels, even though stable, are inferior by some 10 [µS/cm] to the one measured at the very beginning of the survey when the discharge was predominantly sustained by the moraine aquifer, underlining the soil contribution as well.

Outlet 123 under forest in April 2012

Until April 7th discharge in the 123 drain is sustained by the moraine aquifer (Fig. 48). Discharge and electrical conductivity are stable around respectively 15 [L/min] and 530 [µS/cm] (Fig. 49). Nevertheless, in reaction to the 32 [mm] precipitation event between April 3rd to 5th, some soil stored water contributes to the system, which is enhanced by a synchronous radon, CO_2 and slight supersaturation increase. This contribution, even though limited, is instantaneous, happening on April 3rd and could imply a piston effect.

A rainfall of 36 [mm] on April 7th initiates the first arrival of soil water noticeably contributing to the discharge, which reaches 25 [L/min]. Indeed, an 18 [mbar] supersaturation pulse, along with a radon and CO_2 increase is observed, along with turbidity, TOC

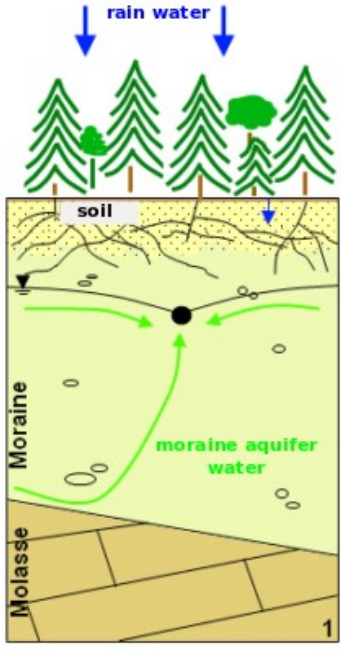

Fig. 48: Conceptual flow model during moraine aquifer predominant contribution (modified after Martini, 2012).

and eC pulses. As no more rainfalls occurred until April 10th, this first soil episode is diluted by the moraine aquifer water, resulting in a radon and CO_2 levels diminishing. The high storage capacity of the soil is enhanced by eC values never showing any negative pulses. Indeed, poorly mineralized rain water is stored in the soil doesn't reach the 123 drain.

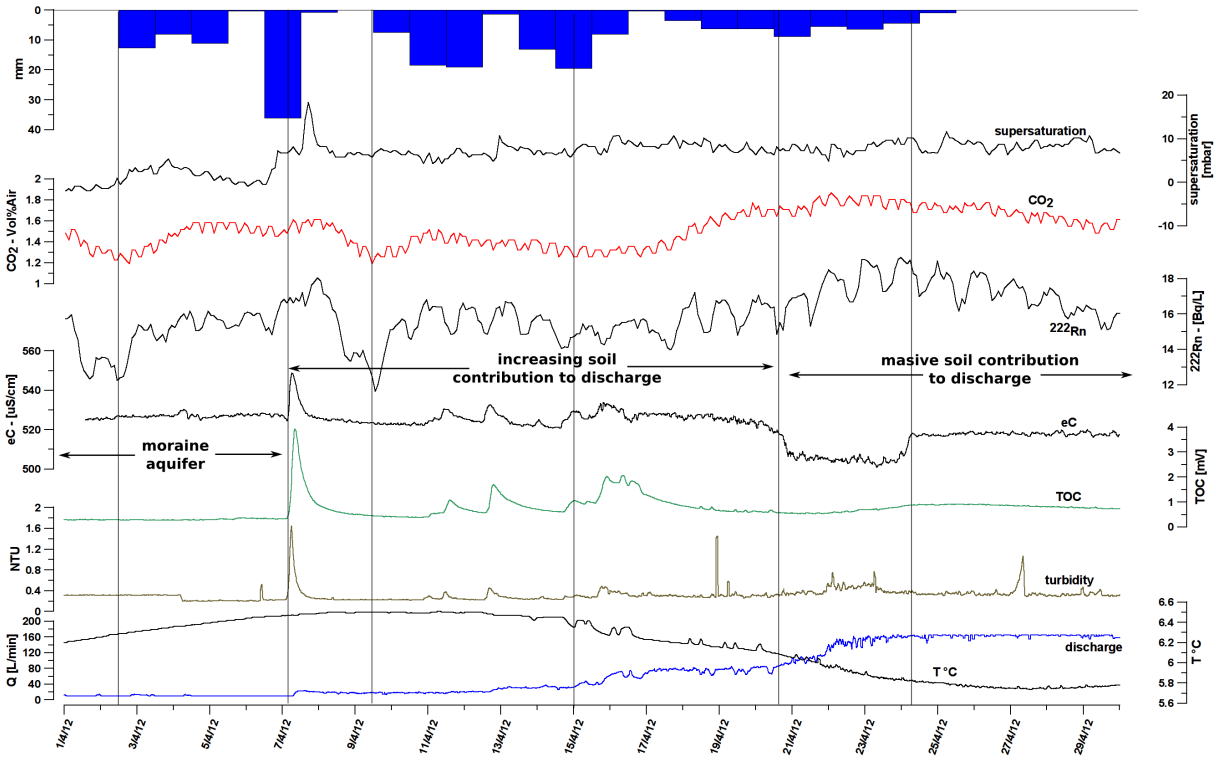

Fig. 49: Dissoved gases in the 123 drain in April 2012. Measurement uncertainties : Rn:~3%, CO2:~7%, supersaturation:~3%.

The rainfall event of 85 [mm] between April 10th to 16th is enhanced by a continuous and progressive discharge increases and eC, TOC and turbidity pulses, accompanied by supersaturation peaks of very limited amplitude. A piston effect is involved as radon and CO_2 levels codependently increase with rainfalls from April 10th to remain stable until April 17th. These characteristics reveal a combined contribution on the hydrodynamic of the system, between water originating from the moraine aquifer and a noticeable pre-event, mineralized, soil water. It also marks the very beginning of fresh soil stored water as the temperature diminishes.

The last slight precipitation event of 42 [mm] between April 18th to 25th continues the progressive discharge increase trend. Fresh soil stored water increasingly contributes to the hydrodynamic of the system, as radon and CO_2 levels increase and temperature shows a negative trend. The soil high storage capacity under forest and vegetation water

interception are underlined on April 21st. Indeed, until this date fresh rain water contribution to the discharge was limited and only characterized by a progressive temperature diminishing. Whereas April 21st is marked by massive fresh soil stored water release as eC undergo a noticeable negative evolution, and radon, CO_2 and discharge reach their highest levels.

On April 24th the contribution of the moraine aquifer to the discharge is noticeable again, as can be seen by the eC increase. It coincides with the end of the last precipitation event. Nevertheless, soil water highly influences the system, as radon and CO_2 levels, even though diminishing, remain high and temperature reaches a low point, accompanied by a discharge maximum.

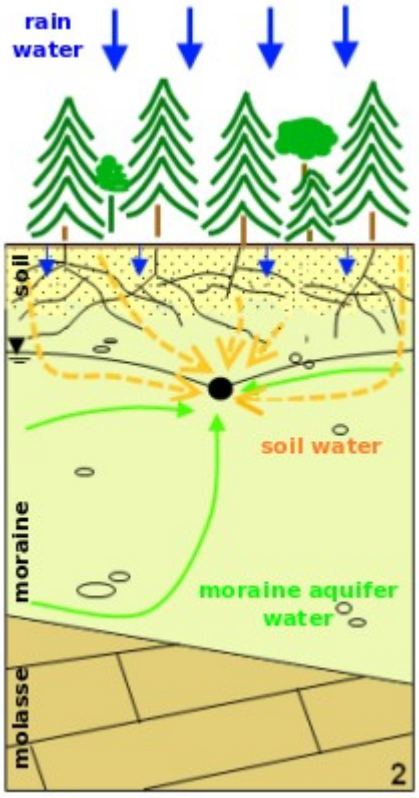

Fig. 50: Conceptual flow model during soil predominant water contribution (modified after Martini, 2012).

2.3.5.1.6 Conclusion

The monitoring of dissolved gases at the Mont Gibloux test site allowed to assess soil contribution to the hydrodynamic of the system. Moreover, this study allowed to confirm that a codependent evolution of radon and carbon dioxide, reflects the signature of soil stored water, as it is the only production source for both these gases.

The forest cover and pasture land noticeably influence the flow regime of the monitored outlets.
Indeed, the 40 drain, situated under pasture land is depicted by a low storage capacity, as fresh rain water quickly reaches the outlet. In addition, the discharge shows quite a nervous behaviour with sharp peaks. Following a precipitation event, it reaches its base level mainly sustained by the moraine aquifer.

The forest and the forest soil covering the watershed of the 123 drain, play a drastically different role. Indeed, precipitations are intercepted by trees, preventing a high amplitude variation of the discharge. Moreover, the significant storage and buffer capacity of a forest covered soil is enhanced on the one hand by the discharge increasing progressively and on the other hand by a remarkable amount of rainfall needed for fresh water to reach the outlet.

3 Conclusion

Among drinking water resources throughout the world, karst aquifers play a prominent role, as they are accounted for about 25% of the global population supply. Due to their specific hydrogeological features, they are characterized by significant vulnerabilities and may undergo noticeable contaminations (e.g. Ford and Williams, 1989). Therefore, in a karst system it is relevant to discriminate between water originating from the soil reservoir, the epikarst, the low permeability volume and the freshly infiltrated rainwater. To do so, a combined monitoring of radon, CO_2 and TDGP (total dissolved gas pressure), along with more classical parameters such as turbidity, total organic carbon and electrical conductivity was carried out in the Prédernier artificial drainage gallery. Chemical and physical data recovered from the monitoring period allowed to infer some statements regarding the processes governing the hydrodynamics of the test site. Increasing radon, CO_2 and supersaturation concentrations at system outlets underline the soil contribution to the discharge, whereas fresh rain water and low permeability volume seepage is depicted by low levels of these gases and discriminated by means of electrical conductivity. The epikarst input to the flow regime could not be identified as radon and CO_2 evolve codependently, only reflecting soil water. This soil specific feature was confirmed by data obtained at the Mont Gibloux hill, where drains are situated within moraine aquifers.

3.1 Dissolved gases as indicators for soil contribution to a karst system

The continuous monitoring of dissolved gases revealed the importance of the soil sub-system with regards to its influence on the recharge of karst aquifers and on the sustainability of its contribution to the flow regime. In the ideal case where the discharge in the sampling point is sufficient, to prevent the gas phase in water to reach an equilibrium with the surrounding air, the supersaturation base-level may be used as a relevant surrogate to assess the temporal distribution of soil contribution to a karst system flow regime. Whereas, codependent radon, CO_2 and supersaturation peaks or rising levels, depict the influence of soil stored water, enriched in dissolved gases during rainfall events.

The dissolved gases approach also enhanced processes governing soil water storage and release, depending on the intensity of precipitation events and on soil thickness. These intrinsic properties result in a specific dissolved gases signature at the system outlet.

3.1.1 Thin soil cover

Following a precipitation event, the ideal response of a karst system characterized by a thin soil cover would result in the following signals (Fig. 51).

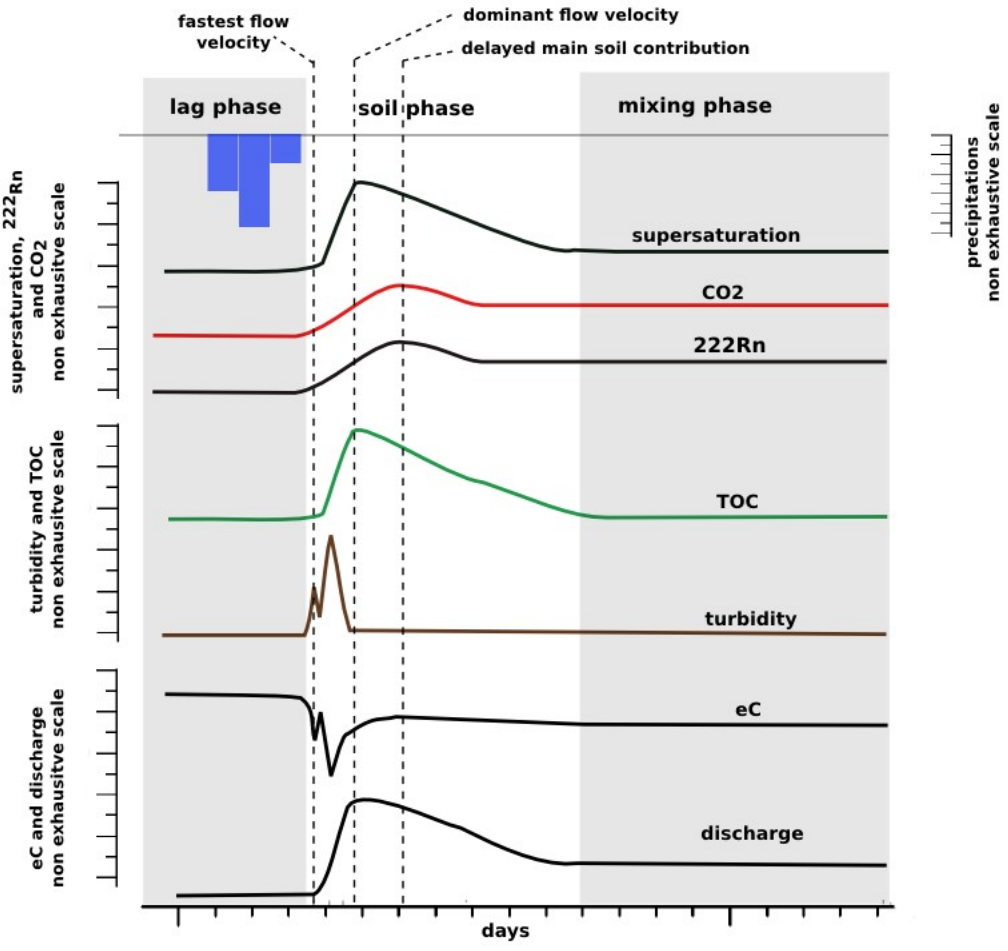

Fig. 51: Conceptual response of a thin soil covered karst system in reaction to rainfalls.

As fresh rain water is used to replenish the soil reservoir, the system outlet shows no reaction. Dissolved gases concentrations, turbidity, TOC and discharge levels are constant and low. The discharge is mainly supplied by seepage-flow through the low permeability volume, which is underlined by higher eC values. These features characterize the lag phase, whose duration depends on the initial water saturation of the soil. During this phase, if the

discharge rate is too low, dissolved gases content in water is in equilibrium with the surrounding air.
Once the soil water content is more than field capacity, water can bypass the soil reservoir through preferential flow paths (roots channels, wetting front contrast, fissures), and contributes to the discharge resumption. This fastest flow velocity event initiates the beginning of the soil phase. It is accompanied by an eC drop and an autochthonous turbidity peak resulting from the remobilisation of intrakarstic material by increasing flow velocities. The progressive influence of the soil cover is enhanced by the ever-growing levels of TOC, supersaturation, radon and carbon dioxide and by an allochthonous turbidity peak. The latter occurs during the rising limb of the TOC curve. This behaviour is linked to exclusion processes, which results in faster transport of particles and colloids, in comparison to solutes. The dominating flow velocity from the soil coincides with TOC, supersaturation and discharge peak values reached simultaneously. Consequently to this dominant flow event, the delayed contribution of both radon and carbon dioxide, which are continuously produced in the soil, may be explained by higher concentrations reached during a reduced flow regime. It enhances the deferred influence of soil stored water to the system. Though the gas enriched soil water contribution diminishes (supersaturation decreasing), radon and carbon dioxide levels remain high, which underlines the soil reservoir noticeable role regarding the recharge of karstic aquifers.
The supersaturation reaching its remanent base level, which is soil thickness dependent, marks the transition to the mixed phase. Following partial recharge of the system, water discharging at outlets is a mixture of soil water, rainwater and of an increasing epiphreatic flow component.

3.1.2 Tick soil cover

Distinguishing features reflecting the sequence of answers characterizing a karst system covered with a thick soil, may be described as follows. The described responses follow a very dry period.

During the lag phase, a first precipitation event has occurred, but the system shows no reaction (Fig. 52). Pre-event water stored in the thick soil has acquired a remanent supersaturation signature. Fresh rain water replenishes the remaining soil volume, resulting in an increasing soil water content and hydraulic head.

Once soil field capacity is reached, fresh water contributes to the resumption of the discharge through preferential flow paths, which is enhanced by a pulse-through turbidity event and a negative eC signal (fastest flow velocity). It is accompanied by the very beginning of deep soil, pre-event water, as the carbon dioxide and radon levels start to rise, while supersaturation is depicted by its base level. Consequently to the newly applied hydrostatic pressure by the fresh water column, pre-event mineralized water undergoes a piston-like effect and is massively released into the system. This results into synchronous radon and carbon dioxide wide peaks, along with a supersaturation constant level and eC increase, which enhances the dominating flow velocity of the deep soil reservoir. The very slight flow-through turbidity and TOC pulses underline the very limited upper soil contribution.

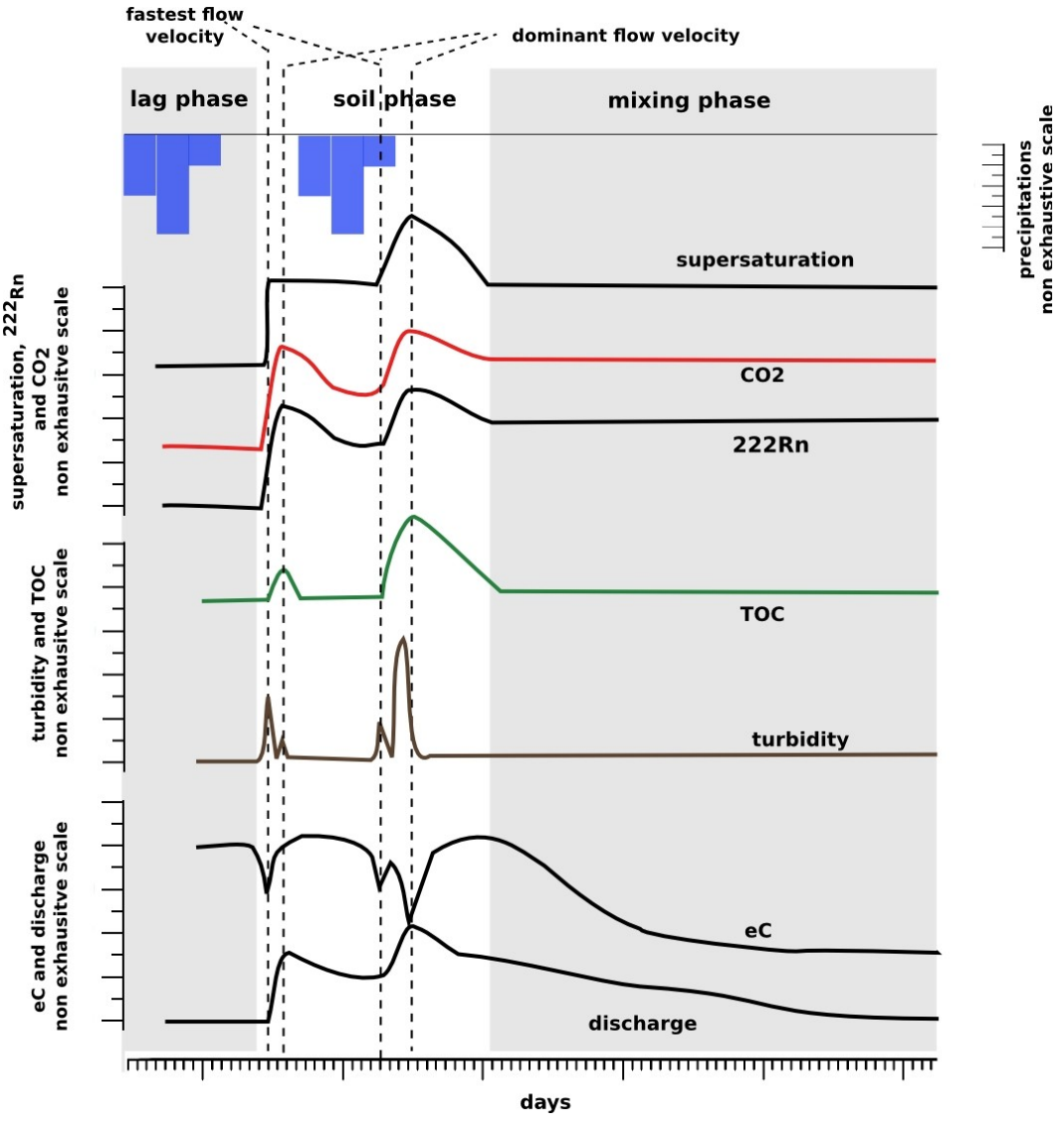

Fig. 52: Conceptual response of a thick soil covered karst system in reaction to rainfalls.

In order for the soil stored water, resulting from the first rainfall event to contribute to the discharge, additional precipitations are necessary. In reaction to this recently applied water head, the gas enriched water volume migrates to the outlet, which is reflected by simultaneous supersaturation, radon, carbon dioxide, TOC and discharge peak values. The flow-through turbidity precedes the associated TOC and supersaturation signal (exclusion phenomenons) and its higher concentrations enhance the upper soil influence on the dynamic of the system. During this sequence no delayed contribution of the soil reservoir is revealed. Indeed, the pre-event water resulting from the first rainfall event, such as the more recent water stored in the soil during the second one, acquired a high radon, carbon dioxide and supersaturation content during their migration trough the tick soil layer.
As no more rainfalls happened, the gas enriched water influence diminishes and the mixed phase is initiated. It reveals a constant contribution of the deeper soil reservoir, depicted by very low TOC and turbidity concentrations and by a constant base level remanent supersaturation level, along with stable and high radon and carbon dioxide values. The progressive epiphreatic predominance is underlined by the decreasing eC level.

3.2 Limitations and perspectives

The presented dissolved gases approach permits identifying the soil sub-system contribution in the selected karst aquifer system, with regards to its influence on the recharge and on the sustainability of its influence to the flow regime.
During high-flow conditions, the continuous monitoring of supersaturation, radon and carbon dioxide proved to be a very valuable method to assess the dynamic governing the different seepages in the Prédernier gallery. Nevertheless, very low discharge rates represent a noticeable drawback. Indeed, it allows the gas phase in water to equilibrate with the air in the drainage gallery, resulting in a set of data not usable for any interpretation. To overcome this issue, the monitoring of these gases in the air surrounding the outlet could be of interest, as it would permit identifying non-relevancy episodes. Moreover, in order to assess more efficiently the transit time of soil stored water, measures of radon concentrations in the soil should be considered. The investigation at other karst aquifer systems, known for their more stable discharge, would permit obtaining valuable data to describe an entire hydrological year.
Furthermore, no evidence was monitored regarding an epikarstic water storage. Thus, the survey of another test site characterized by a well developed epikarst sub-system, would

allow to gain significant insight into the codependent evolution of both radon and carbon dioxide.

Another constraining factor, with regards to radon, highly depends on its half-life of 3.8 days. It implies that the transit time between the radon production origin and the outlet doesn't exceed twenty days. Indeed, after this time range, its concentrations are under detection limits.

As for supersaturation, it definitely deserves more attention among hydrogeologists. Supersaturation seems to be rather the rule than the exception in karst systems (Surbeck, 2005). In order to assess karst system vulnerability, it may be of interest to compare the supersaturation signal with the occurrence of faecal indicator bacteria, such as *Escherichia coli* and enterococci, which indicates the possible presence of pathogenic bacteria, protozoa and viruses.

4 Appendices

Appendix I: Introduction

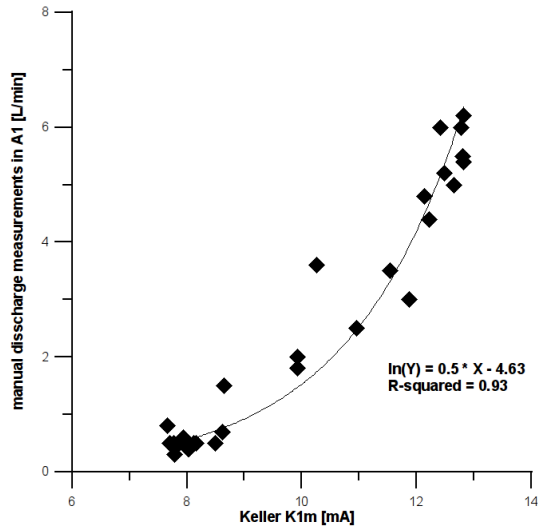

Fig. 53: Discharge calibration in A1 seepage (Keller 1m).

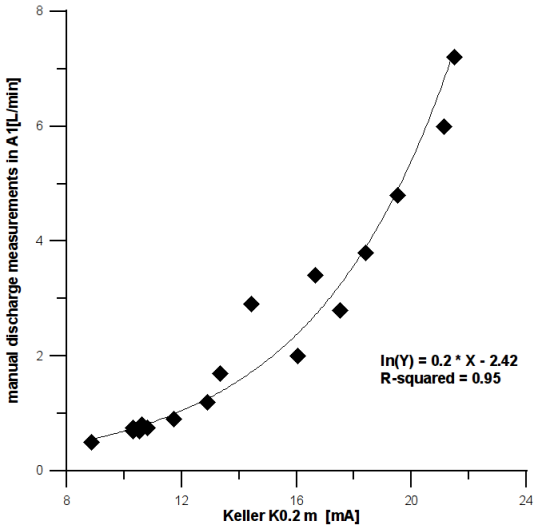

Fig. 54: Discharge calibration in A1 seepage (Keller 0.2 m).

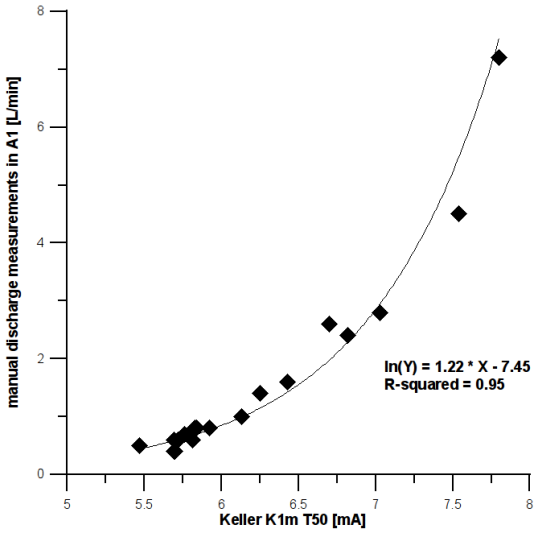

Fig. 55: Discharge calibration in A1 seepage (Keller 1m, DT50).

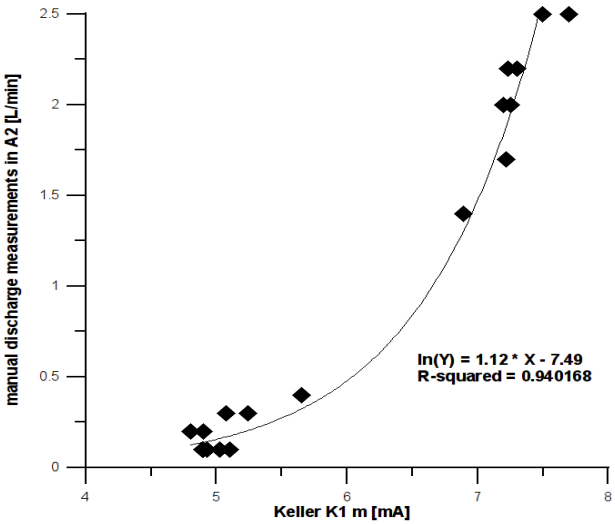

Fig. 56: Discharge calibration in A2 seepage (Keller 1 m).

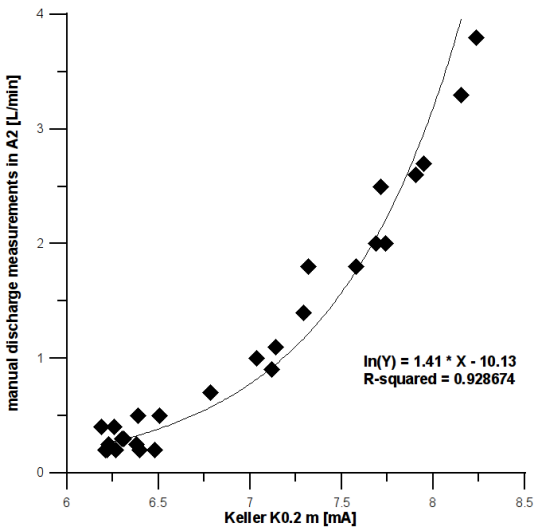

Fig. 57: Discharge calibration in A2 seepage (Keller 0.2 m).

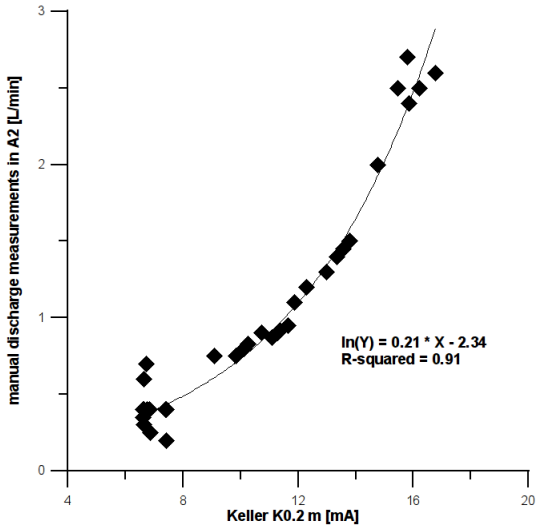

Fig. 58: Discharge calibration in A2 seepage (Keller 0.2 m, DT50).

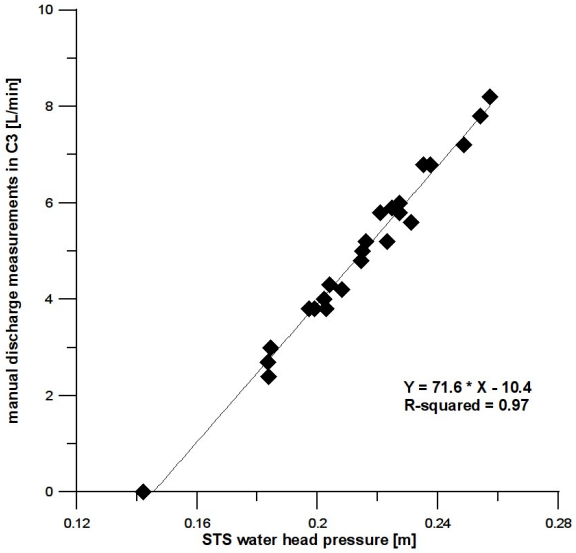

Fig. 59: Discharge calibration at C3 seepage (STS, DL/N 64).

Samples	HCO3 TAC	Li	Na	NH4	K	Mg	Ca	Sr	F	Cl	NO2	Br	NO3	PO4	SO4		cations	anions	balance		date
	mg/L	mg/L	mg/L	mg/L	mg/L	mg/L	mg/L	mg/L	mg/L	mg/L	mg/L	mg/L	mg/L	mg/L	mg/L						
DEV	194.22		0.82	0.14	0.40	5.71	59.14	0.27		1.77			6.33		7.28		3.48	3.49	-0.1 %		11.11.11
A1	185.93		0.79	0.11	0.41	5.14	58.21	0.23		1.58			6.53		7.93		3.38	3.36	0.3 %		11.11.11
A2	182.27		0.74	0.07	0.34	5.14	58.04	0.26		1.59			6.65		9.09		3.37	3.33	0.6 %		11.11.11
DEV	203.98		5.96	0.23	0.68	9.34	75.87	0.49		1.85			6.39		56.77		4.85	4.68	1.8 %		13.12.11
A1	192.27		0.90	0.23	0.46	5.36	63.33	0.20		1.67			6.58		7.52		3.67	3.46	2.9 %		13.12.11
A2	192.27		0.93	0.20	0.47	5.41	63.58	0.20		1.77			6.46		7.98		3.68	3.47	3.0 %		13.12.11
DEV	199.84		3.94	0.20	0.66	8.12	69.62	0.42		1.69			5.64		37.23		4.35	4.19	1.9 %		22.12.11
A1	190.56		0.72	0.13	0.33	4.99	61.93	0.17		1.60			6.33		5.94		3.55	3.39	2.2 %		22.12.11
A2	187.64		0.70	0.12	0.34	5.00	62.07	0.17		1.57			6.21		5.96		3.56	3.34	3.1 %		22.12.11
C3	193.74		0.81	0.08	0.39	5.41	61.50	0.19		1.38			5.13		5.66		3.57	3.41	2.2 %		22.12.11
G4	194.71		9.77	0.19	0.93	13.51	81.59	0.83		1.41			6.01		96.70		5.65	5.34	2.8 %		22.12.11
DEV	198.62		1.82	0.14	0.44	6.17	63.38	0.27		1.41			5.36		16.32		3.77	3.72	0.7 %		12.01.12
A1	187.88		0.71	0.12	0.36	4.52	59.42			1.65			6.29		4.61		3.38	3.32	0.9 %		12.01.12
A2	187.39		0.68	0.11	0.32	4.50	59.62			1.60			6.21		4.55		3.39	3.31	1.2 %		12.01.12
C3	194.22		0.78	0.14	0.38	5.39	62.82	0.21		1.30			4.69		5.19		3.63	3.40	3.3 %		12.01.12
G4	193.49		4.42	0.14	0.61	8.49	67.83	0.45		1.25			5.21		40.05		4.30	4.12	2.1 %		12.01.12
DEV	178.36		1.62	0.12	0.51	5.74	58.68	0.23		1.38			5.82		14.93		3.49	3.37	1.8 %		16.02.12
A1	182.76		0.66	0.05	0.30	4.73	57.62			1.62			7.10		5.79		3.30	3.28	0.4 %		16.02.12
A2	180.56		0.64	0.05	0.29	4.69	57.80			1.62			7.04		5.55		3.31	3.23	1.1 %		16.02.12
C3	181.54		0.65	0.04	0.35	5.07	56.74	0.18		1.07			5.45		6.10		3.29	3.22	1.1 %		16.02.12
G4	179.34		3.27	0.07	0.61	7.37	61.26	0.34		1.20			5.72		32.75		3.83	3.75	1.1 %		16.02.12
DEV	187.88		1.82	0.05	0.43	6.00	58.85	0.22		1.56			6.06		18.84		3.53	3.61	-1.2 %		13.03.12
A1	183.24		0.63	0.04	0.40	4.85	57.26			1.73			6.89		5.90		3.30	3.29	0.2 %		13.03.12
A2	186.66		0.63		0.31	4.88	57.70			1.66			6.96		6.05		3.32	3.34	-0.4 %		13.03.12
C3	178.36		0.65	0.06	0.45	4.99	54.90	0.21		1.17			5.68		6.19		3.20	3.18	0.3 %		13.03.12
G4	182.27		4.20	0.09	0.79	7.88	61.59	0.36		1.72			5.98		42.36		3.93	4.01	-1.0 %		13.03.12
DEV	190.32		1.90	0.03	0.60	5.55	58.56	0.32		2.09			5.76		14.73		3.48	3.58	-1.4 %		12.04.12
A1	187.88		0.67		0.29	4.49	56.85	0.16		1.68			6.06		4.31		3.24	3.31	-1.1 %		12.04.12
A2	191.3		0.71	0.05	0.38	4.50	56.90	0.15		1.66			6.13		4.29		3.26	3.37	-1.7 %		12.04.12
C3	185.44		0.67		0.36	4.93	55.39	0.28		1.25			5.20		5.88		3.21	3.28	-1.1 %		12.04.12
G4	184.46		4.01	0.03	0.53	7.85	62.51	0.48		1.23			5.39		42.94		3.96	4.04	-1.0 %		12.04.12

Table 4: Charge balance error for sampled water.

Appendix II: Results and interpretation

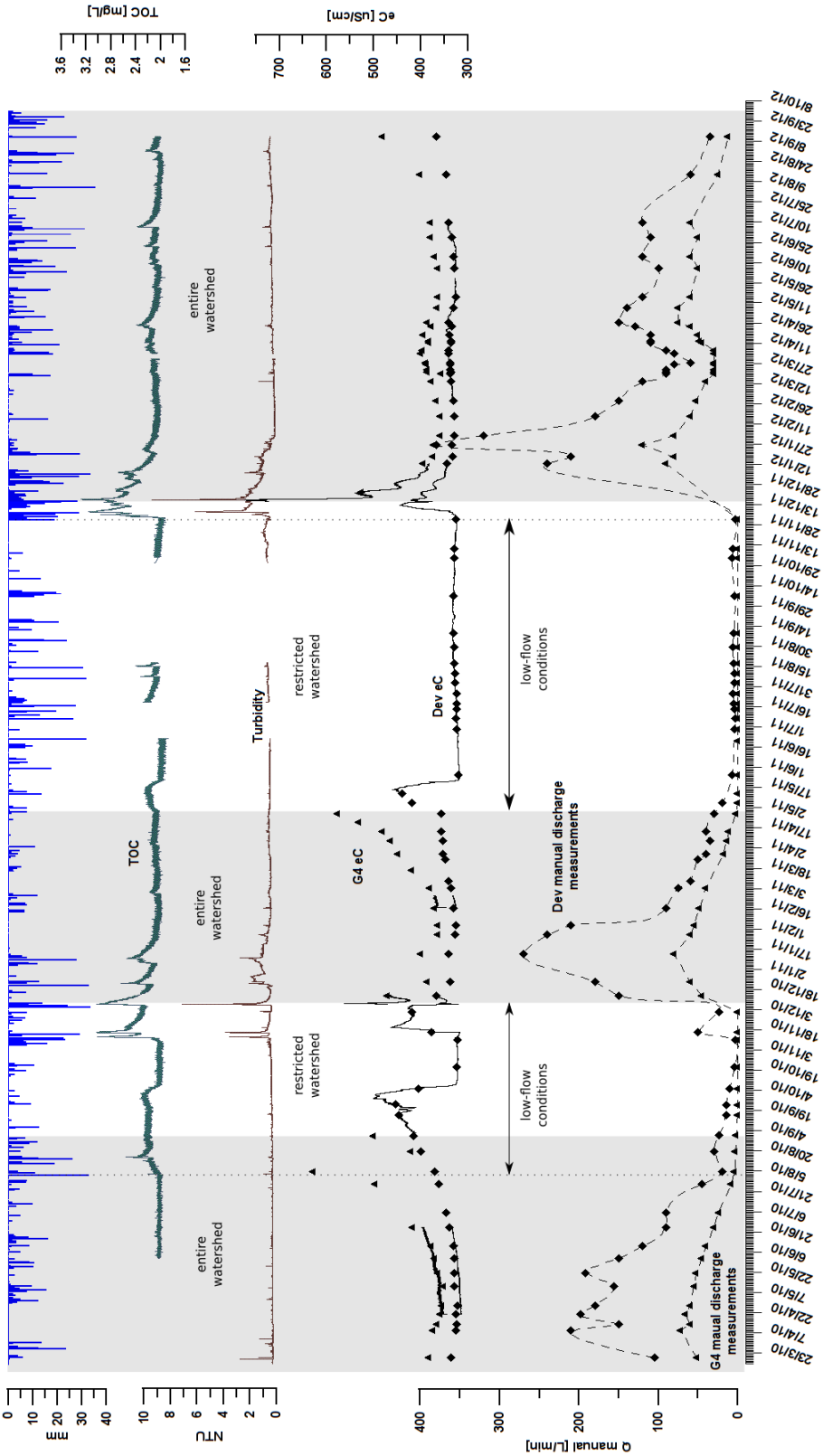

Fig. 60: Monitoring of discharge, electrical conductivity, turbidity and total organic carbon in the Dev spillway, along with discharge and electrical conductivity in the G4 spillway.

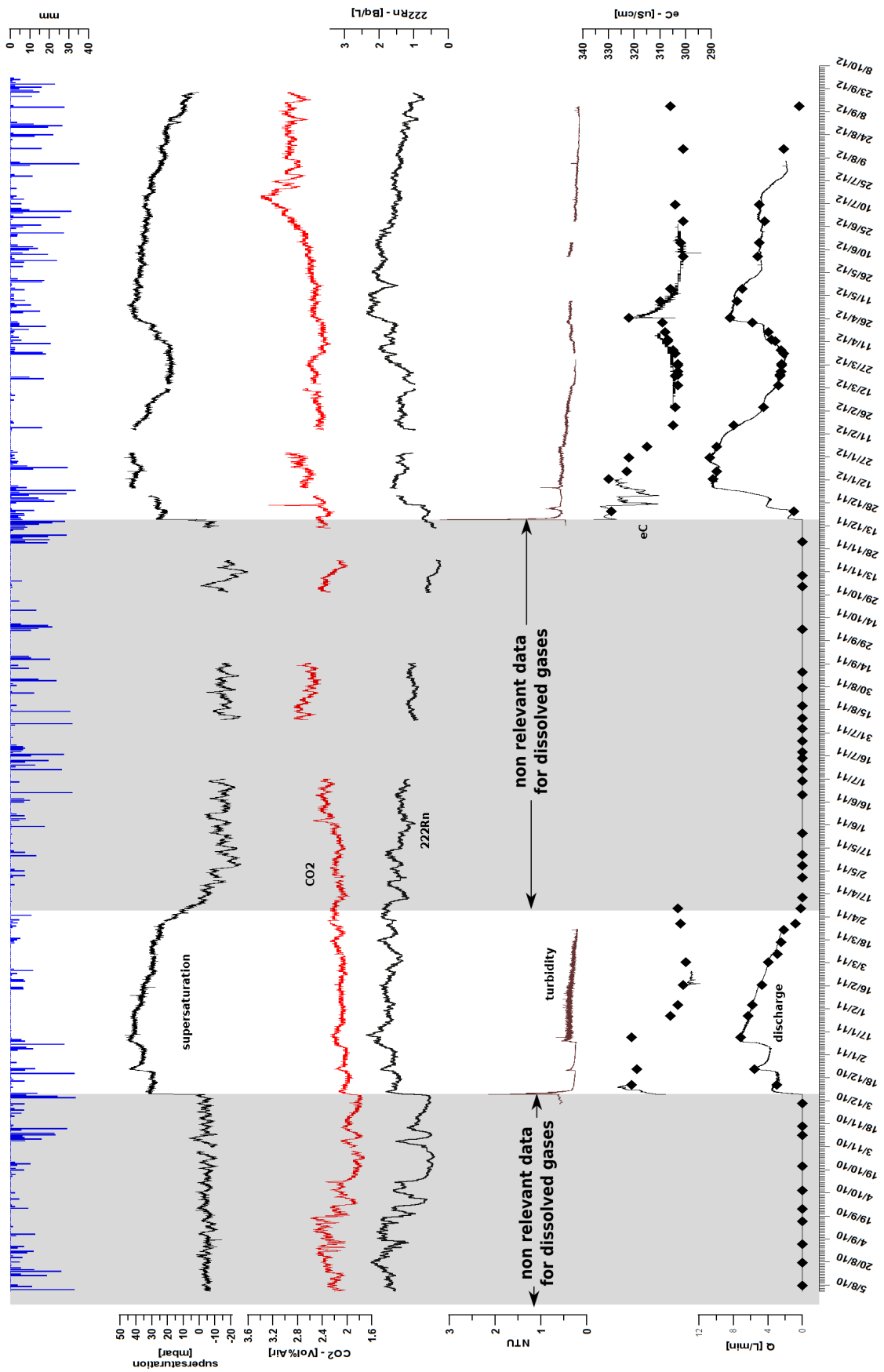

Fig. 61: Long term monitoring of the C3 seepage, with highlighted non relevant data for dissolved gases analysis. Measurement uncertainties : Rn:~3%, CO_2:~7%, supersaturation:~3%.

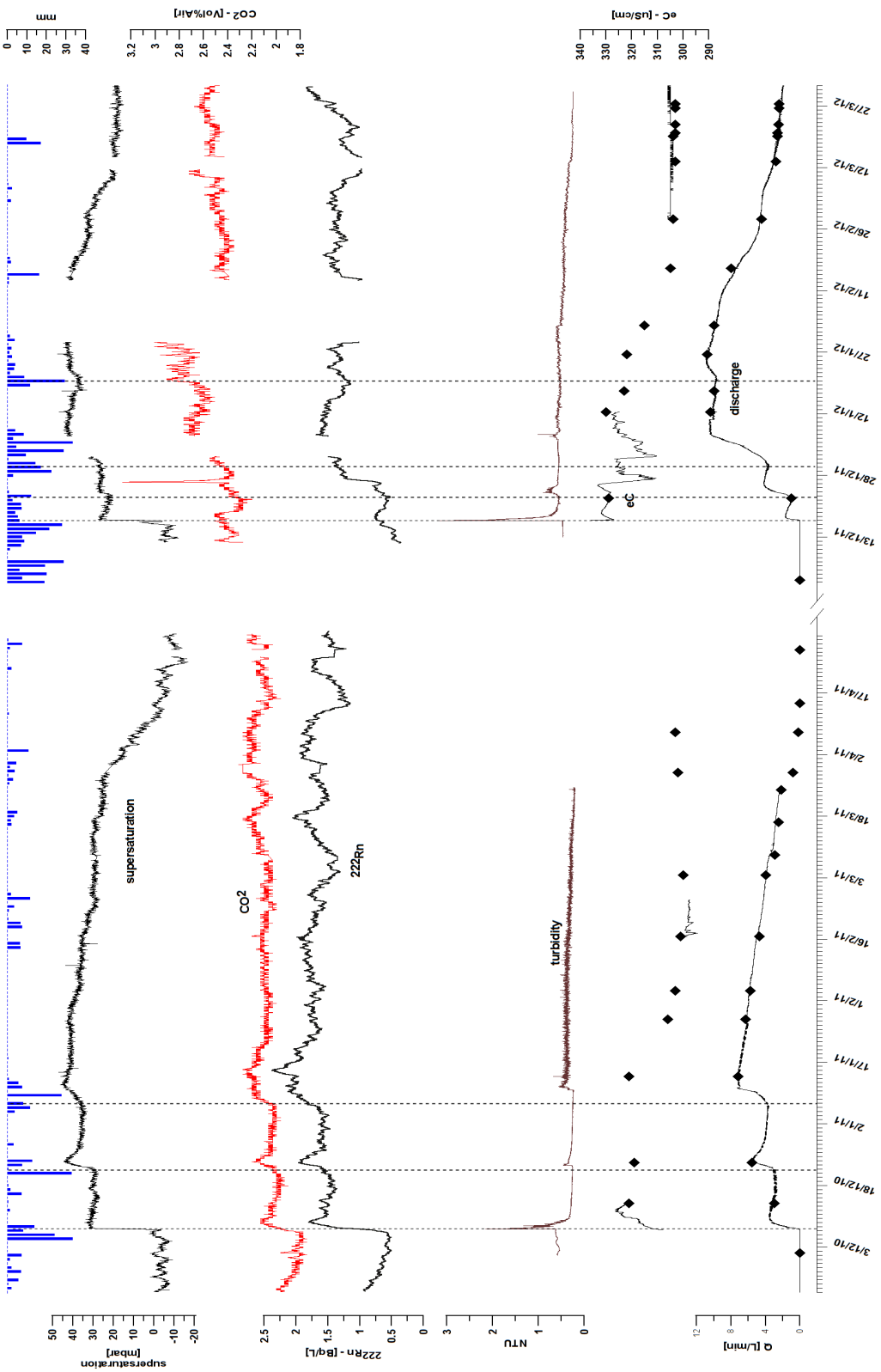

Fig. 62: Relevant periods for dissolved gas (radon, carbon dioxide and supersaturation) interpretation in the C3 seepage. Measurement uncertainties : Rn:~3%, CO_2:~7%, supersaturation:~3%.

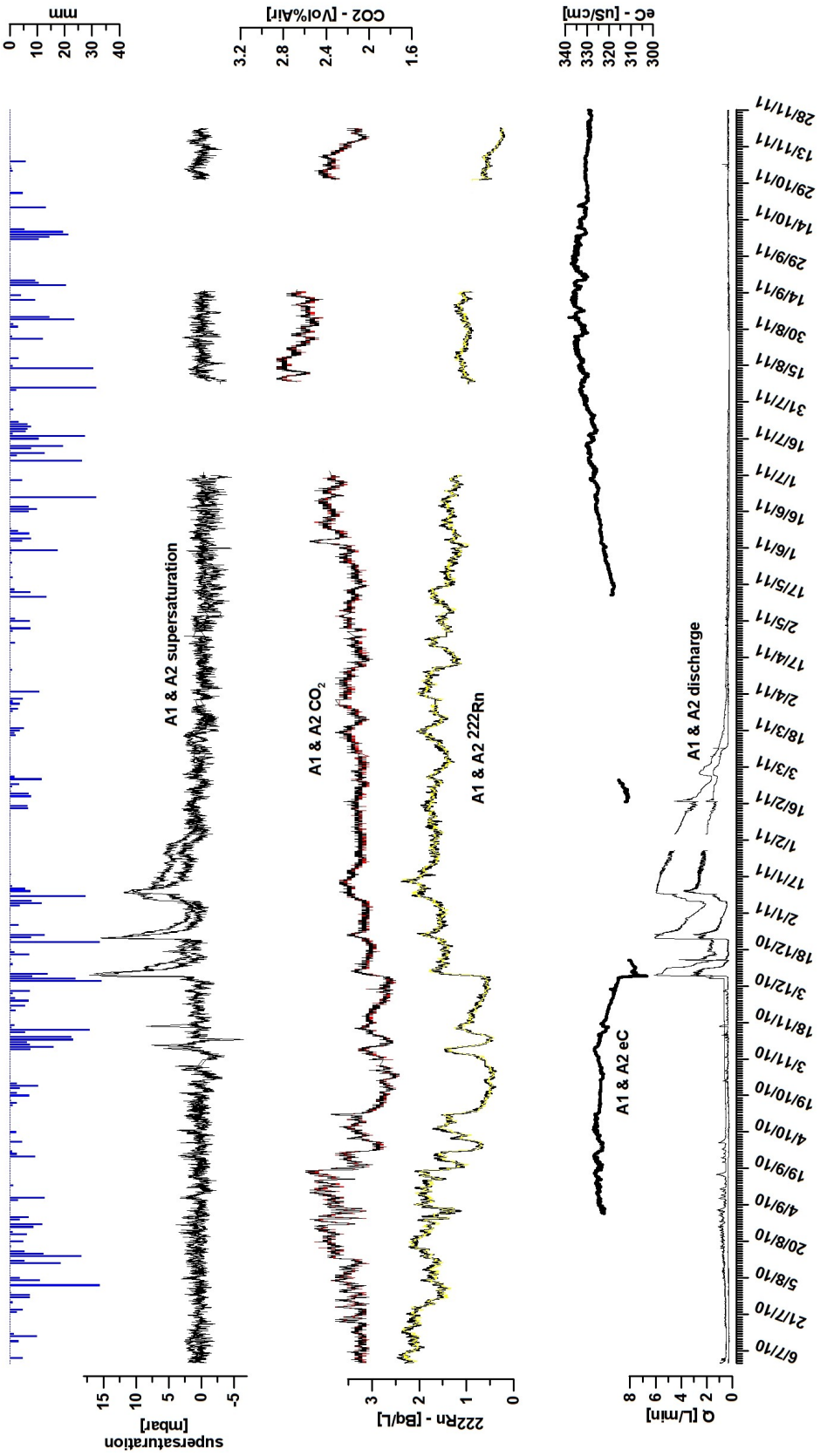

Fig. 63: Discharge, eC, radon, CO_2 and supersaturation in the A1 and A2 seepages. Measurement uncertainties : Rn:~3%, CO2:~7%, supersaturation:~3%.

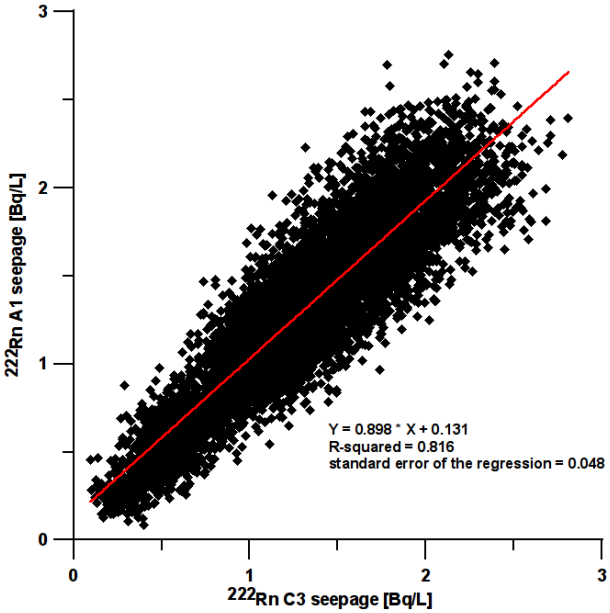

Fig. 65: 222Rn in the C3 seepage vs 222Rn in the A1 seepage during low-flow conditions.

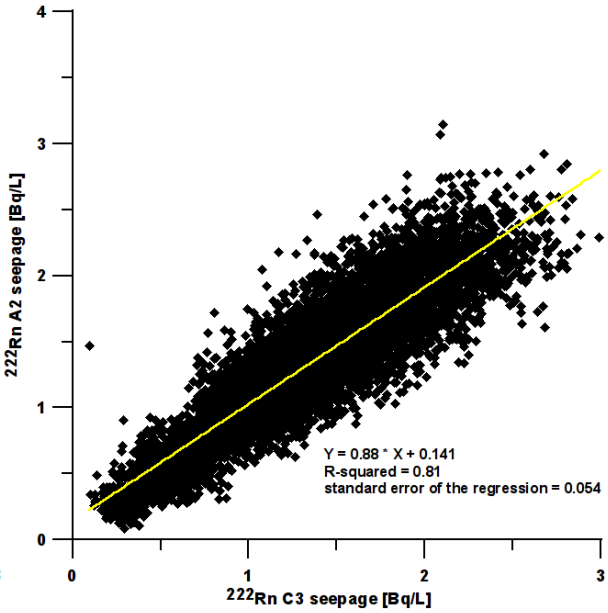

Fig. 64: 222Rn in the C3 seepage vs 222Rn in the A2 seepage during low-flow conditions.

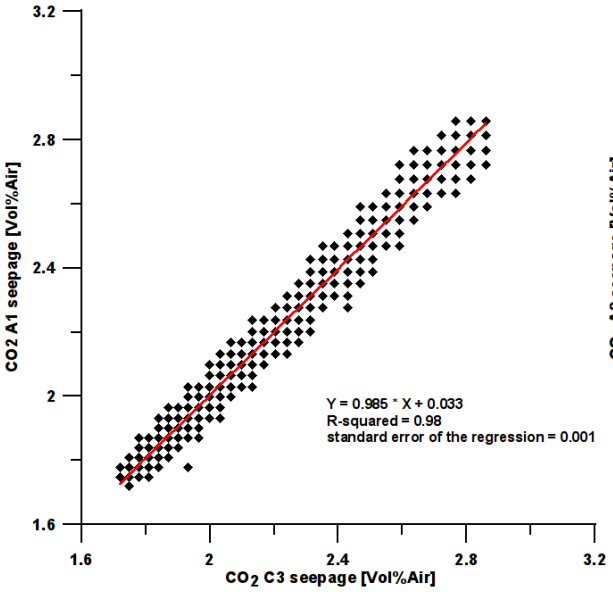

Fig. 66: CO_2 in the C3 seepage vs CO_2 in the A1 seepage during low-flow conditions.

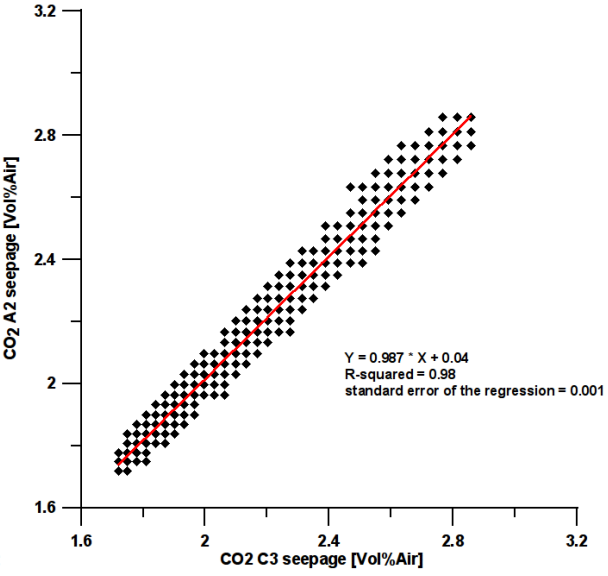

Fig. 67: CO_2 in the C3 seepage vs CO_2 in the A2 seepage during low-flow conditions.

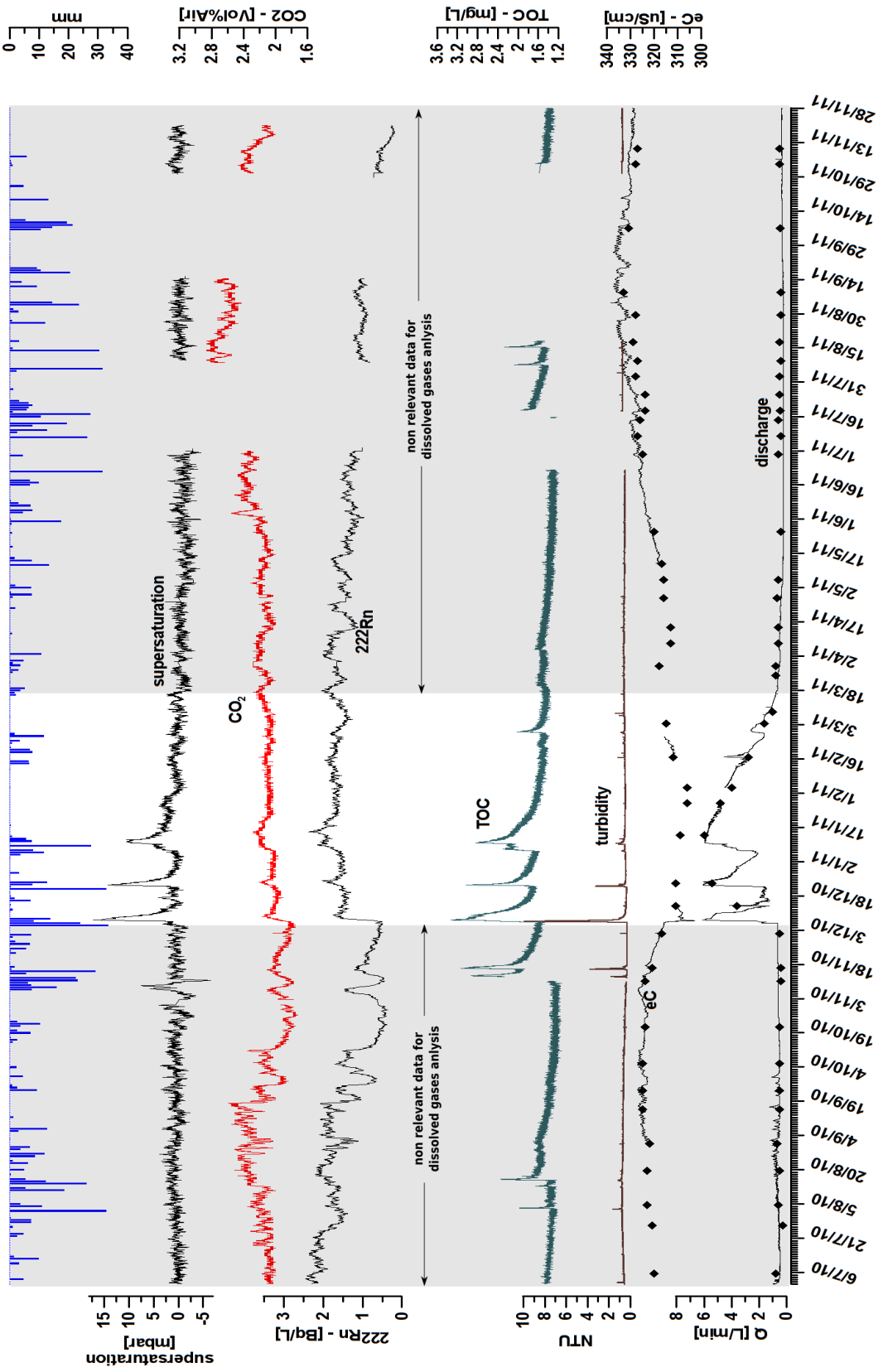

Fig. 68: Non-relevancy period of dissolved gases in the A1 seepage during low-flow conditions. Measurement uncertainties : Rn:~3%, CO2:~7%, supersaturation:~3%.

5 References

ABA-GEOL S.A. 2006. Rapport FR01865. Commune de Sorens : Ouvrages de captage définitifs, Caractéristiques hydrogéologiques. Fribourg.

Afes. 2009. Référentiel pédologique 2008. Paris.

Ames L. L., McGarrah J. E., Walker B. A. and Salter P. F. 1983. Uranium and radium sorption on amorphous ferric oxyhydroxide. Chemical Geology 40: 135-148.

Amraoui F., Razack M. and Bouchaou L. 2003. Turbidity dynamics in karstic systems. Example of Ribaa and Bittit springs in the Middle Atlas (Morocco). Hydrological Sciences Journal – Journal des Sciences Hydrologiques 48 (6): 971-984.

Aubert D. and Pochon M. 1977. Géochimie de la surface et formes du relief. VIII. Aplanissement karstique dans le Jura. Sci. Géol. Bull. 30 (4): 297-302.

Auckenthaler A., Raso G. and Huggenberger P. 2002. Particle transport in a karst aquifer: natural and artificial tracer experiments with bacteria, bacteriophages and microspheres. Water Science and Technology 46 (3): 131-138.

Aust W. M. and Blinn C. R. 2004. Forestry best management practices for timber harvesting and site preparation in the Eastern United States: an overview of water quality and productivity research during the past 20 years (1982-2002). Water, Air, and Soil Pollution 4: 5–36.

Batiot C., Emblanch C. and Blavoux B. 2003. Total Organic Carbon (TOC) and magnesium: two complementary tracers of residence time in karstic systems. Comptes Rendus Géosciences 335: 205-214.

Beven K. and Germann P. 1982. Macropores and water flow in soils. Water Resour. Res. (18):1311-1325.

Blavoux B. and Mudry J. 1983. Décomposition chimique des hydrogrammes du karst. Hydrogéologie-Géologie de l'Ingénieur (4): 270-278.

Booltink H.W.G. and Bouma. J. 1991. Physical and morphological characterization of bypass flow in a well-structured clay soil. Soil Sei. Soc. Am. J. 55: 1249-1254.

Bradford S.A., Simunek J., Bettahar M., van Genuchten M.T. and Yates S.R. 2003. Modelling colloid attachment, straining, and exclusion in saturated porous media. Environmental Science & Technology 37 (10): 2242-2250.

Bundt M. 2000. Highways Through the Soil: Properties of Preferential Flow Paths and Transport of Reactive Compounds. Synthesis. Swiss Federal Institute of Technology.

Burger A. 1987. Itinéraires hydrogéologiques dans les Gorges de l'Areuse. Gaz- Eaux- Eaux usées. 67:9: 561-568.

Climent H. 1996. Transport du Radon à l'interface sol - air, étude de l'influence des paramètres externes. Thèse.Université de Montpellier II - Sciences et techniques du Languedoc.

Davie T. 2006. Forests for soil and water conservation – what does the science say? *NZ Journal of Forestry*, Ma: 8–9.

Dekker L.W. and Ritsema C.J. 1996. Preferential flow paths in a water repellent clay soil with grass cover. Water Resour. Res. 32:1239-1249.

Doerfliger N., Jeannin, P.-Y. and Zwahlen F. 1999. Water vulnerability assessment in karst environments: a new method of defining protection areas using a multi-attribute approach and GIS tools (EPIK method). Environmental Geology,39(2): 165-176.

Drogue C. 1971. Coefficient d'infiltration ou infiltration efficace, sur les roches calcaires, Actes colloque d'hydrologie en pays calcaire, Besançon, pp. 121-131.

Dussart-Baptista L., Massei N., Dupont J.P. and Jouenne T. 2003. Transfer of bacteria-contaminated particles in a karst aquifer: evolution of contaminated materials from a sinkhole to a spring. Journal of Hydrology 284 (1-4): 285-295.

Edward N. T. 1975. Proceedings of Soil Science Society of America Journal, 39: 361-365.

Emblanch C., Blavoux N.,Puig J. et Couren M. 1998. Le marquage de la zone non saturée de karst à l'aide du carbone 13. Comptes Rendus de l'Académie des Sciences - Series IIA - Earth and Planetary Science 326(5) :327-332.

Faybishenko B. A. 1995. Hydraulic behaviour of quasi-saturated soils in the presence of entrapped air: Laboratory experiments. Water Res. Res. 31(10): 2421–2435.

Ford D. and Williams D.W. 1989. Karst geomorphology and hydrology. Unwin Hyman, London.

Fournier M., Massei N., Dussart-Baptista L., Bakalowicz M., Rodet J. and Dupont J. 2006. Study of the transport properties of suspended matter by means of multivariate analysis. 8th conference on limestone hydrogeology, Neuchâtel, Switzerland, 121-124.

Gaiffe M. and Bruckert S. 1990. Origine paléoécologique de l'aptitude des calcaires jurassiques à la fracturation. Conséquences tectoniques, pédogénétiques et écologiques. Bull. Soc. Neuch. Sci. Nat. 113: 191-206.

Gish T. J., Gimenez D. and Rawls W. J. 1998. Impact of roots on ground water quality. Plant and Soil 200: 47–54.

Glass R.J., Steenhuis T.S. and Parlange J.-Y. 1989. Mechanism for finger persistence in homogeneous, unsaturated, porous media: Theory and verification. Soil Sei. 148: 60-70.

Gobat J.-M., Aragno M. and Matthey W. 1998. Le Sol vivant. Lausanne, 568 pp.

Gobat J.-M., Aragno M. and Matthey W. 2010. Le sol vivant : bases de pédologie - biologie des sols. Troisième édition revue et augmentée. Presses Polytechniques et Universitaires Romandes.

Göppert N. and Goldscheider N. 2008. Solute and colloid transport in karst conduits under low- and high-flow conditions. Ground Water 46 (1): 61-68.

Grahammer K., Jawson M. D. and Skopp J. 1991. Soil biology and Biochemistry 23: 77–81.

Greeman D. J. and Rose A. W. 1996. Factors controlling the emanation of radon and thoron in soils of the eastern USA. Chemical Geology 129: 1-14.

Green R. T., Painter S. L., Sun A. and Worthington S. R. H. 2006. Groundwater Contamination in Karst Terranes. Water, Air, & Soil Pollution 6(1-2): 157–170.

Grolander S. 2009. Radon as a groundwater tracer in Forsmark and Laxemar. SKB Rapport R-09-47, Stockholm.

Havlicek E. and Gobat J.-M. 1996. Les apports éoliens dans les sols du Jura. *Etude et Gestion des Sols*, *3*(3): 167–178.

Heaton T. H. E. and Vogel J. C. 1979. Gas concentrations and ages of groundwaters in Beaufort Group sediments, South Africa. Water SA. 5(4): 160–170.

Hogue J. R., Rose A. W. and Jester W. A. 1997. Patterns of disequilibrium among 238U, 234U, 230Th and 226Ra in total soil and soil phases in two soil profiles. In: Generation and mobility of radon in soils. Final Report to U.S. Dept. of Energy, Contract DE-FG02- 87ER60577. Pennsylvania State University, Department of Geosciences.

Holkko J. and Liukkonen S. 1993. Radon diffusion in Finnish glacial till soil. Radiation Protection Dosimetry 45(1/4): 231-233.

Hubbard L. M. and Hagberg N. 1996. Time-variation of the soil gas radon concentration under and near a Swedish house. Environmental International 22 (1): 477-S482.

Hubbard L. M., Hagberg N. and Enflo A. 1992. Temperature effect on radon dynamics in two Swedish dwellings. Radiation Protection Dosimetry 45: 381-386.

Hudson N., Reynolds D. and Baker A. 2007. Fluorescence analysis of dissolved organic matter in natural , waste and polluted waters 649: 631–649.

Jacobsen O.H., Moldrup P., Larsen C., Konnerup L. and Petersen L.W. 1997. Particle transport in macropores of undisturbed soil columns. J. Hydrol. 196: 185-203.

Jacot C. 2011. Le rôle filtre du sol forestier dans la qualité de l'eau. Approches descriptive et expérimentale d'une catena des Gorges de l'Areuse (Neuchâtel, Suisse). Travail de Master, Université de Neuchâtel, Suisse.

Jeannin P.-Y. 1996. Structure et comportement hydraulique des aquifères karstiques. Thèse. CHYN. University of Neuchâtel, Suisse.

Johnson D., Geisinger D., Walker R., Newman J., Vose J., Elliot K. and Ball T. 1994 Plant Soil 165: 129–138.

Kaess W. 1998. Tracing Technique in Geohydrology, Balkema, Rotterdam.

Katz B.G., Catches J.S., Bullen T.D. and Michel R.L., 1998. Changes in the isotopic and chemical composition of ground water resulting from a recharge pulse from a sinking stream. Journal of Hydrology 211(1-4): 178-207.

Keller A.A., Sirivithayapakorn S. and Chrysikopoulos C.V. 2004. Early breakthrough of colloids and bacteriophage MS2 in a water-saturated sand column. Water Resources Research 40 (8), article n°: W08304.

Kiraly L.1975. Rapport sur l'état actuel des connaissances dans le domaine des caractères physiques des roches karstiques. In: A. Burger and L. Dubertet (Editors), Hydrogeology of karstic terrains. International Union of Geological Sciences, pp. 53-67.

Kiraly L. 1998. Modelling karst aquifers by the combined discrete channel and continuum approach. Bulletin d'Hydrogéologie 16: 77-98.

Kiraly L. 2002. Evolution of karst: from prekarst to cessation. Postojna-Ljubljana, Zalozba ZRC Gabrovšek, F. Ed., 155-190.

Klapproth J. C. and Johnson J. E. 2000. Understanding the Science Behind Riparian Forest Buffers: Effects on Water Quality. Virginia Cooperative Extension, Publication 420-151.

Klimchouk A. 1997. The nature and principal characteristics of epikarst. 12th International Congress of Speleology La Chaux-de-Fonds, pp. 306.

Klimchouk A.B. 2000. The formation of Epikarst and Its role in Vadose Speleogenesis. In: A.B. Klimchouk, D.C. Ford, A.N. Palmer and W. Dreybrodt (Editors), Speleogenesis. Evolution of Karst Aquifers. National Speleological Society, pp. 91-99.

Klimchouk A. 2004. Towards defining, delimiting and classifying epikarst: Its origin, processes and variants of geomorphic evolution. Speleogenesis and Evolution of Karst Aquifers 2 (1):1-13.

Kralik M. 2001. Strategie zum Schutz der Karstwassergebiete in Österreich. Report BE-189, Environment Agency, Vienna.

Lacroix M., Rodet J., Wang H. Q., Masséi N. and Dupont J. 2000. Origine des matières en suspension dans un système aquifère karstique : apports de la microgranulométrie. Earth and Planetary Sciences 330: 347–354.

Lakowicz J.R. 1999. Principle of Fluorescence Spectroscopy 2nd Edition. Kluwer Academic/Plenum Publishers: New York. Lombardi AT, Jardim WF. 1999. Fluorescence spectroscopy of high performance liquid chromatography fractionated marine and terrestrial organic materials. Water Research 33(2): 512–520.

Lange B., Luescher P. and Germann P.F. 2008. Significance of tree roots for preferential infiltration in stagnic soils. Hydrology and Earth System Sciences Discussions 5: 2373– 2407.

Lee E.S. and Krother N.C. 2001. A four-component mixing model for water in a karst terrain in south-central Indiana; USA. Using solute concentration and stable isotopes as tracers. Chemical Geology 179: 129-143.

Lozet J. and Mathieu C. 2002. Dictionnaire de science du sol. Coll. Tec & Doc.

MacCraith B., Grattan K.T.V., Connolly D., Briggs R., Boyle W.J.O. and Avis M. 1993. Cross comparison of techniques for the monitoring of total organic-carbon (TOC) in water sources and supplies. Water Science and Technology 28 (11-12): 457-463.

Macfadyen A.1970. Methods of Study in Soil Ecology. IBP/UNESCO Symp., Paris. pp. 167– 172.

Mahler B.J. and Lynch F.L. 1999. Muddy waters: temporal variation in sediment discharging from a karst spring. Journal of Hydrology 214 (1-4): 165-178.

Maloszewski P., Stichler W., Zuber A. and Rank D. 2002. Identifying the flow systems in a karstic-fissured-porous aquifer, Scheealpe, Austria, by modelling of environmental 18O and 3H isotopes. Journal of Hydrology 256: 48-59.

Mangin A. 1975. Contribution à l'étude hydrodynamique des aquifères karstiques. Thèse. Université de Dijon. Annales de spéléologie 29/3: 283-332, 29/4: 495-601, 30/1: 21-124.

Markkanen M. and Arvela H. 1992. Radon emanation from soils. Radiation Protection Dosimetry 45: 269-272.

Martini N. 2012. Influences des sols sur les eaux souterraines : une approche par l'étude des gaz dissous, au mont gibloux. University of Neuchâtel.

Massei M., Wang H.Q., Dupont J.P., Rodet J. and Laignel B. 2003. Assessment of direct transfer and resuspension of particles during turbid floods at a karstic spring. Journal of Hydrology 275 (1-2): 109-121.

Monroe, W. H. 1970. A Glossary of Karst Terminology. Geological Survey Water-Supply Paper 1899-K. U.S. Geological Survey. U.S. Government Printing Office. Washington, D.C.

Moore S. E. 1999. Forests, Hydrology, and Water Quality: Impacts of Silvicultural Practices. Florida Cooperative Extension Service, Gainesville.

Moore T. R. and Dalva M. 1993. The influence of temperature and water table position on methane and carbon dioxide emissions from laboratory columns of peatland soils. Journal of Soil Science 44:651–664

Mukhtar S., Baker J.L., Horton R. and Erbach D.C. 1985. Soil water infiltration as affected by the use of the paraplow. Transac- tion of ASAE 28: 1811–1816.

Mullinger N. J., Binley A. M., Pates J. M. and Crook N. P. 2007. Radon in Chalk streams: Spatial and temporal variation of groundwater sources in the Pang and Lambourn catchments, UK. Journal of Hydrology 339: 172 – 182.

Nagy H. É., Szabó Z., Jordán G., Szabó C., Horváth A. and Kiss A. 2012. Time variations of 222Rn concentration and air exchange rates in a Hungarian cave. Isotopes in environmental and health studies 48(3): 464–72.

Nebbache S., Loquet M., Vinceslas-Akpa M. and Feeny V. 1997. Turbidity and microorganisms in a karst spring. European Journal of Soil Biology 33 (2): 89-103.

OFEV 2009. Résultats de l'observatoire national des eaux souterraines (NAQUA) – Etat et évolution de 2004 à 2006. Etat de l'environnement n° 0903, Office fédéral de l'environnement, Berne, 144 p.

Perrin J. 2003. A conceptual model of flow and transport in a karst aquifer based on spatial and temporal variations of natural tracers. Thesis, University of Neuchâtel, Switzerland.

Perrin J., Jeannin P.-Y. and Zwahlen F. 2003. Epikarst storage in a karst aquifer: a conceptual model based on isotopic data, Milandre test site, Switzerland. Journal of Hydrology 279(1-4): 106-124.

Pronk M. 2009. Origin and behaviour of microorganisms and particles in selected karst aquifer systems. PhD thesis, Centre of Hydrogeology, University of Neuchâtel, Switzerland.

Radke J.K. and Berry E.C. 1993. Infiltration as a tool for detecting soil changes due to cropping, tillage, and grazing livestock. American Journal of Alternative Agriculture 8: 164–174.

Rommel K. 1980. Die kleine Leitfähigkeits-Fibel – Einführung in die Konduktometrie für Praktiker, WTW GmbH, Weilheim, Deutschland.

Ryan M. and Meiman J. 1996. An examination of short-term variations in water quality at a karst spring in Kentucky. Ground Water 34 (1): 23-30.

Sauter M. 1992. Quantification and forecasting of regional groundwater flow and transport in a karst aquifer (Gallusquelle, SW Germany), Tübingen.

Savoy L. 2007. Use of natural and artificial reactive tracers to investigate the transfer of solutes in karst systems. PhD thesis, Centre of Hydrogeology, University of Neuchâtel, Switzerland.

Savoy L., Surbeck H. and Hunkeler D. 2011. Radon and CO_2 as natural tracers to investigate the recharge dynamics of karst aquifers. Journal of Hydrology 406: 148-157.

Scanlon B. R., Nicot J. P. and Massmann, J. W. 2002. Soil Gas Movement in Unsaturated Systems (pp. 297–341).

Schnegg P.A. 2003. A new field fluorometer for multi-tracer tests and turbidity measurement applied to hydrogeological problems. Proceedings of the 8th International Congress of the Brazilian Geophysical Society, Rio de Janeiro (Brazil), 14-18 Sept. 2003.

Schnegg P.A. and Costa R. 2003. Tracer tests made easier with field fluorometers. Technical note. Bulletin d'Hydrogéologie 20: 89-91.

Schott B. and Wiegand J. 2003. Processes of radionuclide enrichment in sediments and groundwaters of Mont Vully (Canton Fribourg, Switzerland). Eclogae Geologicae Helvetiae 96: 99- 107.

Schürch M., Herold T. and Kozel R. 2003. Grundwasser – die Funktion des Waldes. Beitrag aus Bündner Wald Nr. 4/2003, 71-76. BWG, Bern.

Schwertmann U. 1985. The effect of pedogenic environments on iron oxide minerals. Advances in Soil Science 1:171-200.

Selker J.S., Steenhuis T.S. and Parlange J.-Y. 1992. Wetting front instability in homogeneous sandy soils under continuous infiltration. Soil Sei. Soc. Am. J. 56: 1346-1350.

Semkow T. M. 1990. Recoil-emanation theory applied to radon release from mineral grains. Geochimica et Cosmochimica Acta 54: 425-440.

Smart P.L. and Friederich H. 1986. Water movement and storage in the unsaturated zone of a maturely karstified carbonate aquifer, Mendip Hills, England. In: D. National Water Well Association, Ohio. (Editor), Proc. Conf. env. problems of karst terrains and their solutions, pp. 59-87.

Sottas J. 2010. Caractérisation des facteurs pédologiques du site du Gibloux. Diplôme, Univ. Neuchâtel.

Stadler H., Skritek P., Sommer R., Mach L., Zerobin W. and Farnleitner A.H. 2008. Microbiological monitoring and automated event sampling at karst springs using LEO-satellites. Water Science and Technology 58 (4): 899-909.

Surbeck H. 2005. Dissolved gases as natural tracers in karst hydrogeology : radon and beyond, proceedings of Multidisciplinary Approach to Karstwater Protection strategy, Unesco Course, Budapest, Hungary.

Surbeck H. 1991. Radium und Radon im Boden, messtechnische und geologische As- pekte, In: Messung von Radon und Radon-Folgeprodukten, Völkle, H. and Borchert, D. (Eds.), Publication Series Progress in Radiation Protection, Fachverband für Strahlenschutz, TUV Rheinland, Köln 1991

Taylor M., Mulholland M. and Thornburrow D. 2009. Infiltration Characteristics of Soils Under Forestry and Agriculture in the Upper Waikato Catchment, Vol. 4005.

Thüler L. 2010. Hydrogéologie Karstique en milieu forestier: site des Gorges de l'Areuse. Univeresité de Neuchâtel.

Thurman E.M. 1985. Organic geochemistry of natural waters. Developments in Biogeochemistry; 2. Martinus Nijhoff/Dr W. Junk, Dordrecht, Boston.

Tissier G. 2012. Ressource en eaux karstique de montagne: analyse des impacts de l'anthropisation dans un contexte de changement climatique. PhD thesis, Université de Grenoble, France.

Von Gunten H.R., Surbeck H. and Rössler E. 1996. Uranium series disequilibrium and high thorium and radium enrichments in karst formations, Environ.Sci. & Technol. 30/4: 1268-1274

Washington J. W. and Rose A. W. 1990. Regional and temporal relations of radon in soil gas to soil temperature and moisture. Geophysical Research Letters 17: 829-832.

Washington J. W. and Rose A. W. 1992. Temporal variability of radon concentration in the interstitial gas of soils in Pennsylvania. Journal of Geophysical Research: 97(B6): 9145-9159.

White W.B. and White E.L. 2005. Ground water flux distribution between matrix, fractures, and conduits: constraints on modelling. Speleogenesis and Evolution of Karst Aquifers: 3(2), 6 pages.

Williams P.W. 1983. The role of the subcutaneous zone in karst hydrology. Journal of Hydrology 61: 45-67.

Williams P.W. 1985. Subcutaneous hydrology and the development of doline and cockpit karst. Zeit. Geomorph. NF. 29: 463-482.

Zheng H., Chen F., Ouyang Z., Tu N., and Xu, W. 2008. Impacts of reforestation approaches on run-off control in the hilly red soil region of Southern China. Journal of Hydrology 356: 174–184.